UC San Diego

UC San Diego Electronic Theses and Dissertations

Title

The Origin and Function of CNS Fibrosis

Permalink

https://escholarship.org/uc/item/94k6s720

Author

Dorrier, Cayce

Publication Date

2020

Peer reviewed|Thesis/dissertation

eScholarship.org Powered by the California Digital Library
University of California

UNIVERSITY OF CALIFORNIA SAN DIEGO

The Origin and Function of CNS Fibrosis

A dissertation submitted in partial satisfaction of the requirements for the degree Doctor of Philosophy

in

Biomedical Sciences

by

Cayce Elizabeth Dorrier

Committee in charge:

Professor Richard Daneman, Chair
Professor Joan Heller Brown
Professor Mark Ginsberg
Professor Tracy Handel
Professor Binhai Zheng

2020

©

Cayce Elizabeth Dorrier, 2020

All rights reserved

The dissertation of Cayce Elizabeth Dorrier is approved, and it is acceptable in quality and form for publication on microfilm and electronically:

_____

_____

_____

_____

_____

Chair

University of California San Diego

2020

TABLE OF CONTENTS

LIST OF FIGURES

ACKNOWLEDGEMENTS

I would first like to thank my advisor Richard Daneman for his continued support throughout my time in graduate school. He has been an outstanding mentor and shaped the way I think about approaching and answering scientific questions. I have learned so much from him and hope to continue doing so throughout my career. In addition to dedicating so much time answering questions, editing my work, and chatting about science with me, Rich has also been a positive presence in my life over the past five years and a great person to talk to. I would also like to thank all of the members of the Daneman lab, as they have been so helpful in every aspect of my graduate career. I could not have done any of this without them, and will miss each person immensely. The group that we had in the lab was special, and I am not sure I will work with people who I both respect and cherish so much again.

I would also like to thank my thesis committee, the BMS program, and the Molecular Pharmacology Training Program for guiding me through the different requirements of graduate school. Pat and Leanne in the BMS office were especially helpful throughout this process. The Pharmacology Training Grant not only provided me with funding for two years, but also a community of students and mentors to ensure I always felt supported.

Finally, I would like to thank all of my family and friends for always being there for me and encouraging me to pursue a scientific career. My parents and sister Jamie supported my decision to move so far away for graduate school, were always available to chat and were excited with me for every bit of progress I made throughout my time here. My visits to and from my friend Bailey kept me sane during tough patches, and my BMS classmates were always available to commiserate about our shared experiences. Meeting Javier was one of the best moments of my graduate career, and I am excited to keep learning from him about science and life.

Chapter 1, in part, is currently being prepared for submission for publication of the material. Dorrier CE, Pintarić L, Daneman R. The dissertation author was the primary investigator and author of this material.

Chapter 2, in part, has been submitted for publication of the material as it may appear in Nature Neuroscience, 2020, Dorrier CE, Aran D, Haenelt EA, Sheehy RN, Hoi KK, Pintarić L, Chen Y, Lizama CO, Cautivo KM, Weiner GA, Popko B, Fancy SPJ, Arnold T, Daneman R. The dissertation author was the primary investigator and author of this paper.

Chapter 4, in part, is currently being prepared for submission for publication of the material. Miller J, Dorrier CE, Daneman R, Nudleman E. The dissertation author was the primary investigator and author of this material.

VITA

2015 Bachelor of Science in Chemistry, University of North Carolina at Chapel Hill

2020 Doctor of Philosophy in Biomedical Sciences, University of California San Diego

PUBLICATIONS

Dorrier CE, Aran D, Haenelt EA, Sheehy RN, Hoi KK, Pintarić L, Chen Y, Lizama CO, Cautivo KM, Weiner GA, Popko B, Fancy SPJ, Arnold T, Daneman R. CNS fibroblasts form a fibrotic scar in response to neuroinflammation. Under revision for resubmission to Nature Neuroscience.

Miller J*, Dorrier CE*, Daneman R, Nudleman E. Extended OIR protocol results in pericyte driven pre-retinal fibrosis. In preparation for eLife. *authors contributed equally,

Blanchette M, Bajc K, Ruderisch N, Dorrier CE, Profaci CP, Zhong G, Pant D, Cuevas-Diaz Duran R, Harvey SS, Garcia-pak IH, Isoherranen N, Tsai L, Wu J, Daneman R. Regional specializations of the blood-brain barrier regulate local brain function. In preparation for Science.

Marcinkiewcz CA, Bierlein-De La Rosa G, Dorrier CE, McKnight M, DiBerto JF, Pati D, Gianessi C, Hon O, Tipton GJ, McElligott ZA, Delpire E, Kash TL. Sex-dependent modulation of anxiety and fear by 5-HT1A receptors in the bed nucleus of the stria terminalis. ACS Chem Neurosci. 2019 Jul 17;10(7):3154-3166.

Marcinkiewcz CA, Mazzone CM, D'Agostino G, Halladay LR, Hardaway JA, DiBerto JF, Navarro M, Burnham N, Cristiano C, Dorrier CE, Tipton GJ, Ramakrishnan C, Kozicz T, Deisseroth K, Thiele TE, McElligott ZA, Holmes A, Heisler LK, Kash TL. Serotonin engages an anxiety and fear-promoting circuit in the extended amygdala. Nature. 24 Aug 2016; 537(7618):97-101.

Marcinkiewcz CA, Dorrier CE, Lopez AJ, Kash TL. Ethanol induced adaptations in 5-HT2c receptor signaling in the bed nucleus of stria terminalis: Implications for anxiety during ethanol withdrawal. Neuropharmacology. 13 Sep 2014; 89:157-67.

ABSTRACT OF THE DISSERTATION

The Origin and Function of CNS Fibrosis

by

Cayce Elizabeth Dorrier

Doctor of Philosophy in Biomedical Sciences

University of California San Diego, 2020

Professor Richard Daneman, Chair

Fibrosis is a common pathological response to inflammation in many peripheral tissues and can prevent tissue regeneration and repair. Despite the potential importance, very little is known about the fibrotic response in the central nervous system (CNS), and how this may impact the regenerative process. We identified persistent fibrotic scarring in the brain and spinal cord following neuroinflammation. Using lineage tracing and single-cell sequencing in the EAE mouse model of multiple sclerosis, we determined that this fibrotic scar is derived from

proliferative CNS resident fibroblasts, not pericytes or infiltrating bone marrow-derived cells. Ablating proliferating fibroblasts using the fibroblast-specific expression of herpes thymidine kinase led to an increase in oligodendrocyte lineage cells within inflammatory lesions and a reduction in motor disability. We further identified that interferon gamma pathway genes are enriched in CNS fibroblasts, and the fibroblast-specific deletion of *Ifngr1* resulted in a reduced fibrotic scar in EAE. Additionally, we identified that platelet derived growth factor receptor signaling affects brain fibroblast development and fibroblast migration. In the retina, fibrosis occurs following retinopathies and can lead to retinal detachment and blindness, and yet little is known about the origin of this fibrosis as it has been difficult to model in mice. We generated a novel mouse model of oxygen-induced retinopathies that exhibits persistent fibrotic pathology, and used histology and single-cell sequencing to determine that the origin of the fibrotic scar in the retina is likely pericytes. These data delineate a framework for understanding CNS fibrosis.

CHAPTER ONE:

Introduction to CNS fibrosis and fibroblasts

Fibrosis of the central nervous system

Fibrosis, or the pathologic formation of scar tissue made up of extracellular matrix proteins, occurs in many organs throughout the body in response to inflammation and injury. Fibrosis can have devastating consequences such as organ failure, which occurs when fibrotic tissue replaces normal organ tissue to an extent where the organ is no longer able to perform its normal functions. Fibrosis forms largely through the activation of fibroblasts, a cell type that plays a major role in structural support of connective tissues. Much less is known about fibrosis in the CNS including the full spectrum of triggers that lead to fibrosis, the cell type producing the extracellular matrix and the consequences of the scarring.

Recent data has demonstrated that fibroblasts are present in the meninges and perivascular spaces of the brain and spinal cord. The origins and functions of these cells are largely unknown, although they have been shown to play roles in fibrotic scar formation in the CNS following injury and inflammation which have also been attributed to other perivascular cell types such as pericytes. This introduction will describe what is known about the location and identity of CNS perivascular cell types and then focus on these newly described CNS fibroblasts-specifically their origin, subtypes, and role in health and disease, in particular fibrotic scarring.

Perivascular cell types and their potential for wound repair

CNS perivascular spaces are home to a variety of cell types that play important roles in communicating between the periphery and the brain and spinal cord parenchyma. These spaces are continuous with the meninges subarachnoid space allowing for fluid transfer with the meninges and are also a major route of solute clearance from the CNS (Lam et al., 2017; Mastorakos and McGavern, 2019). They are bordered on either side by the endothelial basement

membrane and the astrocyte endfeet basement membrane. In arterioles and capillaries these membrane are adjacent, and they separate beginning at postcapillary venules to form a fluid-filled cavity often referred to as the Virchow-Robin space (Mastorakos and McGavern, 2019; Zhang et al., 1990). Many different functions, including CNS fibrosis, have been attributed to perivascular cells, described in more detail below. However, without good markers to distinguish between them, it is difficult to examine the specific roles of each cell type. With new imaging techniques and single-cell sequencing technology we will be able to more definitively describe these major cell populations and deconvolute the role of each cell type in health and disease.

Pericytes are located within the endothelial basement membrane of capillaries and have been widely noted to play important roles in the development and maintenance of the blood-brain barrier (Armulik et al., 2011; Armulik et al., 2010; Daneman et al., 2010). On CNS capillaries there is approximately one pericyte for every one to three endothelial cells, and they extend cytoplasmic processes along the endothelium and form peg and socket contacts with endothelial cells at holes in the basement membrane (Armulik et al., 2011; Shepro and Morel, 1993). They are replaced by smooth muscle cells as capillaries transition into larger arterioles and venules, although exactly when on the vascular tree this transition takes place has been debated (Attwell et al., 2016). Common CNS pericyte markers include PDGFRβ and NG2, but neither are specific to pericytes as they also mark fibroblasts and oligodendrocyte progenitor cells, respectively, and to some extent vSMCs (Bergers and Song, 2005). Many of the functions of pericytes were determined using these markers as reporters or by knocking their respective genes out to assess functional changes, and therefore may not be pericyte-specific. Sequencing studies have proposed more specific markers including Kcnj8 and Abcc9, although these markers are still

rarely used to delineate this cell type (Bondjers et al., 2006; Vanlandewijck et al., 2018). A subtype of pericytes found using a Glast-CreER reporter mouse and denoted as type A pericytes have been shown to upregulate collagen expression in disease and form the fibrotic scar following spinal cord injury (Göritz et al., 2011). Other studies using different markers, such as a TBX18CreERT2 reporter mouse, found that in contrast pericytes do not proliferate during CNS trauma (Guimarães-Camboa et al., 2017; Soderblom et al., 2013). In other organs pericyte-like cells such as hepatic stellate cells in the liver have been proposed to be an origin of fibrotic tissue (Bataller and Brenner, 2005; Birbrair et al., 2014). Other functions of CNS pericytes include regulating transcytosis and leukocyte transport across endothelial cells, influencing the differentiation of oligodendrocyte lineage cells, and aiding in waste clearance (Daneman et al., 2010; De La Fuente et al., 2017; Sagare et al., 2013; Sweeney et al., 2016). There is competing evidence as to whether pericytes can act as stem cells and regulate blood flow (Dore-Duffy, 2008; Guimarães-Camboa et al., 2017; Hall et al., 2014; Hill et al., 2015; Peppiatt et al., 2006). Future studies using more pericyte-specific markers will enable us to answer these remaining questions and determine whether the functions attributed to pericytes are also performed by other cell types.

Vascular smooth muscle cells form continuous sheets around blood vessel walls. They are found on both the arterial and venular portion of the vascular tree and are absent from the capillary bed (Mastorakos and McGavern, 2019). Compared to arterioles, which have only one or two layers of vSMCs, larger arterial vessels have more concentric layering of circumferentially oriented vSMCs (Aldea et al., 2019; Welsh et al., 2018). Post-capillary venules contain sparse vSMCs that start to form into stellate multi-layered structures on venules (Welsh et al., 2018). In the

CNS, they perform the critical role of controlling cerebral blood flow by acting on the deformable basement membrane through contracting cytoskeletal proteins actin and myosin. While it was traditionally thought that vessel tone is primarily controlled by vSMCs that are found on larger arterioles, which encompasses less than 10% of the overall cerebral vasculature, recent studies propose that pericytes surrounding capillaries also play a role in regulating blood flow (Fernández-Klett et al., 2010; Hall et al., 2014). One of the key concerns when studying different cells of the neurovascular unit is the lack of marker specificity. Like other perivascular cell types, vSMCs express PDGFRβ, αSMA, CD13, NG2, CD146, and desmin *in situ* and *in vitro* (Smyth et al., 2018). However, differentiation of pericytes and vSMCs is critical. Vascular smooth muscle cells express αSMA, CD146, and desmin in higher quantity compared to pericytes, but lower amounts of NG2 (Smyth et al., 2018). Smooth muscle cells have been implicated in fibrosis in various pathologies throughout the body with the most common including atherosclerosis and asthma (Schuliga, 2015). Phenotypic switching of vSMCs in vascular pathologies alters their activity to release pro-inflammatory mediators, produce ECM proteins implicated in fibrosis and increase cellular proliferation and/or size (Douillet et al., 2000; Hu et al., 2019).

Perivascular macrophages (PVM) are part of the immune surveillance system in the brain that can be distinguished from other boarder-associated macrophages due to their specific location in the Virchow-Robin space. PVMs have been implicated in many mechanisms during steady state and brain pathology. During tissue homeostasis they have been shown to aid in maintaining BBB integrity by supporting tight junctions between endothelial cells and impeding inflammation by phagocytosing debris and potentially harmful pathogens (Faraco et al., 2017; Lapenna et al.,

2018). PVMs have shown to alter their phenotype upon tissue injury. They are activated by PAMPs, DAMPS and cytokines derived from neutrophils. At site of trauma, the activated PVMS are a source of many pro-inflammatory mediators (TNF-a, IL-6 and IL-1b) which can activate fibroblasts and induce growth, migration and subsequent secretion of ECM proteins (Mescher, 2017). The most widely used markers for perivascular macrophages are CD163, CD206, and Lyve-1 (Faraco et al., 2017). However, certain limitations on marker specificity are still observed. CD206 is a superior marker to CD163 since CD163 can also recognize monocytes (Yang et al., 2019). However, if immunohistochemistry is performed on a brain which has been subject to brain injury such as ischemic stroke, CD206+ cell populations increase to include brain resident microglia and infiltrating macrophages (Faraco et al., 2017). CD206 and CD163 are also found on meningeal and choroid plexus macrophages, while LYVE1 is specific to MGM and PVMs (Yang et al., 2019).

CNS fibroblasts are located in the meninges in the dura, arachnoid and pia mater, and in the perivascular spaces adjacent to arterioles and venules. In these areas they are sparsely populated in the Virchow-Robin space; outside of the endothelial basement membrane but within the astrocyte end feet (Lam et al., 2017; Mastorakos and McGavern, 2019). These cells are positive for both PDGFRα and PDGFRβ, but finding a single, specific marker for fibroblasts throughout the body has been difficult. PDGFRβ is often used as a marker for pericytes, but because it is also present in fibroblasts it is possible that fibroblasts are contributing to the functions attributed to PDGFRβ+ cells. The ER-TR7 antigen on reticular fibroblasts and their adjoining extracellular network is often used to mark fibroblasts, although the molecular identity of this antigen is unknown (Van Vliet et al., 1986; Van Vliet et al., 1984). A recent single-cell sequencing paper

of the CNS vasculature noted these cells express the epithelial marker Lama1, unlike many peripheral fibroblasts, and used a Lama1 antibody to label these cells in the brain (Vanlandewijck et al., 2018). Recent papers by the Lee lab have demonstrated that this cell type expands in number during CNS trauma and forms the fibrotic scar (Soderblom et al., 2013; Yahn et al., 2020). In other organs such as the lung, heart and skin, fibroblasts are widely implicated in scar formation (Kendall and Feghali-Bostwick, 2014; Lederer and Martinez, 2018; Travers et al., 2016; Wynn, 2008).

CNS fibroblast origin and role in development

While the development of perivascular CNS fibroblasts has not been studied, the development of meningeal fibroblasts has been well characterized. The meninges forms a protective sheet around the brain parenchyma and contains 3 membranes with distinct histological characteristics – the dura mater, arachnoid mater and the pia mater. The development of the meninges is initiated by mesenchyme cell migration and establishment of the primary meninx. This primordium is formed by the fifth week of gestation in humans and embryonic day 9.5 in mice (Angelov and Vasilev, 1989). The barrier between the meninges and the brain tissue is established by fibroblasts which produce ECM proteins to form the pial basement membrane (Dasgupta and Jeong, 2019). By embryonic day 13 in mice (6th week of gestation in humans), there are distinct meningeal layers around the brain. Below the calvarial layer, which contains the precursors of the skull, the meningeal primordium is divided by the dural limiting layer which establishes the border between the pachymeninx, or dura mater, and the leptomeninges (Dasgupta and Jeong, 2019). The membranes continue to differentiate and the cavitation process in the leptomeninx is initiated, leading to the formation of the sub-arachnoid

space and arachnoid trabeculae (Dasgupta and Jeong, 2019). The cellular origins of the meninges in the hind and midbrain derive from the mesoderm, while cells in the forebrain migrate from the neural crest (O'Rahilly and Müller, 1986).

Fibroblasts play important roles throughout meningeal and CNS development. Fibroblasts deposit ECM proteins which form the deformable pial basement membrane and excrete chemokines such as SDF1 which support neuronal migration and positioning (Dasgupta and Jeong, 2019; Halfter et al., 2002). Meningeal ECM proteins regulate cortical layer formation, while meningeal fibroblasts produce retinoic acid which directs cortical neurogenesis and cerebrovascular development (Siegenthaler et al., 2011). Mice with mutations in the transcription factor Foxc1, largely expressed in meningeal fibroblasts throughout development, have deficiencies in the maturation of the meninges ranging from abnormal meningeal fibroblast counts to an underdeveloped sub-arachnoid space (Dasgupta and Jeong, 2019; Zarbalis et al., 2007). *Foxc1* knockout mice showed complete loss of retinoic acid synthesis and confirmed that retinoic acid signaling is critical in regulating the neurogenic switch from symmetric lateral division to asymmetric radial expansion of the cortex (Siegenthaler et al., 2011; Siegenthaler and Pleasure, 2011). Furthermore, mice with a complete knockout or hypomorph of *Foxc1* show a distinct phenotype of a laterally expanded forebrain and a reduction in neuronal production. This leads to calvarial osteogenesis and a defective cortical phenotype (Siegenthaler and Pleasure, 2011; Vivatbutsiri et al., 2008; Zarbalis et al., 2007).

Mouse telencephalic meningeal fibroblasts at e14.5 were recently profiled through single-cell RNA sequencing, which revealed that there are distinct meningeal fibroblast populations (DeSisto et al., 2020). Pial fibroblasts can be differentiated from the dura and arachnoid cluster by expression of the novel marker *s100a6*, and also highly express *Lum*, *Mfpa2* and *Ngfr*.

Compared to dura and arachnoid fibroblasts, pial fibroblasts show enrichment in many genes responsible for the production of ECM proteins such as collagens, laminins and glycoproteins. Additionally, pial fibroblasts together with arachnoid fibroblasts exhibit a key role in retinoic acid synthesis. Pial fibroblasts are responsible for retinaldehyde production, while arachnoid fibroblasts have enriched expression of *Aldh1a12*, which is implicated in retinoic acid production, and *CRABP2*, which encodes for a retinoic acid transporter. Arachnoid fibroblasts also show enrichment in various genes encoding for sulfate, magnesium and GABA transporters, glycoprotein Agnptl2 and other ECM proteins implicated in fibroblast regulation. Dural fibroblasts have increased expression of genes encoding for small and large ribosomal subunits, the ion transport regulator Fxyd5 and the transcription factors Foxp1 and Six1. Novel markers for differentiating meningeal fibroblasts which are conserved across human and mouse brains include CRABP2 for arachnoid fibroblasts and s100a6 for pial fibroblasts.

CNS Fibroblasts in the healthy adult: functions and subtypes

The role of CNS fibroblasts in the healthy adult, especially those outside of the meninges, has not been well studied. In the periphery the foremost role of fibroblasts is to provide structural support to connective tissues through extracellular matrix (ECM) secretion, particularly of collagens I and III (Kendall and Feghali-Bostwick, 2014). Fibroblasts in some tissues can also differentiate into other cells when needed, such as fat cells or cartilage cells, and produce a wide array of cytokines and growth factors (Alberts B, 2002). They play critical roles in angiogenesis as they secrete matrix proteins to facilitate tube formation as well as vascular endothelial growth factor (VEGF), which promotes angiogenesis (Newman et al., 2011). They also sense and

respond to mechanical stress by remodeling tissue as necessary and altering their membrane potential (Camelliti et al., 2005; Herum et al., 2017).

Fibroblasts in the CNS are much more numerous in the meninges than in perivascular spaces and have been shown to play structural support roles within and between the different meningeal layers. In the dura, fibroblasts and collagen fibers attach this outer layer of the meninges to the skull, and a thin layer of fibroblasts without adjoining ECM proteins separates the dura and arachnoid (Haines et al., 1993; Kirmi et al., 2009). In the arachnoid, fibroblasts and collagens form the arachnoid trabeculae which connect this layer to the pia (Alcolado et al., 1988). In the pia, a thin layer of fibroblasts and basement membrane separates the pia and glia limitans (Lam et al., 2017). These roles in separating the different layers of the meninges are incredibly important as these layers have varying degrees of vascular leakage and therefore contact with the periphery (Mastorakos and McGavern, 2019).

The role of perivascular fibroblasts in the Virchow-Robin space and surrounding blood vessels in the subarachnoid space is less clear. There is little evidence that these perivascular fibroblasts are differentiating and there is not widespread angiogenesis in the adult, human CNS. It has been proposed that fibroblasts covering pial vessels facilitate fluid exchange between the CSF and perivascular spaces (Mastorakos and McGavern, 2019), but more in depth studies are needed to validate this claim.

In the healthy, adult CNS, fibroblasts residing in the meninges and Virchow-Robin spaces in adult mice have only recently been transcriptionally profiled at the bulk and single cell level, revealing information about the transcriptional identity of CNS fibroblasts and the presence of various subtypes. The first study to characterize these cells was a comprehensive single-cell sequencing study of the brain vascular and perivascular cells in healthy mice

(Vanlandewijck et al., 2018). The authors found 2 clusters of fibroblasts which they denoted as F1 and F2. These fibroblasts highly express extracellular matrix proteins such as collagens in both clusters, and a comparison of CNS fibroblasts with lung fibroblasts found that 45/50 of the CNS fibroblast-enriched transcripts were also found in lung fibroblasts.

A single-cell transcriptomic study of meningeal fibroblasts in development found multiple subtypes between the meningeal layers (DeSisto et al., 2020). It still remains to be determined how these populations relate to the 2 populations from the studies mentioned above, and if these 2 populations correlate to meningeal support vs. perivascular fibroblasts or morphological differences between cells in both locations. Further studies using techniques such as spatial single-cell sequencing and in situ hybridization should be performed to further characterize these subtypes.

Meningeal fibroblasts contribute to a fibroblastic reticular network following inflammation

In the lymph nodes following inflammation a fibroblastic reticular network forms to serve as an immune cell niche (Aloisi and Pujol-Borrell, 2006; Chang and Turley, 2015; Junt et al., 2008). It has been recently shown that a similar network forms in the meninges during inflammation, most notably in the neuroinflammatory disease Multiple Sclerosis (MS) (Magliozzi et al., 2007). These networks consist of T cells, B cells, other immune cells and fibroblasts held together by ECM secreted from the fibroblasts (Bajénoff et al., 2006). In mouse EAE, a model for MS, TH17 cells have been shown to be necessary for the formation of this network (Pikor et al., 2015). Specifically, IL17 and IL22 from these cells was shown to remodel CNS fibroblasts and upregulate fibrotic gene expression both *in vitro* and *in vivo*.

The overall role of this meningeal network in disease progression is just beginning to be studied. In human MS it has been shown to occur near areas of grey matter demyelination, implicating it in grey matter lesion formation (Magliozzi et al., 2007; Magliozzi et al., 2010). In mouse EAE, blocking IL17 and IL22 and reducing the size of this meningeal network led to a decrease in the EAE motor disability score (Pikor et al., 2015). However, the exact signaling contribution from the individual cells in this network including fibroblasts is unclear as no cell type specific deletions have been tested.

This fibroblastic reticular network has also been described following CNS infections such as mouse coronavirus (Watanabe et al., 2016) and Lymphocytic choriomeningitis virus (LCMV) infection (Kim et al., 2009). The latter study revealed that the LCMV infected cell population in the meninges was ER-TR7^{+} stromal cells. An additional study characterized this network following an infection of the mouse hepatitis virus (MHV) strain A59 and further showed that CCR7 ligands produced by stromal cells in the network played a role in supporting the recruitment of antiviral CD8+ cells (Cupovic et al., 2016). Many questions remain about the conditions that lead to the formation of this meningeal network, its overall role in disease progression as it appears to be beneficial to recovery following infection and harmful in demyelination, and the exact role of fibroblasts in its formation and signaling. It has been proposed that specific signals from fibroblasts help to maintain the immune cell niche, and transcriptional profiling of fibroblasts in this network could help to reveal these signaling mechanisms upregulated in fibroblasts in the network vs. those in the healthy meninges.

Outside of the reticular network, meningeal fibroblasts have been implicated in headache propagation, where LPS- and NE- treated dural fibroblast conditioned media induces facial allodynia, (Wei et al., 2014; Wei et al., 2015) and neuropathic pain, where mice deficient in

PI16, found mainly in fibroblasts in the meninges of the dorsal root ganglia, were protected against neuropathic pain (Singhmar et al., 2020). More work is needed to understand the complete profile of how meningeal fibroblasts interact with their surroundings in these conditions.

CNS fibroblasts form a fibrotic scar following injury and inflammation

Following injury to the CNS a scar forms around the site of trauma consisting of 2 parts: a glial scar made up of reactive astrocytes that forms almost immediately after injury and an inner fibrotic scar in the disease core that seals up the injury site and forms in the days and weeks following the trigger (Fernández-Klett and Priller, 2014a; O'Shea et al., 2017). This glial scar has been widely characterized, and new research shows that it can have an overall beneficial role in disease repair (Anderson et al., 2016; Burda and Sofroniew, 2014; Faulkner et al., 2004; Sofroniew, 2009a). The inner fibrotic scar has been much less studied although it has also been implicated in disease repair and recovery following injury and inflammation in the CNS. Below, we summarize the main CNS injuries and diseases where fibrotic scarring has been implicated and describe what has been proposed as the cell type forming the scar, the role of the scar in recovery following specific triggers and the mechanisms that lead to CNS fibroblast proliferation and collagen production. Many of these questions remain incompletely answered, however, suggesting that studies probing the origin, role, and mechanisms leading to fibrotic scarring in many CNS diseases would be useful to fully understand how scarring influences CNS repair.

Spinal cord injury (SCI) is the most widely studied trigger for CNS fibrotic scarring in both humans and animal models. Several studies have suggested that this scar arises from Type A

pericytes that upregulate collagen expression following injury. The major study proposing this cellular origin used a Glast-CreER mouse model, generally a promotor thought to be most active in astrocytes, to identify scar-forming cells and classified them as pericytes due to their expression of PDGFRβ (Göritz et al., 2011). Other studies using the Col1a1GFP mouse model have suggested that the origin of the fibrotic scar is CNS fibroblasts, as the collagen-producing cells do not express pericyte markers such as NG2. Light sheet microscopy images of an injured mouse spinal cord suggested that the Col1a1GFP+ cells were likely coming from the meninges, although no definitive studies have determined the proportion of the scar arising from meningeal vs. perivascular fibroblasts (Soderblom et al., 2013). It is likely that these differing reports have actually been classifying the same cell type as both pericytes and fibroblasts express PDGFRβ. Genetic lineage tracing studies could provide further insight into the cellular origin of the scar. It has been thought that this fibrotic scar contributes negatively to disease progression as it blocks progenitor cells from entering the injury core and axon regeneration, and therapies have been proposed to target this scar to advance recovery (Brazda and Müller, 2009). It has been shown, however, that when fibrotic scar formation was completely blocked in mice that the injury site fails to close, resulting in an open tissue defect (Göritz et al., 2011). In contrast, if this scar is largely diminished in size, there is an increase in recovery from disease as shown by both motor tests in mice and optogenetic stimulation of regenerating axons (Dias et al., 2018). This study used a combination knockout of *HRas*, *NRas* and a cell-specific deletion of *KRas* to prevent fibroblast proliferation and scar formation. This pathway is not one specific to fibroblasts, however, and unlikely to be used in a clinical setting. Other studies have shown that inhibiting microtubule formation prevents fibrotic scarring and dampening immune cell signaling can also

be used to reduce scarring and enhance disease recovery (Brazda and Müller, 2009; Hellal et al., 2011; Klapka et al., 2005; Vangansewinkel et al., 2019).

Traumatic brain injury (TBI) like spinal cord injury is a physical injury to the CNS. There are many different mouse models of TBI that lead to brain injuries of varying sizes and intensities, and fibrotic scarring has been exhibited in the more severe models. As in SCI there have been differing reports of the cellular origin of this scar. It has been widely noted that PDGFRβ+ cells accumulate in the injury core of rodents, with the identity of these cells attributed to either pericytes or meningeal fibroblasts (Kyyriäinen et al., 2017; Zehendner et al., 2015). Inhibiting PDGFRβ signaling following TBI has been shown to decrease scar formation in mice, although how this manipulation affected overall tissue recovery was not studied (Pei et al., 2017). It has also been shown that scar-forming cells highly express TGFβ receptors following TBI, (Komuta et al., 2010) and that inhibiting TGFβ signaling following TBI in rodents reduced scar formation and promoted the regeneration of dopaminergic neurons (Logan et al., 1994; Yoshioka et al., 2011). Reducing scar formation by preventing Col4 helix formation has also been shown to promote axonal regeneration following brain injury (Yoshioka et al., 2010). Future studies will be needed to conclusively determine the origin of the scar and how fibrotic scar deposition and manipulation contributes to recovery for all types of TBI.

Stroke is caused by loss of blood flow to specific areas of the CNS. The resulting hypoxia leads to blood-brain barrier breakdown, tissue damage and CNS scarring. It has been shown that both PDGFRβ+ and Col1a1GFP+ cells, referred to as stromal cells, increase in number in the lesion core surrounded by fibrotic proteins following the MCAO mouse model of stroke (Fernández-

Klett et al., 2013; Kelly et al., 2016). In *PDGFRβ*+/- mice following MCAO, fibrotic scar formation was reduced but the overall infarct volume was larger, implicating PDGFR signaling in fibrotic scar formation in this model and a potential role for the fibrotic scar in managing infarct size (Makihara et al., 2015). Whether this change in infarct size results in changes in disease recovery and tissue repair remains unknown.

Multiple sclerosis is a neuroinflammatory disease characterized by concentrated areas of inflammation and demyelination. ECM depositions occur around blood vessels in human MS and a recent study has shown that Col1a1GFP+ cells increase in number in the spinal cord parenchyma following symptom onset in the EAE mouse model of MS. (Mohan et al., 2010; van Horssen et al., 2006; van Horssen et al., 2007; Yahn et al., 2020).

Infection Following *Staphylococcus aureus* infection in the mouse brain, an abscess forms that is surrounded by a fibrotic wall (Aldrich and Kielian, 2011). It has been reported that a small population of bone marrow-derived cells in the area of the fibrotic wall were positive for markers of fibrosis such as collagen I. It remains unknown how bone marrow-derived cells contribute to fibrosis following other CNS triggers.

Retinopathies: Fibrotic scarring occurs in the retina following conditions such as diabetic retinopathy and retinopathy of prematurity (ROP) and can lead to tractional retina detachments and blindness (Friedlander, 2007). The proposed origin of this fibrotic scar varies with the location of the fibrosis and the extent of tissue damage to specific layers of the retina. For example, when there is a physical injury to the retina pigment epithelium (RPE), these cells have

been proposed to migrate to the surface of the retina and deposit scar tissue (Hiscott et al., 1999; Machemer et al., 1978). In other cases, Müller glial cells have been proposed to extend their processes to the surface of the retina and deposit scar tissue (Bringmann et al., 2006). While there is an extensive retinal vasculature, the presence of perivascular fibroblasts in the retina has not been reported. A single-cell transcriptomic study of the murine retina picked up a few cells denoted as fibroblasts, however these cells were reported to be contamination (Friedlander, 2007; Macosko et al., 2015). More in depth sequencing studies are needed to confirm whether or not there are fibroblasts in the retina of mice and humans and if they play a role in the devastating process of retinal scarring.

In sum, fibrosis occurs in the CNS as a consequence of triggers such as injuries, hypoxia and inflammation. This scar may play multiple roles in tissue repair following CNS injury, but the overall roles in recovery following each specific trigger are largely unknown. The origin of the scar needs to be more fully characterized, with existing data suggesting it arises from pericytes and/or CNS fibroblasts. CNS fibroblasts are a recently characterized cell type that plays important roles in processes such as CNS wound healing and infection responses. Very little is known about the role of these cells in the healthy CNS and the factors driving them to participate so robustly in disease.

Chapter 1, in part, is currently being prepared for submission for publication of the material. Dorrier CE, Pintarić L, Daneman R. The dissertation author was the primary investigator and author of this material.

CHAPTER TWO:

CNS fibroblasts form a fibrotic scar in response to inflammation

INTRODUCTION

Fibrosis, defined as the pathological deposition of collagen I (Col1)-rich extracellular matrix, is a common response to injury and inflammation in peripheral organs such as the heart, kidney, liver and lung (Bataller and Brenner, 2005; Lederer and Martinez, 2018; Lee and Kalluri, 2010; Mack, 2018; Travers et al., 2016). Following tissue damage, extracellular matrix deposits provide essential structure to areas of injury. Fibrotic scarring occurs if the secretion of these proteins is left unchecked and the matrix overcomes the tissue, which can cause organ damage and in severe cases organ failure (Rockey et al., 2015; Wynn, 2008). Only a handful of reports have evaluated fibrosis in the CNS, and have largely done so in the context of spinal cord injury (SCI) (Fernández-Klett and Priller, 2014a; Kawano et al., 2012; O'Shea et al., 2017). Little is known about the presence or extent of fibrosis in the CNS in response to neuroinflammation and its role in disease recovery.

Following SCI, a scar forms that has two components: an outer glial scar made up of reactive astrocytes that surrounds the site almost immediately following injury and an inner fibrotic scar made up of ECM proteins, predominately Col1, that appears a few days post injury (Cregg et al., 2014; O'Shea et al., 2017). While the origin and role of the glial scar have been studied (Anderson et al., 2016; Faulkner et al., 2004; Yiu and He, 2006), much less is known about the fibrotic component. The fibrotic scar is significant as it seals the injury site, which has been hypothesized to limit the influx of blood cells and toxins into the brain parenchyma, but also prevents repair in the long term as axons are not able to grow past ECM proteins (Brazda and Müller, 2009; Kawano et al., 2012). Interestingly, if fibrotic scar formation is completely ablated following SCI, the lesion does not seal leaving a cavity that is not compatible with regeneration (Göritz et al., 2011). Meanwhile reducing, but not completely inhibiting, fibrotic

scar formation following SCI promotes functional recovery by enabling axon regeneration (Dias and Göritz, 2018; Hellal et al., 2011; Yoshioka et al., 2010; Zhu et al., 2015). This suggests that modulating specific aspects of fibrotic scarring may be an important therapeutic strategy to improve CNS repair.

Much less is known about the presence of fibrotic scarring in response to neuroinflammation and how this may affect tissue repair. In multiple sclerosis (MS), a neuroinflammatory disease characterized by CNS lesions with immune cell infiltration and demyelination, a number of studies have reported Col1 deposition surrounding blood vessels and an increase in fibrotic gene expression in lesions (Mohan et al., 2010; van Horssen et al., 2006; van Horssen et al., 2007; Yahn et al., 2020). In EAE, a mouse model for MS, an increase in collagen-producing cells has been reported in demyelinating lesions (Yahn et al., 2020). Following neuroinflammation, such as that which occurs in MS, this fibrotic scar may act to lessen the severity of disease by limiting immune cell infiltration or it may inhibit repair by limiting neuronal function and/or inhibiting the entry of progenitor cells into the lesions. As there are no approved treatments for MS that repair damaged tissue, understanding what factors prevent tissue repair in neuroinflammatory conditions such as MS could lead to new therapeutics.

Determining the origin and mechanisms of fibrotic scar formation could influence treatment options for any CNS disorder with fibrotic scarring. In SCI, the origin of Col1-producing fibrotic cells has been controversial. Some reports propose that a subset of pericytes are activated to give rise to Col1-expressing cells in the scar, whereas other groups have suggested these cells derive from the proliferation and migration of resident CNS fibroblasts which produce Col1 at rest (Birbrair et al., 2014; Göritz et al., 2011; Guimarães-Camboa et al.,

2017; Kelly et al., 2016; Soderblom et al., 2013). A recent single-cell sequencing paper showed that indeed these are distinct populations in health: pericytes are embedded in the basement membrane of capillaries, and fibroblasts are associated with large vessels in the parenchyma and meninges (Vanlandewijck et al., 2018). Furthermore, very little is known about the molecular mechanisms that lead to CNS fibrotic scar formation and how these mechanisms can be targeted to modulate fibrotic scar formation and enhance recovery.

Here, we show that there is extensive fibrotic scar formation following neuroinflammation which contributes to disease severity. This fibrotic scar is found in every neuroinflammatory lesion and lasts for months following lesion formation. Using lineage tracing and single-cell sequencing we demonstrate that the scar forms from the proliferation and migration of CNS fibroblasts, and that inhibiting CNS fibroblast proliferation leads to decreased fibrotic scarring and reduced disability in the chronic stages of disease. We further show that IFNγ signaling regulates the amplitude of fibrotic scar formation, identifying a potential therapeutic target to modulate levels of scar formation.

RESULTS

Neuroinflammation drives CNS fibrosis

To determine if a fibrotic scar forms following neuroinflammation, we induced EAE in Col1a1GFP mice and examined both collagen 1 (Col1) protein expression and the number and localization of Col1a1GFP-expressing cells in the spinal cord. In health, Col1 protein and Col1a1GFP+ cells were found in the meninges and associated with large parenchymal vessels (Fig 1a, S1a). In EAE, a robust Col1+ fibrotic scar was found in every lesion examined starting at 5 days post symptom onset (PSO) and remained for the duration of the experiment (60 days

PSO) (Fig 1a, S1b-d). Col1 deposition coincided with a massive increase in the number of Col1a1GFP+ cells throughout the parenchymal lesions that peaked at 10 days PSO, and maintained their numbers throughout the course of the experiment (Fig 1a,b, S1e,f). Fibrotic scar formation and expansion of Col1a1GFP+ cells were observed secondary to the initial influx of immune cells and the onset of motor symptoms (Fig 1b-d, S1b,d,), suggesting that fibrosis is likely a response to, and not causal of, neuroinflammation and symptom initiation.

We further immunostained fibrotic spinal cords with a series of cellular markers to determine which colocalize with the Cola1GFP+ fibrotic cells. Col1a1GFP+ cells were immune-reactive for both PDGFRα and PDGFRβ which together commonly mark fibroblasts in peripheral organs. The Col1a1GFP+ cells did not stain positive for markers of astrocytes (Sox9, GFAP), microglia/macrophages (Iba1, CD11b) or mural cells (Ng2, Desmin) (Fig 1e). Additionally, while Col1a1GFP+ cells increased significantly during disease, there was not a comparable increase in Desmin + cells in the lesions over time (Fig 1c,d). Staining for Olig2, a marker for oligodendrocyte lineage cells, demonstrated that these cells were outside the Col1-stained region, suggesting that this scar may be blocking oligodendrocyte lineage cells from entering the lesion site and repairing demyelinated axons (Fig 1e). In contrast to the clear lamination of the fibrotic and glial scars that occurs following SCI[9], we observed intermixing of GFAP+ reactive astrocyte processes and Col1a1GFP+ fibrotic cells (Fig S1c). These results demonstrate that a robust Col1+ fibrotic scar forms in response to neuroinflammation, and the Col1-secreting cells increase in the lesion over time and are immunoreactive for both PDGFRα and PDGFRβ.

To determine the relative contributions of inflammation and demyelination to fibrotic scarring, we inhibited inflammation in EAE using fingolimod, or FTY720, which prevents

immune cell exit from lymph nodes and is used as a treatment for MS in human patients (Aktas et al., 2010; Chun and Hartung, 2010). Mice administered saline following EAE had robust demyelination, motor symptoms, fibrotic scarring and Col1a1GFP+ cell expansion, whereas mice administered FTY720 did not experience motor symptoms or demyelination and had no discernable fibrotic scar or increase in scar-forming cells (Fig 1f-h). Thus inhibition of neuroinflammation in the EAE model reduced both demyelination and fibrotic scarring. To further delineate the roles of inflammation and demyelination we looked for fibrotic scarring in mice with the cuprizone and lysolecithin (LPC) models of demyelination. Through immunostaining for collagen 1 protein and infiltrating immune cells, we found that mice administered cuprizone, which does not lead to widespread CNS inflammation, did not have fibrotic scarring in the areas of demyelination, while mice administered LPC, which does lead to immune cell entry into demyelinated areas, did have a fibrotic scar (Fig S2). Together, these experiments suggest that fibrotic scarring results from neuroinflammation driven demyelination.

CNS fibroblasts form the fibrotic scar in neuroinflammation

Conflicting studies have reported that CNS fibrotic scar formation is derived from either the expansion of Col1-expressing CNS fibroblasts or pericytes turning on the expression of collagen. Single-cell sequencing of vascular cells in the CNS has demonstrated that there are indeed distinct populations of pericytes (along capillaries and post-capillary venules) and fibroblasts (associated primarily with large vessels), however, it is likely that these cells have been confused for each other in the literature as both cell types express PDGFRβ (Vanlandewijck et al., 2018).

To determine the identity of the scar forming cells we performed lineage tracing experiments with the Rosa-lsl-tdTomato reporter mouse line mated to tamoxifen-inducible cre transgenic lines: NG2CreER^{TM} to label mural cells (pericytes and vascular smooth muscle cells [vSMCs]) and oligodendrocyte precursor cells, SMACreER^{T2} to label vSMCs and Col1a2CreER^{T} to label cells that express Col1 at rest. We injected mice from each strain with tamoxifen at 6 weeks of age to induce expression of tdTomato within the specific cell population and induced EAE at 12 weeks of age. We collected spinal cords at 10 days PSO to assess the presence of any cells that were downstream of the genetically labeled NG2, aSMA, or Col1a2 cells within the Col1+ fibrotic scar. We observed a 70-fold increase in the number of Col1a2CreER^{T} labeled cells in the injury site that colocalized with the Col1+ fibrotic scar, without a similar increase in the NG2CreER^{TM} or aSMACreER^{T2} traced cells (Fig 2a-d). We then bred the Col1a2CreER^{T} reporter mice with the Col1a1GFP mice and found that over 90% of GFP+ cells were also tdTomato positive in health and over 80% in EAE (Figure S3c,d). This demonstrates that the vast majority of fibrotic scar-forming cells arose from the expansion of cells that expressed Col1 at rest, and not mural cells turning on Col1 expression.

To determine whether the CNS fibrotic cells derive from the bone marrow, we transplanted wild type mice with bone marrow from either Col1GFP or UBC-GFP (pan-cellular ubiquitous expression of GFP) mice. Recipients of UBC-GFP bone marrow displayed massive infiltration of GFP+ cells into fibrotic EAE lesions. Col1GFP bone marrow recipients displayed a robust Col1+ fibrotic scar, but had no Col1GFP+ cells in these lesions. These results indicate that Col1 expressing fibrotic cells were derived from the host, and not bone marrow derived fibrocytes or immune cells that migrated into EAE lesions (Fig 2e).

To further evaluate the cellular identities of Col1-secreting cells in health and EAE, we performed single-cell RNA sequencing of GFP+ cells from Col1a1GFP mice in health and EAE at 5-7 days PSO. The cells clustered into 8 clusters (0-7), which could be subdivided into three major classes: Class 1 (clusters 0,2,3,4,6), Class 2 (clusters 1,5) and Class 3 (cluster 7) (Fig 3b). Cells from both health and EAE were found in each cluster, suggesting that there is not a unique cell population that turns on the expression of Col1a1 in EAE. This is consistent with the lineage tracing results which demonstrate that the fibrotic cells result from cells that express Col1 in health. Class 1 and Class 2, representing 98% of cells, were characterized as fibroblasts and Class 3 as stromal cells using SingleR, a computational method for unbiased cell type recognition of single-cell data sets using thousands of bulk RNAseq reference datasets from all organs (Fig 3a-d) (Aran et al., 2019; Philippeos et al., 2018; Xie et al., 2018). Indeed, the expression of pericyte and vSMC-specific genes were low in clusters 0-6, whereas canonical fibroblast-specific genes where highly expressed, and cluster 7 expressed a combination of pericyte and vSMC-specific genes (Fig 3e, S4e) (Vanlandewijck et al., 2018). Fine SingleR analysis revealed that Class 1 and Class 2 fibroblasts can be differentiated by the expression of MTS15 (Fig S4c) (Gray et al., 2007). Although there were Col1-GFP+ mural cells identified in cluster 7, these represented a small minority (<2%) of the collagen 1 producing cells, and this cluster displayed the lowest collagen1 expression of any of the clusters, suggesting that mural cells are not major contributors to fibrotic scar formation.

The proportions of each cell population were very similar in health versus EAE, with small increases in Class 1 clusters (0, 2, 3, 4) and decreases in Class 2 clusters (1,5) in EAE (Fig 3a-c). Proliferation analysis of the cells revealed that cells in each cluster have some proportion of cells with a transcriptional profile indicative of the S and G2/M phases of the cell cycle, with

cells in cluster 2 having the largest proportion of cells in the G2/M stage (Fig 3f,g). Cluster 0 has the most enriched expression of extracellular matrix proteins such as collagens, and cluster 3 is enriched for the transcription factors Fos, Fosb and Junb, which are expressed in activated fibroblasts and required for stretch-induced ECM production (Fig S4d) (Ramachandran et al., 2011; Xie et al., 2018). Therefore, these data indicate that there are two classes of Col1+ fibroblasts that produce the fibrotic scar which can be divided into clusters that define specific states of these cells, including activated, dividing and actively producing high levels of ECM.

Taken together these lineage tracing and single-cell sequencing studies indicate that fibrotic cells arise overwhelmingly from the expansion of CNS fibroblasts expressing Col1 in health, and not pericytes/vSMCs that turn on Col1 production or infiltrating bone marrow derived cells. These studies further identify potential fibroblast cell states specifically associated with neuroinflammatory fibrotic scar formation.

Ablation of proliferating fibroblasts reduces disease severity in EAE

To determine how fibrotic scar formation affects the progression of neuroinflammatory disease, we generated transgenic mice expressing the herpes simplex virus thymidine kinase (HTK) in Col1-expressing cells, where the administration of ganciclovir (GCV) would kill dividing fibroblasts following EAE induction (Chen et al., 2004; Voskuhl et al., 2009). Test (Col1a2CreER^{T}; lox-stop-lox-HTK [fHTK]) and littermate control (lox-stop-lox-HTK) mice were injected with tamoxifen at 6 weeks to induce HTK expression specifically in the fibroblasts of the fHTK mice, and EAE was induced at 12 weeks. GCV (25 mg/kg) was administered to all mice daily starting at day 8 post EAE induction to continually prevent fibroblast proliferation in the fHTK mice and tissue was collected 30 days post EAE induction. This resulted in a

significant ablation of the Col1+ fibrotic scar in fHTK mice with most residual Col1 expression observed around blood vessels (Fig 4a,b). Extracellular matrix proteins such as periostin and collagen 3 and the fibroblast antigen ER-TR7 were also reduced by this paradigm (Fig S5a). There was no apparent effect on immune cell infiltration or reactive gliosis (Fig 4c,j, S5a-c). Therefore, a reduction in fibroblast proliferation led to a major reduction in parenchymal fibrotic scar formation but still left some perivascular Col1.

While there was no difference in the onset of EAE motor symptoms, fHTK mice had EAE scores around 0.5 points lower than littermate controls at the chronic stages of disease (Fig 4d). While numerically small, a scoring difference of 0.5 at this point in the EAE curve represents the difference between mice with the use of both back paws and mice that have at least one hind limb paralyzed. Thus, a reduction in the fibrotic scar led to a significant reduction in the deterioration of motor ability. Additionally, fHTK mice had more Olig2+ cells per lesion area than controls although there were no differences in total myelin areas between groups (Fig 4f-i). To further characterize the identity of the Olig2+ cells, we co-labeled these cells for the mature oligodendrocyte marker CC1. We found no difference between the percentages of Olig2+ CC1+ cells between groups, suggesting that the increase in Olig2+ cells in lesions of fHTK mice were not specific to a particular stage in the oligodendrocyte lineage (Fig S5d).

To understand how fibrosis, and specifically depositions of collagen 1, would decrease Olig2+ cell entry into lesions, we performed *in vitro* experiments with primary, cultured OPCs to determine how collagen 1 affects OPC proliferation, differentiation, and migration. For these experiments we examined primary OPCs seeded in cell culture wells treated with poly-L-lysine (PLL) alone, PLL + collagen 1, PLL + fibronectin, and PLL + laminin in order to compare the effects of collagen 1 to those of other extracellular matrix proteins of the basement membrane.

We found that collagen 1 did not have an effect on cell proliferation or differentiation but significantly decreased OPC migration across a transwell insert (Fig S6). Interestingly, the basement membrane matrix proteins fibronectin and laminin both significantly increased migration, which corresponds to the fact that OPCs migrate along CNS vessels during development (Tsai et al., 2016).

These results suggest that fibrosis impairs recovery in EAE and may limit the ability of myelin-forming oligodendrocyte linage cells to migrate into the lesions. However, ablation of proliferative fibroblasts alone does not promote axonal remyelination or full symptomatic recovery in EAE. We found a profound loss of neurofilament positive axons within lesions in both control in fHTK mice, suggesting that although more oligodendrocyte lineage cells were able to enter the lesion, there was a lack of axons to myelinate (Fig S5e). This was further demonstrated by electron microscopy images where both control and fHTK mice had significantly less myelinated axons than healthy, wild type mice (Fig 4j,k). Therefore, combining anti-fibrotic approaches with therapeutics to maintain axon integrity might prove synergistic in the treatment of diseases such as MS.

Fibrotic scar formation in neuroinflammation is due in part to interferon gamma signaling

To gain deeper insight into the molecular mechanisms of neuroinflammatory fibrosis, we performed bulk RNA sequencing on Col1a1GFP+ cells sorted from spinal cords of healthy mice, mice with EAE (5 and 10 days PSO), and whole spinal cord homogenate. Col1a1, Col1a2 and Col3a1 were some of the most highly enriched genes in both the healthy and EAE GFP+ cells compared to the whole spinal cord, and their expression continued to increase throughout the course of EAE (Fig S7). When comparing CNS fibroblasts in health and EAE, there were more

significant differentially expressed genes 5 days PSO (2516 upregulated, 2278 downregulated) than 10 days PSO (1414 upregulated, 1122 downregulated). Many of the genes highly upregulated at 5 days PSO are involved in inflammatory signaling, (Fig 5a, S7) and their expression largely peaked at 5 days PSO and moderately decreased by 10 days PSO (Fig 5a). A smaller subset of genes was increased at 5 days PSO and continued to increase at 10 days PSO, and included many genes encoding collagen subunits (Fig S7). These data suggest that CNS fibroblasts turn on inflammatory signaling pathways early in disease progression when there is the most fibroblast proliferation and continue depositing extracellular matrix once their expansion is complete (Fig S7).

Pathway analysis identified IFNγ signaling is enriched in EAE fibroblasts compared to the whole spinal cord (Fig S7). We found that CNS fibroblasts express IFNγ receptors (Ifngr1, Ifngr2) and downstream signaling molecules (Jak1, Jak2, Stat1, Stat5a, Stat5b) in both health and EAE, and upregulate IFNγ target genes CXCL9 and CXCL10 following EAE (Fig 5b)(Rawlings et al., 2004; Saha et al., 2010; Schroder et al., 2004). In the single-cell sequencing dataset, interferon gamma pathway genes were expressed throughout each of the different clusters (Fig 5d). Interferon gamma target genes Cxcl9 and Cxcl10 were expressed mainly in cluster 2, which is the cluster with the highest proportion of actively dividing cells, suggesting that this interferon gamma signaling may regulate fibroblast proliferation. Taken together these data reveal that CNS fibroblasts express the machinery to respond to IFNγ signaling, but this signaling cascade is only induced following EAE. To determine which cells in the EAE lesion are secreting IFNγ, we performed single-cell sequencing on whole spinal cords from EAE mice. IFNγ was highly expressed in a cluster of cells that were identified as T-cells (Fig 5e). These data suggest that during EAE, T-cells secreted IFNγ signals to CNS fibroblasts.

The role of IFNγ signaling in fibrosis in peripheral tissues has been debated (Chen et al., 2001; Kim et al., 2005; King et al., 2009; Oldroyd et al., 1999; Poosti et al., 2015; Wang et al., 2015). To determine whether IFNγ signaling in fibroblasts is necessary for CNS fibrotic scar formation, we selectively deleted *Ifngr1* from fibroblasts prior to EAE induction. Mice with fibroblast-specific Ifngr1 deletion ($Infgr1^{f/f}$;$Col1a2CreER^{T}$ [fIFNγ]) and littermate controls ($Infgr1^{f/f}$) were injected with tamoxifen at 6 weeks of age, induced with EAE at 12 weeks of age, collected 30 days post EAE induction, and analyzed for the extent of fibrotic scar formation. fIFNγ mice had a significant reduction in fibrotic scar formation (Fig 6a,b), although not to the extent of the reduction in the cell ablation paradigm. There were no differences in motor disability, lesion size, or myelination between groups (Fig 6c-f). To determine if interferon gamma is sufficient for scar formation, we analyzed tissue from mice administered cuprizone for 5 weeks with astrocyte-specific overexpression of interferon gamma (Lin et al., 2006). We found no fibrotic scar in the areas of demyelination, suggesting that an induction of interferon gamma is not sufficient for scar formation (Fig S2b). Together, these experiments confirm that interferon gamma signaling in CNS fibroblasts regulates the amplitude of fibrotic scarring, but on its own is not sufficient to initiate fibrotic scarring. Therefore, IFNγ signaling may provide a molecular target to modulate the amount of fibrotic scarring following neuroinflammation in combination with other treatments.

DISCUSSION

In this study we demonstrate that a dense Col1+ fibrotic scar forms following neuroinflammation and plays a role in regulating disease severity. This study, combined with the identification of fibrotic scarring following SCI, suggests that there is a robust fibrotic response to both injury and inflammation in the CNS, and that activation and proliferation of CNS

fibroblasts may be a common response across many different neurological disorders. This has wide implications for our understanding of the pathophysiology and repair of a wide array of neurological diseases, and a more thorough analysis of the fibrotic response needs to be characterized in different human neurological and neurodegenerative diseases and mouse models.

Using lineage tracing and single-cell sequencing, we illustrate that this fibrotic scar derives overwhelmingly from the proliferation and migration of CNS fibroblasts found in the meninges and surrounding large blood vessels in health. This is in contrast to previous studies reporting that a subtype of pericytes form the fibrotic scar following SCI[16,17]. This inconsistency is likely due to the expression of PDGFRβ and similar perivascular localization of both of these cell types, leading to a mischaracterization of the identity of the scar-forming cells as pericytes. The proportion of this scar that comes from the CNS fibroblasts in the meninges vs. those surrounding large blood vessels remains unknown, but we hypothesize that both cell types play a role in scar formation. Techniques such as *in vivo*, two-photon imaging could be used to further delineate the roles of CNS fibroblasts from different regions.

Interestingly, when we ablated proliferating fibroblasts, although the fibrotic scar was greatly diminished, there was still Col1 deposition largely restricted to the area around blood vessels. This remaining Col1 deposition may derive from the incomplete recombination of the Col1a2CreER^{T} used in the ablation paradigm, scar tissue deposition by CNS fibroblasts that aren't actively proliferating, and/or scar deposition by vascular cells such as endothelial cells, pericytes or VSMCs. A recent study found that in EAE, endothelial cells take up myelin debris which leads to an endothelial-mesenchymal transition and an upregulation in the expression of extracellular matrix proteins (Zhou et al., 2019). While we did not find Col1a1GFP reporter

expression in CNS endothelial cells, it is possible that CNS endothelial cells express Col1 protein without turning on the Col1a1GFP promoter, thus leading to perivascular Col1 accumulation. Interestingly, we found a small proportion of mural cells secrete Col1 suggesting that these cells may regulate the perivascular Col1 deposition.

Fibrotic scarring could influence the course of neuroinflammatory disease by restricting immune cell entry to inflammatory lesions thus lessening disease severity, or by preventing tissue repair and regeneration. We found that reducing fibrotic scar formation by preventing CNS fibroblast proliferation decreases motor disability and increases the number of oligodendrocyte lineage cells in the lesion in the chronic stages of disease without affecting immune cell entry or myelination. Additionally, collagen proteins inhibit OPC migration *in vitro*. This suggests that fibrotic scarring limits the ability of cells with repair potential (oligodendrocyte lineage cells) from entering the demyelinating lesion, however, these cells are still not capable of remyelination. This lack of remyelination may stem from either the presence of oligodendrocyte precursor differentiation inhibition cues, or from axon degeneration that occurs in the EAE model. Indeed, we found robust axon degeneration in this EAE model (Fig 4j,k, S5c). Therefore, combining therapeutics that inhibit scar formation with those that preserve axon integrity may synergize to enhance repair following neuroinflammation. As there are no changes in myelination after reducing fibrotic scarring, it is not completely clear how reducing the fibrotic scar decreases the EAE score in the chronic stages of disease.

This study also implicates interferon gamma signaling in CNS fibrotic scar formation, unveiling a new molecular mechanism that could be of interest for CNS disorders with scar tissue deposition. As *Ifngr1* deletion from CNS fibroblasts did not completely ablate the fibrotic scar in neuroinflammatory lesions, other pathways are also likely involved in fibrotic scar

formation. Additionally, interferon gamma is mainly secreted by adaptive immune cells, and thus this signal may be utilized to amplify fibrotic scar formation when adaptive immunity is involved in neuroinflammatory lesion formation. Pathways involved in fibrosis in peripheral tissues such as the TGFβ pathway and Wnt pathway could also be playing a role in CNS fibrosis following a variety of triggers (Burgy and Königshoff, 2018; Wynn, 2008). Our RNA sequencing dataset of CNS fibroblasts in health and EAE will be widely useful to understand other drivers of CNS scar formation. This data, along with the discovery of the origin of the scar, could influence treatment options for SCI, stroke and other neurological injuries and inflammatory diseases with fibrotic scarring.

FIGURES

Figure 2.1: Fibrotic scar formation occurs in EAE lesions.
a. Spinal cord sections from Col1a1GFP mice in health or with EAE were stained for collagen I (red) to label the fibrotic scar, DAPI to label nuclei (blue) and visualized for the GFP reporter (green). Left: whole spinal cord cross sections (top) with specific area magnified (bottom) for Col1a1GFP mice in health or 30 days EAE post symptom onset (PSO). Right: Magnified spinal cord cross section areas from Col1a1GFP mice 5, 10 or 60 days PSO. b. Quantification of the number of Col1a1GFP+ cells per lesion (bar graph) was compared with EAE motor symptoms (line graph) over the course of EAE, (± s.e.m; n=3–6 per time point for cell quantification, 4-11 for EAE score). c. Spinal cord sections from Col1a1GFP mice were stained with desmin, CD4 or CD8 (red) over the course of EAE, which is quantified in (d), n= 3-4 per condition. e. Spinal cords from Col1a1GFP mice with EAE at 10 or 30 days PSO were stained with DAPI (blue) and molecular markers for various cell types (red). GFP+ cells are immune-reactive for both PDGFRα and PDGFRβ, but not for markers of astrocytes (Sox9), microglia/macrophages (Iba1), oligodendrocyte lineage cells (Olig2) or mural cells (Ng2). f. Col1a1GFP mice with EAE were treated with either saline or 2 mg/kg FTY720 and collected 8-10 days PSO. The collagen area and number of cells per area is quantified in g, h, n = 3 per condition, $^{**}p < 0.01$, $^{***}p < 0.001$. Scale bars = 100 μm.

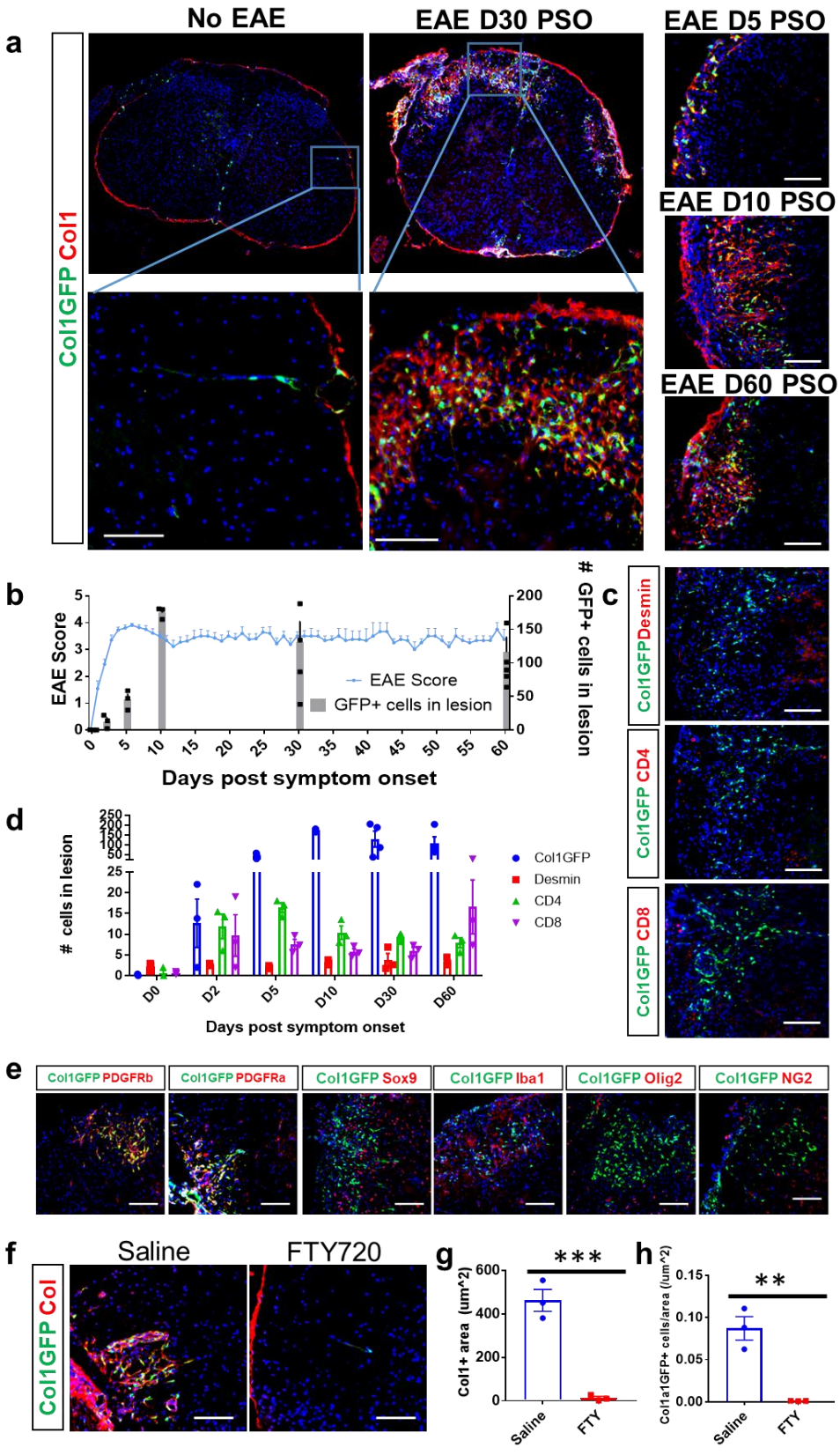
a
No EAE
EAE D30 PSO
EAE D5 PSO
EAE D10 PSO
EAE D60 PSO
Col1GFP Col1
b
EAE Score
GFP+ cells in lesion
EAE Score
GFP+ cells in lesion
Days post symptom onset
c
Col1GFP Desmin
Col1GFP CD4
Col1GFP CD8
d
cells in lesion
Col1GFP
Desmin
CD4
CD8
D0
D2
D5
D10
D30
D60
Days post symptom onset
e
Col1GFP PDGFRb
Col1GFP PDGFRa
Col1GFP Sox9
Col1GFP Iba1
Col1GFP Olig2
Col1GFP NG2
f
Saline
FTY720
Col1GFP Col
g
***
Col1+ area (um^2)
Saline
FTY
h
**
Col1a1GFP+ cells/area (/um^2)
Saline
FTY

Figure 2.2: Scar-forming cells arise from CNS fibroblast expansion.
a-d. Sections from spinal cords of Col1a2CreER^{T};Rosa-tdTomato (a), NG2CreER^{TM};Rosa-tdTomato (b), or aSMACreER^{T2};Rosa-tdTomato (c) mice with EAE were stained for Col1 (green) and DAPI (blue) and visualized for tdTomato reporter (red). d. The number of reporter cells in EAE lesions was normalized to the number of reporter cells in white matter in health (n=7 health, 9 EAE for Col1a2CreER^{T}, n=7 health, 8 EAE for NG2CreER^{TM}, n=4 health, 7 EAE for aSmaCreER^{T2}, $p<0.0001$ using a one way ANOVA with multiple comparisons, $p<0.0001$ for Col1a2CreER^{T} vs. NG2CreER^{TM}, $p=0.0001$ for Col1a2CreER^{T} vs. aSMACreER^{T2} and $p>0.9999$ for NG2CreER^{TM} vs aSMACreER^{T2}). e. Spinal cord sections from mice with Col1a1GFP donor bone marrow (left) or UBC-GFP donor bone marrow (right) with EAE at 10 days PSO were stained with Col1 (green), and the GFP was visualized in red (n=8 for Col1a1GFP, n=5 for UBC-GFP). All scale bars = 100 μm.

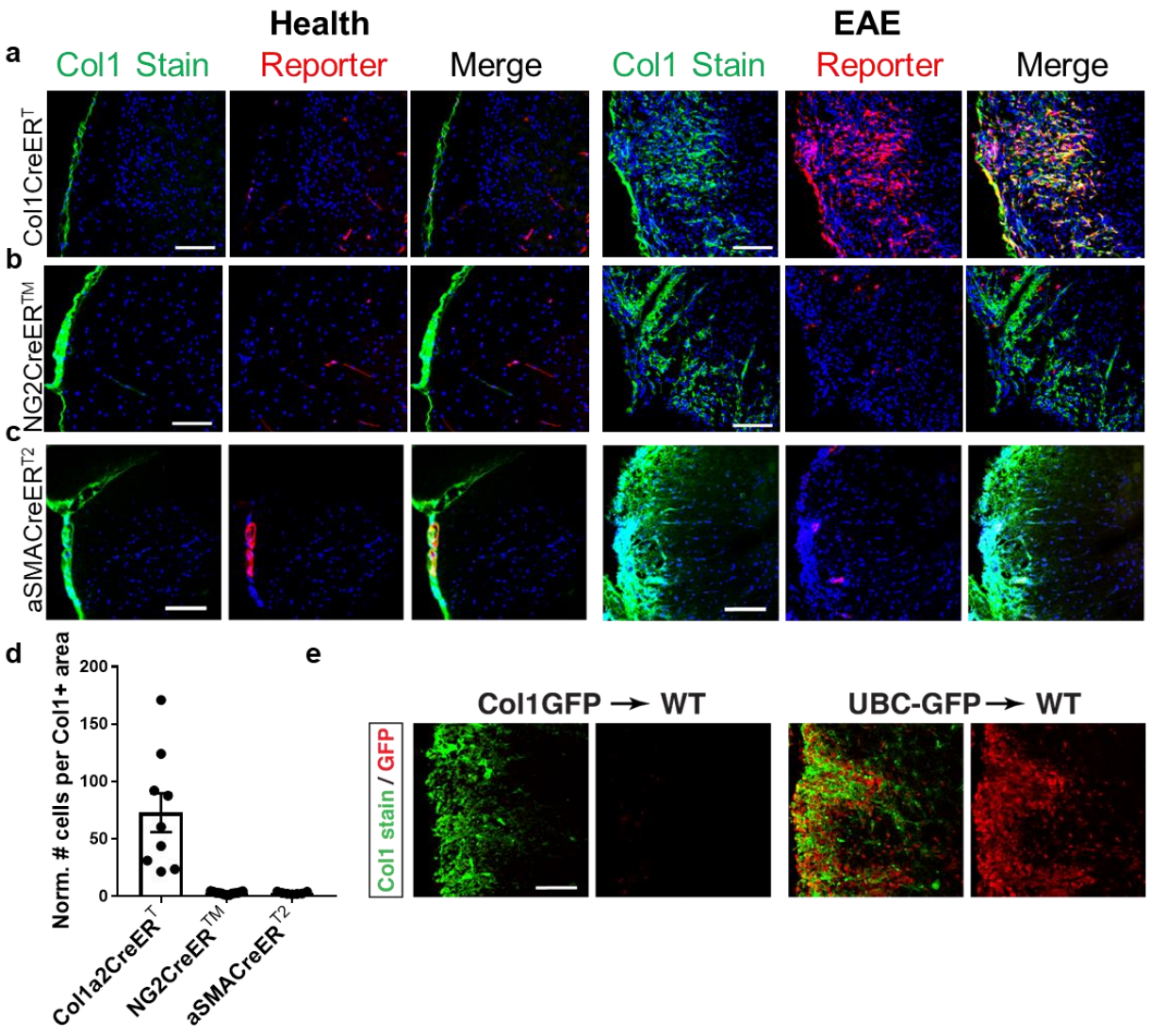
Health
EAE
a
Col1 Stain
Reporter
Merge
Col1 Stain
Reporter
Merge
Col1CreER^T
b
NG2CreER^TM
c
aSMACreER^T2
d
Norm. # cells per Col1+ area
200
150
100
50
0
Col1a2CreER^T
NG2CreER^TM
aSMACreER^T2
e
Col1GFP → WT
UBC-GFP → WT
Col1 stain / GFP

Figure 2.3: Scar-forming cells have the transcriptional profile of fibroblasts at the single cell level. a-d. Col1a1GFP+ cells from spinal cords of healthy mice (n=3 samples with 2-3 spinal cords each) and mice with EAE 5-7 days PSO (n=2 samples, 2 spinal cords each) were transcriptionally profiled at the single cell level and clustered using Seurat v3. a. UMAP plot with the sample identity (Health vs. EAE) labeled for each cell. b. UMAP plot of the clustering analysis reveals 8 clusters that could be subdivided into three classes: Class 1 (clusters 0,2,3,4,6), Class 2 (clusters 1,5), and Class 3 (cluster 7). c. Pie charts showing the percentage of each cluster relative to the total number of cells in health or EAE. d. UMAP plot with each cell labeled with its cellular identity determined using SingleR and the Immgen reference dataset. e. Violin plots of the expression levels of pericyte, vSMC and fibroblast- specific genes per cluster. f. UMAP plot showing the transcriptional cell cycle identity per cell. g. Bar graph showing the percentage of each cluster with the transcriptional signatures of the different steps of the cell cycle.

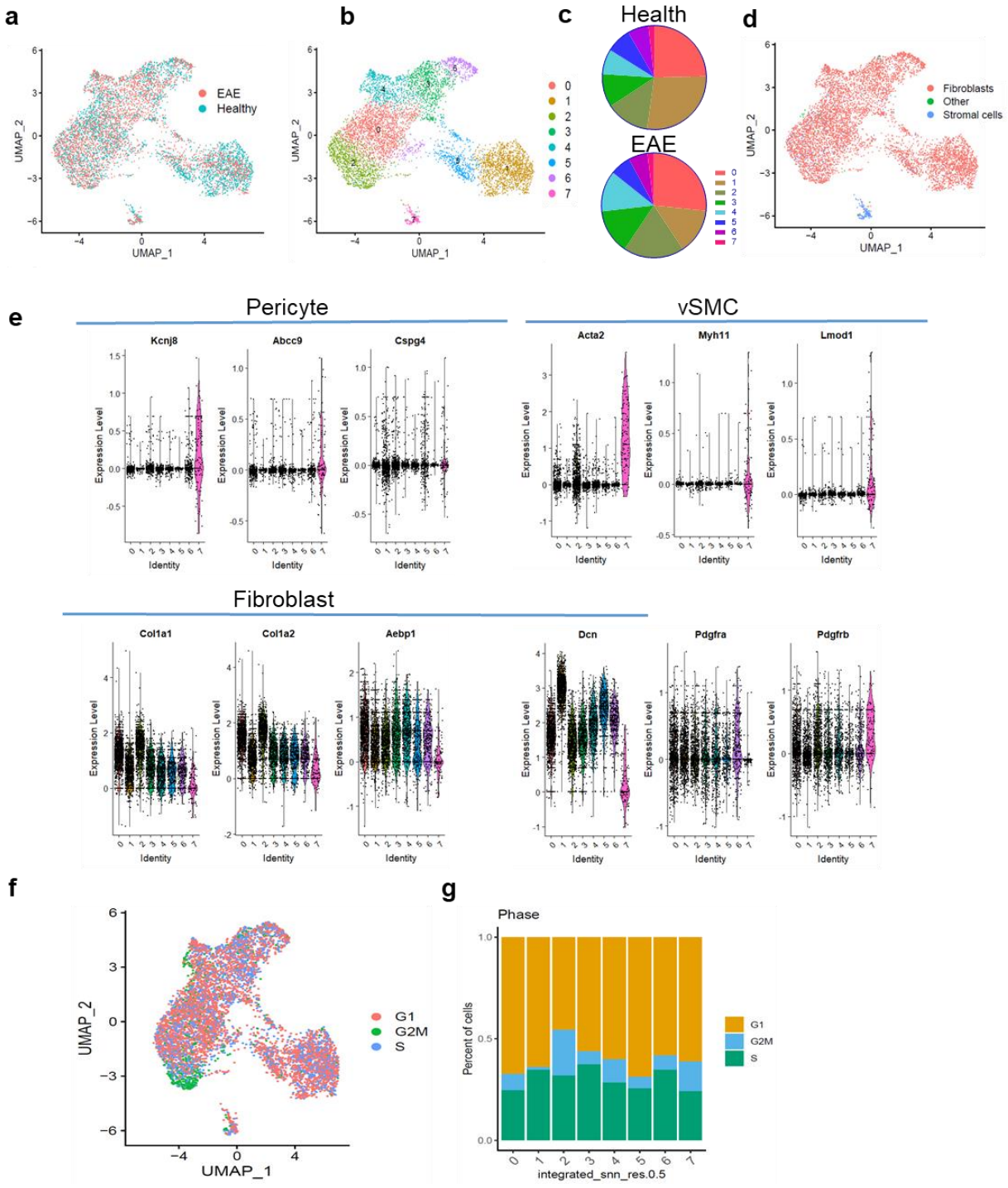
a
b
c
d
e
f
g
EAE
Healthy
UMAP_1
UMAP_2
Health
EAE
Fibroblasts
Other
Stromal cells
Pericyte
vSMC
Fibroblast
Kcnj8
Abcc9
Cspg4
Acta2
Myh11
Lmod1
Col1a1
Col1a2
Aebp1
Dcn
Pdgfra
Pdgfrb
Expression Level
Identity
G1
G2M
S
Phase
Percent of cells
integrated_snn_res.0.5

Figure 2.4: Reducing fibrotic scar formation reduces disease severity in neuroinflammation.

a. Spinal cord sections from fibroblast-specific herpes thymidine kinase (fHTK) mice and littermate controls 30 days after EAE immunization were stained for Col1 (green), DAPI (blue) and CD11b (top, red) to label immune cells or CD31 (bottom, red) to label endothelial cells. b. Quantification of the percentage of the area of immune infiltration (denoted by CD11b) that is Col1+, **p <0.01 by Student's one-tailed t-test, n=21 control, 19 fHTK. c. Quantification of the total lesion size, denoted by Cd11b staining, n = 21 control, 19 fHTK, p = 0.33 by Student's two-tailed t-test. d. EAE score for the fHTK mice and controls up to 30 days post EAE induction, **p<0.01, *p <0.05 by two-tailed Mann-Whitney test, n=22 control, 19 fHTK. e. Pie charts depicting the percentages of control and fHTK mice that were paralyzed at day 24 and day 30 post EAE induction. f. Spinal cords from control and fHTK mice were stained for Olig2 (green), CD11b (red) and DAPI (blue) with the area of the CD11b+ lesion traced with a dotted white line. g. The number of Olig2+ cells per CD11b+ lesion was quantified comparing the fHTK and control mice, *p = 0.038 by Student's one-tailed t-test. f.. Spinal cord sections from fHTK mice and controls at 30 days post EAE induction were stained for FluoroMyelin (red) and DAPI (blue) with the area of the CD11b+ lesion traced with a dotted white line. i. Quantification of the percentage of the total white matter area that is FluoroMyelin positive, p = 0.96 by Student's two-tailed t-test. j. Electron microscopy images of spinal cord sections from healthy wild type mice, fHTK mice and controls at 30 days post EAE induction. k. Quantification of the # of myelinated axons from the 3 groups per 3000x picture frame, ***p < 0.001, **p < 0.01, using a one-way ANOVA with multiple comparisons. All scale bars = 100 μm.

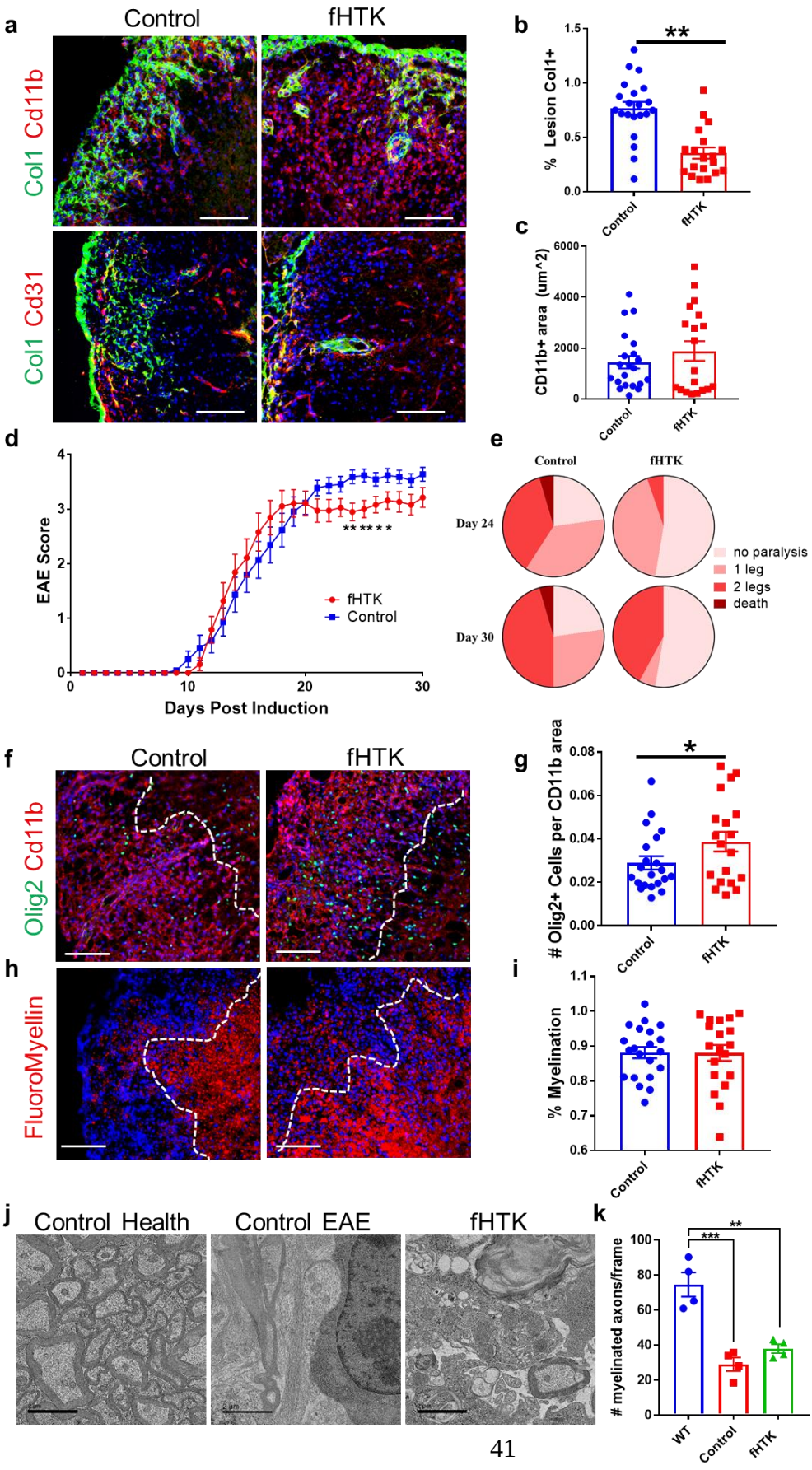
a
Control
fHTK
Col1 Cd11b
Col1 Cd31
b
% Lesion Col1+
**
Control
fHTK
c
CD11b+ area (um^2)
Control
fHTK
d
EAE Score
Days Post Induction
fHTK
Control
e
Control
fHTK
Day 24
Day 30
no paralysis
1 leg
2 legs
death
f
Control
fHTK
Olig2 Cd11b
g
Olig2+ Cells per CD11b area
*
h
FluoroMyellin
i
% Myelination
j
Control Health
Control EAE
fHTK
k
myelinated axons/frame
***
**
WT
Control
fHTK

Figure 2.5: CNS fibroblasts upregulate interferon gamma pathway genes in EAE. a. Heat map of the expression levels of the top 100 differentially expressed genes by FDR in Col1a1GFP+ cells from EAE 5 days PSO and 10 days PSO (CNS Fibro EAE D5, D10) compared to Col1a1GFP+ cells from health (CNS Fibro Health) in each of the 3 samples of these conditions. b. mRNA levels in counts per million (CPM) of interferon gamma pathway and target genes from the sequencing of whole spinal cord tissue (Whole SC) and CNS Fibro Health, CNS Fibro EAE D5 and CNS Fibro EAE D10, *FDR < 0.05, **FDR < 0.01 to Whole SC, #FDR < 0.05, ##FDR < 0.01 to CNS Fibro Health. c. Spinal cord sections from Col1a1GFP mice in health (left) and EAE (right) were stained with CXCL10 (red). d. Violin plots from the single-cell sequencing dataset depicting the total RNA counts for genes in the interferon gamma pathway. e. UMAP plot of individual cells sequenced from a whole spinal cord a of wild type mouse with EAE with their assigned cell type identity using SingleR and the Immgen reference dataset. e. Interferon gamma expression is indicated in blue, and is found predominately in T cells in EAE. All scale bars = 100 μm.

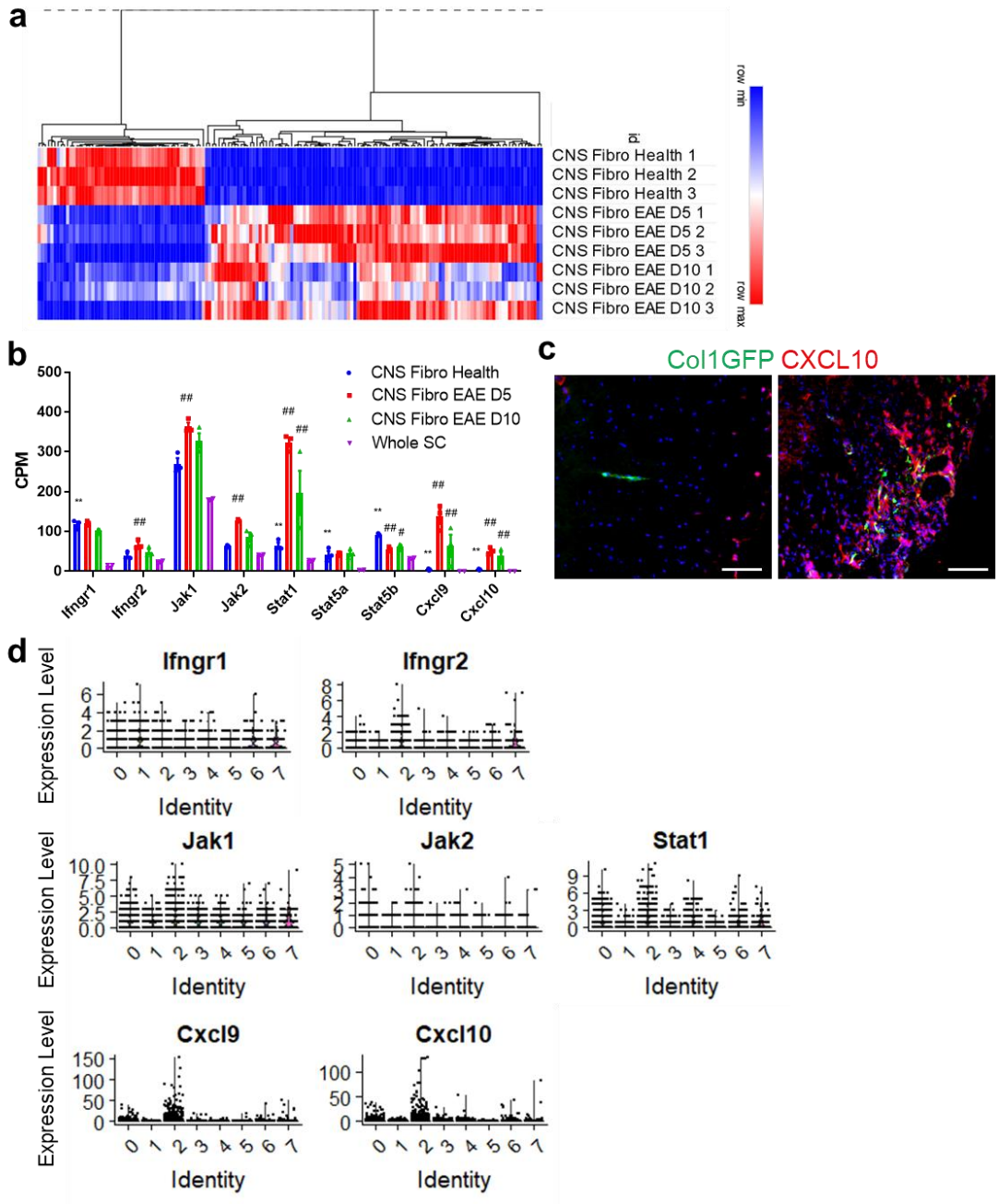
a
id
CNS Fibro Health 1
CNS Fibro Health 2
CNS Fibro Health 3
CNS Fibro EAE D5 1
CNS Fibro EAE D5 2
CNS Fibro EAE D5 3
CNS Fibro EAE D10 1
CNS Fibro EAE D10 2
CNS Fibro EAE D10 3
row min
row max
b
CPM
CNS Fibro Health
CNS Fibro EAE D5
CNS Fibro EAE D10
Whole SC
Ifngr1
Ifngr2
Jak1
Jak2
Stat1
Stat5a
Stat5b
Cxcl9
Cxcl10
c
Col1GFP CXCL10
d
Expression Level
Ifngr1
Ifngr2
Jak1
Jak2
Stat1
Cxcl9
Cxcl10
Identity
e
Whole Spinal Cord EAE
IFNg expression
B cells
Dendritic cells
Endothelial cells
Epithelial cells
Fibroblasts
Granulocytes
Macrophages
Monocytes
Neurons
NK cells
Oligodendrocytes
T cells
UMAP_1
UMAP_2

Figure 2.6: Interferon gamma signaling regulates scar formation following neuroinflammation.
a. Spinal cord sections from fibroblast-specific IFNγ knockout mice (fIFNγ, $IFN\gamma^{fl/fl}$; $Col1a2CreER^{T}$) and littermate controls ($IFN\gamma^{fl/fl}$) stained for Col1 (green), CD11b (red) or CD31 (red), and DAPI (blue). The amount of fibrotic scar covering the lesion was quantified in (b), *p <0.05 by Student's two-tailed t-test, n=14 control, 15 fIFNγ. c. EAE score for the fIFNγ mice and controls up to 30 days post EAE induction (n= 14 control, 15 fIFNγ). d. Quantification of the CD11b+ immune cell area in the control and fIFNγ groups 30 days post EAE immunization, p = 0.61 by Student's two-tailed t-test, n= 14 control, 15 fIFNγ. e. Quantification of the percentage of the total white matter area that is FluoroMyelin positive for the control and fIFNγ groups, p = 0.44 by Student's two-tailed t-test, n= 14 control, 15 fIFNγ. f. Quantification of Olig2+ cells per CD11b+ lesion area between the control and fIFNγ groups, p = 0.76 by Student's two-tailed t-test, n= 14 control, 15 fIFNγ.

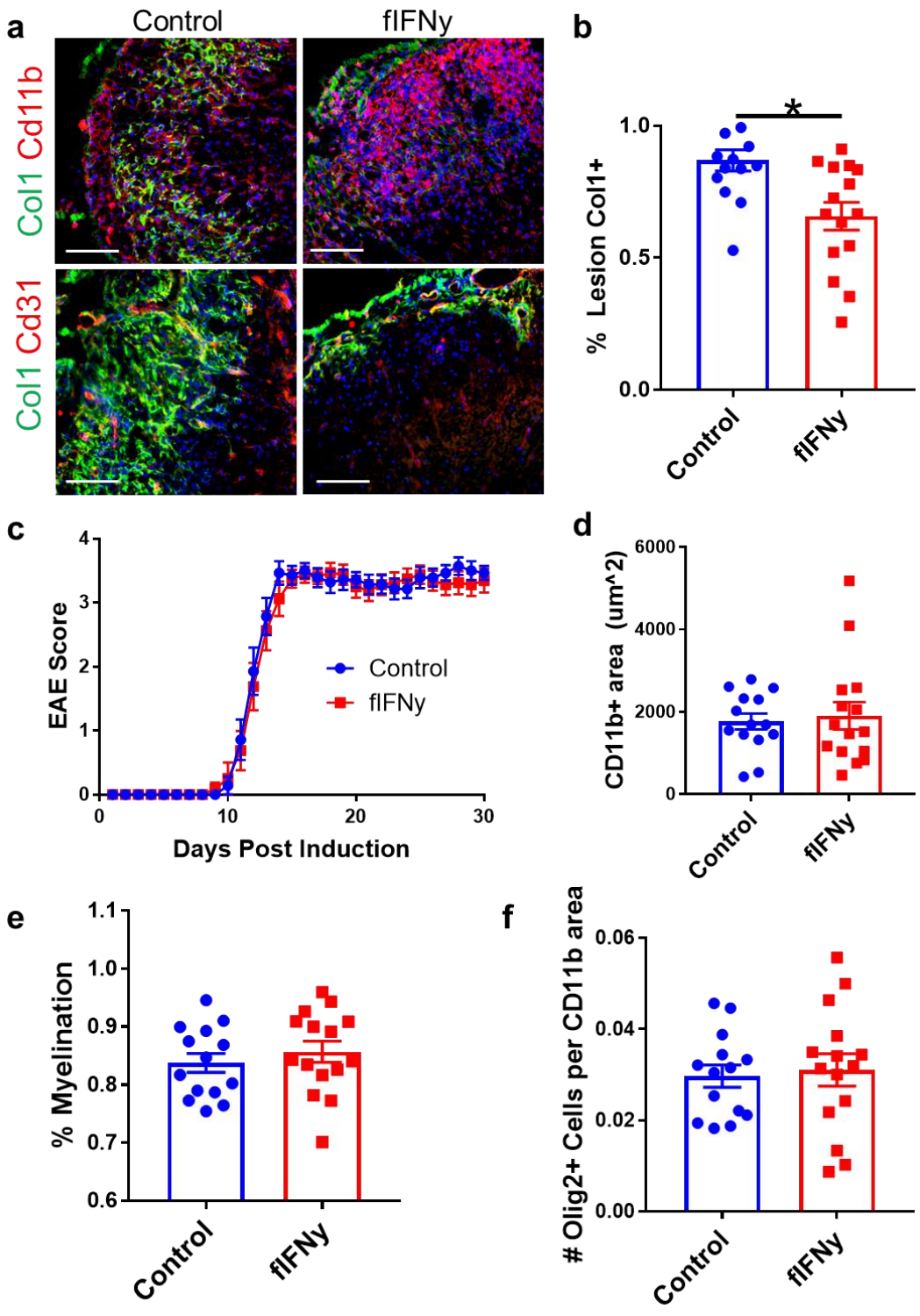
a
Control
fIFNy
Col1 Cd11b
Col1 Cd31
b
% Lesion Col1+
1.0
0.5
0.0
*
Control
fIFNy
c
EAE Score
4
3
2
1
0
0
10
20
30
Days Post Induction
Control
fIFNy
d
CD11b+ area (um^2)
6000
4000
2000
0
Control
fIFNy
e
% Myelination
1.1
1.0
0.9
0.8
0.7
0.6
Control
fIFNy
f
Olig2+ Cells per CD11b area
0.06
0.04
0.02
0.00
Control
fIFNy

Figure 2.S1: Fibrosis and CNS fibroblast characteristics in health and EAE

a. Analysis of the number of Col1a1GFP+ cells per total vascular length and smooth muscle actin (SMA)+ vascular length in different CNS regions in healthy adult mice. CP= choroid plexus, SC= spinal cord white or grey matter, n=4, Col1a1GFP mice. b-d. Spinal cord sections from wild type mice in health or with EAE at 2, 5 or 10 days PSO were stained with Col1 (red), DAPI (blue) and CD11b (b, green), GFAP (c, green), or CD4 (d, green) Scale bars = 100 µm. e. Light sheet microscopy image of a Col1a1GFP mouse in health (right) and one with EAE (left) 10 days PSO perfused with tomato lectin and optically cleared. f. Confocal microscopy images of Col1a1GFP spinal cords from health (left) and EAE (right) stained for CD31 in red, scale bars = 10 µm.

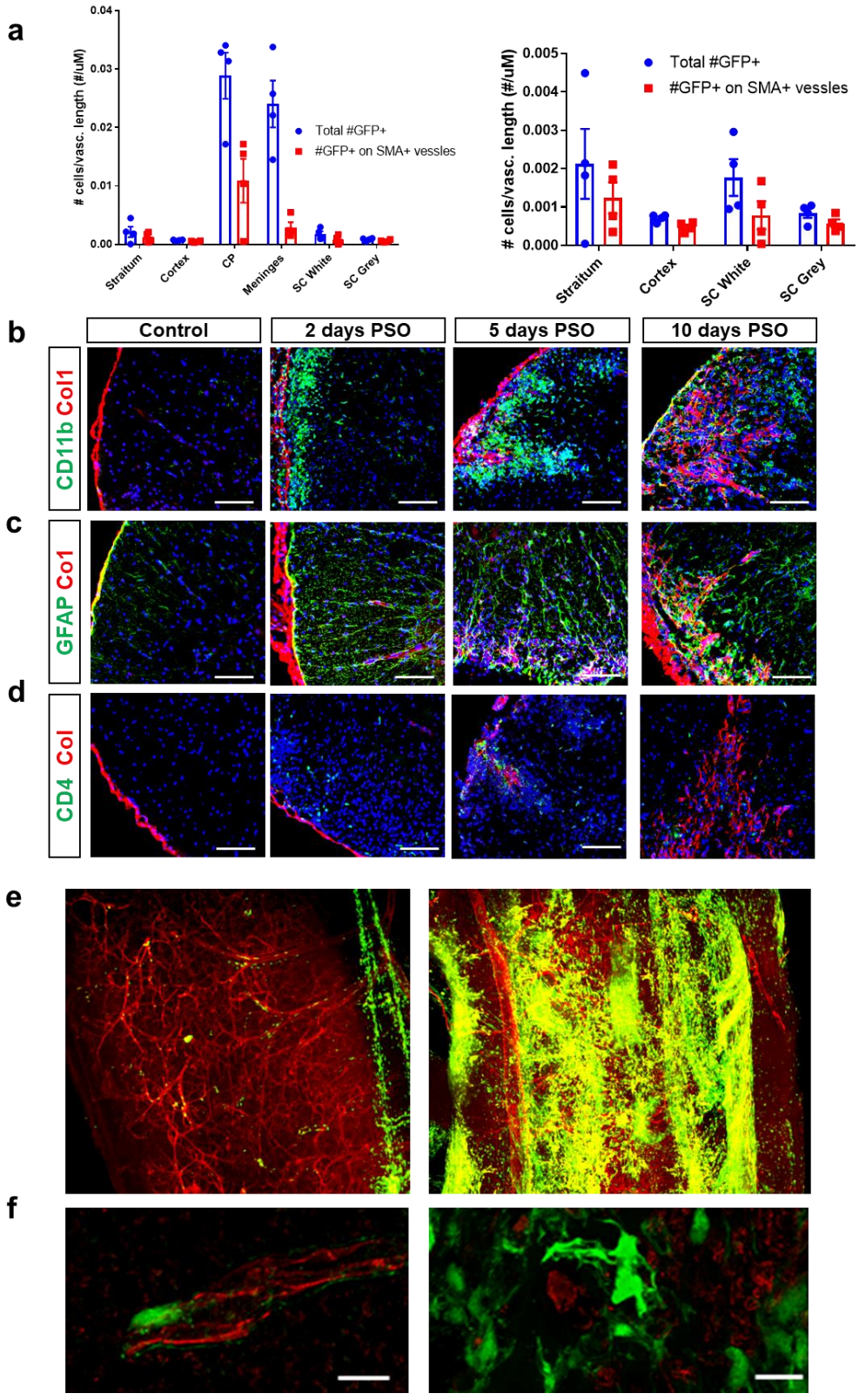
a
cells/vasc. length (#/uM)
Total #GFP+
#GFP+ on SMA+ vessles
Straitum
Cortex
CP
Meninges
SC White
SC Grey
b
Control
2 days PSO
5 days PSO
10 days PSO
CD11b Col1
c
GFAP Co1
d
CD4 Col
e
f

Figure 2.S2: Fibrosis is present in the LPC but not cuprizone models of demyelination
a. Spinal cord sections from mice either 5, 7, or 14 days post LPC injection into the spinal cord stained for either Col1 (green) and FluoroMyelin (red) or myelin basic protein (MBP) (red) and Cd11b (green). b. Brain sections in the area of the corpus callosum from mice administered cuprizone for 5 weeks and collected at the end of the 5 weeks or 3 weeks later with or without doxycycline administration stained for either Col1 (green) and FluoroMyelin (red) or myelin basic protein (MBP) (red) and Cd11b (green). Scale bar = 100 μM.

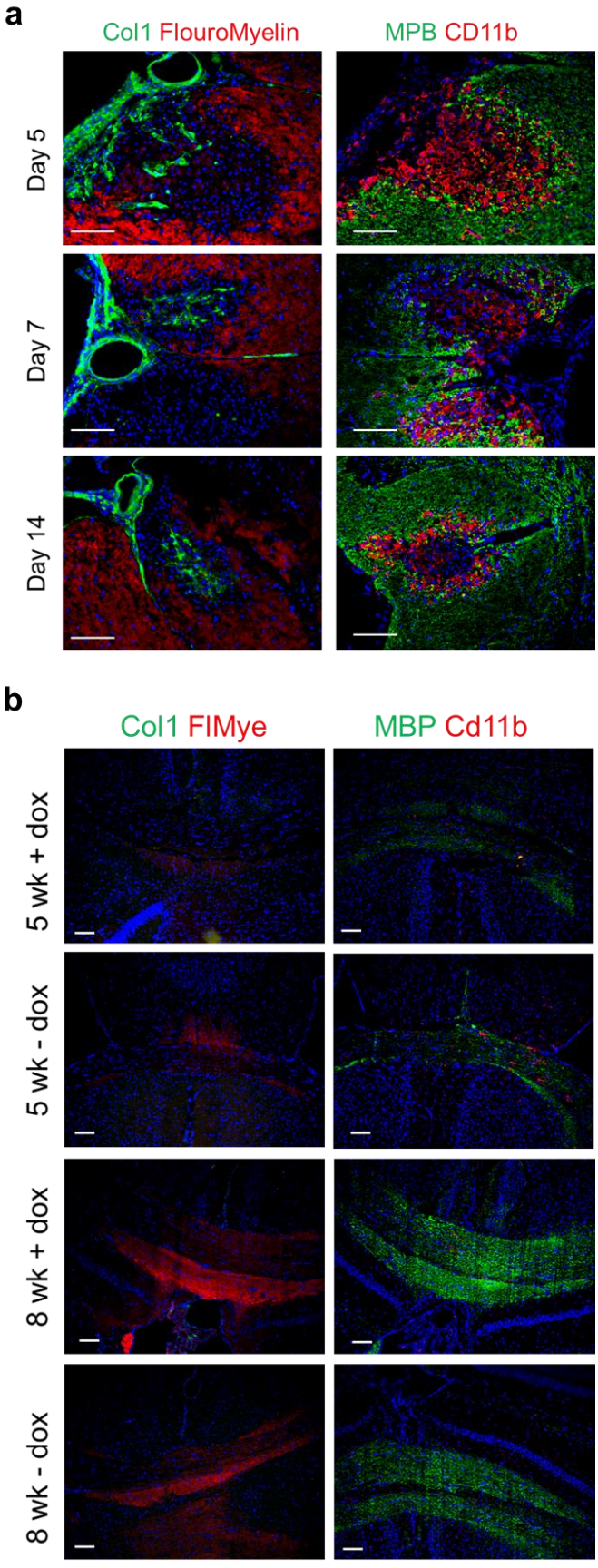
a
Col1 FlouroMyelin
MPB CD11b
Day 5
Day 7
Day 14
b
Col1 FlMye
MBP Cd11b
5 wk + dox
5 wk - dox
8 wk + dox
8 wk - dox

Figure 2.S3: Lineage tracing reporter expression
Spinal cords of Col1a2CreER^{T};Rosa-tdTomato (a) or NG2CreER^{TM};Rosa-tdTomato or NG2CreER^{TM} (b) mice in health or 10 days EAE PSO were stained with CD31 in green and DAPI in blue. Scale bars = 100 µm. c. Spinal cords of Col1a2CreER^{T};Rosa-tdTomato;Col1a1GFP mice in health or 10 days EAE PSO were imaged for both reporters. The percentage of GFP+ cells that were also positive for the tomato reporter in health and EAE is quantified in (d).

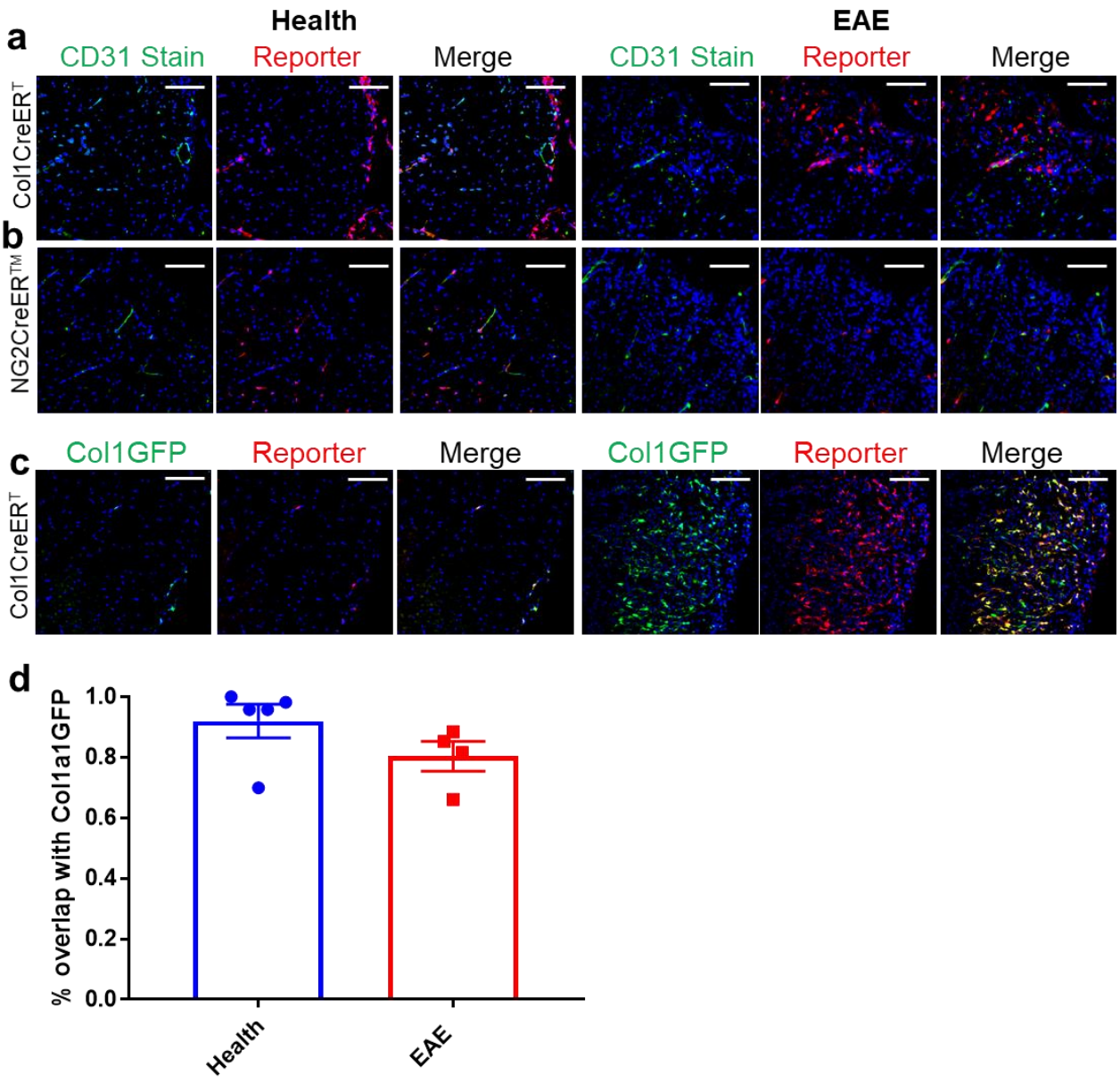
a
Health
EAE
CD31 Stain
Reporter
Merge
CD31 Stain
Reporter
Merge
Col1CreER™
b
NG2CreER™
c
Col1GFP
Reporter
Merge
Col1GFP
Reporter
Merge
Col1CreER™
d
% overlap with Col1a1GFP
1.0
0.8
0.6
0.4
0.2
0.0
Health
EAE

Figure 2.S4: Single-cell sequencing analysis of CNS fibroblasts in health and EAE

a. Sample FACS plots for the single-cell sequencing analysis. b. UMAP plot with the individual sample identity labeled for each cell. c. UMAP plot with each cell labeled with its cellular identity determined using SingleR fine analysis and the Immgen reference dataset. d. Heat map depicting the expression of the 10 most differentially expressed genes in each cluster based on the logFC of the dataset. e. Heat map depicting the expression levels of genes specific to the labeled cell types, Olig = oligodendrocyte.

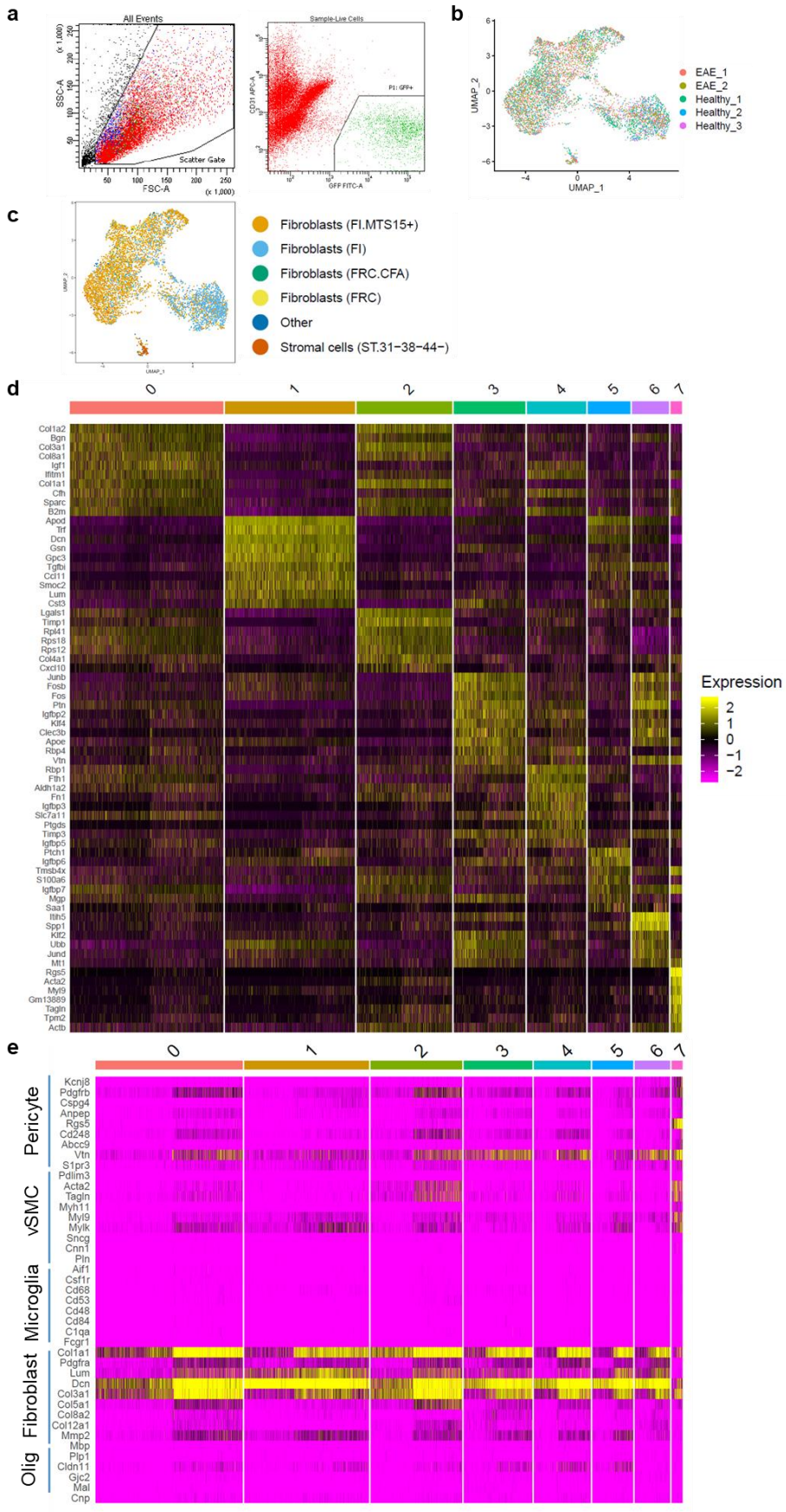
a
All Events
SSC-A
FSC-A
Scatter Gate
Sample-Live Cells
P1: GFP+
b
EAE_1
EAE_2
Healthy_1
Healthy_2
Healthy_3
UMAP_1
UMAP_2
c
Fibroblasts (Fl.MTS15+)
Fibroblasts (Fl)
Fibroblasts (FRC.CFA)
Fibroblasts (FRC)
Other
Stromal cells (ST.31−38−44−)
d
Expression
e
Pericyte
vSMC
Microglia
Fibroblast
Olig

Figure 2.S5: Tissue analysis following fibrotic scar reduction in EAE
a. Spinal cord sections from fHTK mice and controls were stained for DAPI (blue) and periostin (green), ER-TR7 (green), Col3 (green) and CD11b (red), or GFAP (green) and Cd11b (red). b. Spinal cord sections from fHTK mice and controls were stained for CD4 (red, left) and DAPI (blue) and the number of CD4+ cells per lesion area was compared between groups (right), $p = 0.38$ by Student's two-tailed t-test, n=21 control and 19 fHTK. c. Spinal cord sections from fHTK mice and controls were stained for CD8 (red, left) and DAPI (blue) and the number of CD8+ cells per lesion area was compared between groups (right), $p = 0.22$ by Student's two-tailed t-test, n=21 control and 19 fHTK. d. Spinal cord sections from fHTK mice and controls were stained for Olig2 in green and CC1 in red, and the percent of Olig2+ cells that were also CC1+ was quantified, $p = 0.26$ by Student's two-tailed t-test e. Spinal cord sections from fHTK mice and controls were stained for neurofilament heavy polypeptide (NF) in green and CD11b in red, and the number of healthy, blebbed and total axons was quantified. Scale bars = 100 μm

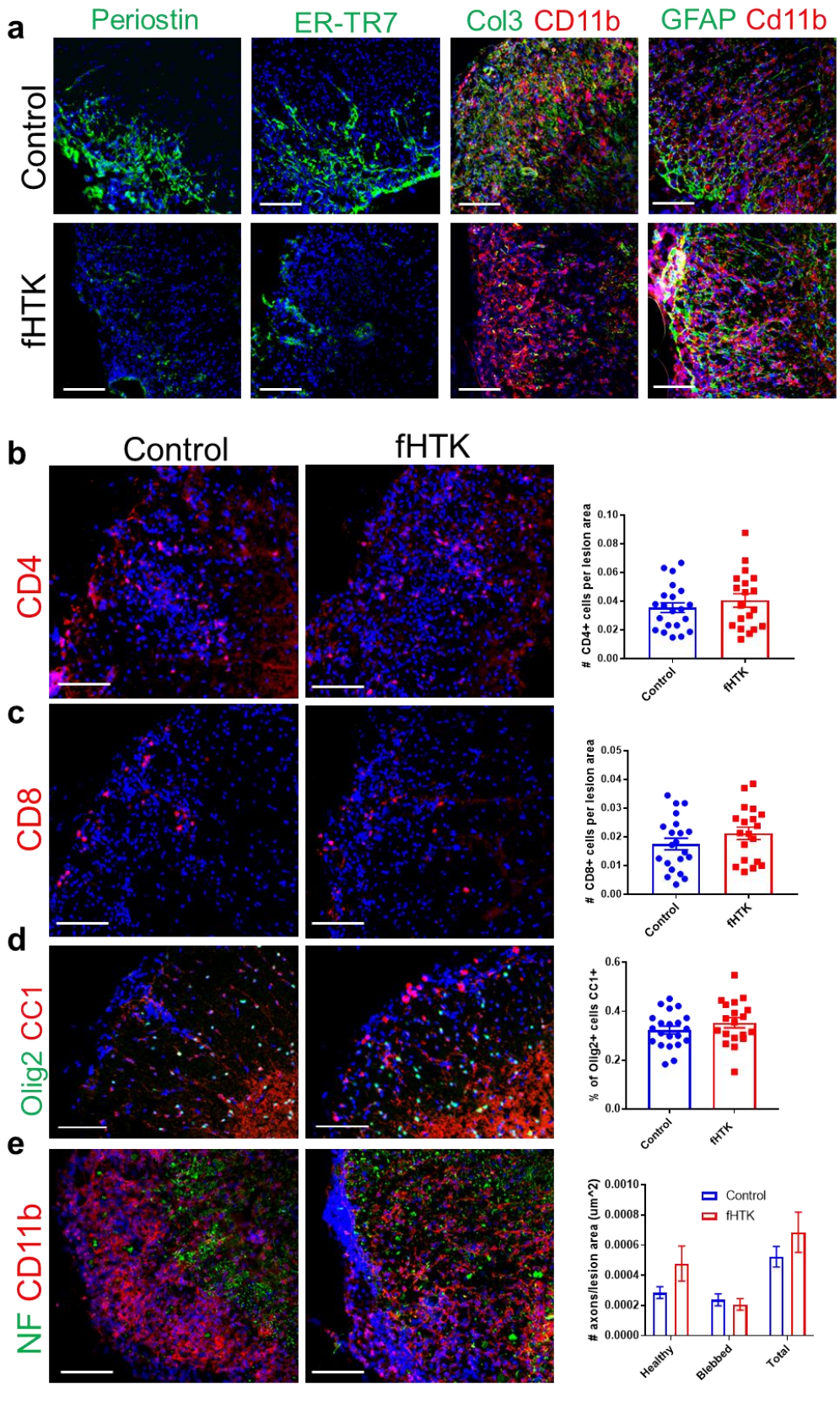
a
Periostin
ER-TR7
Col3 CD11b
GFAP Cd11b
Control
fHTK
b
Control
fHTK
CD4
CD4+ cells per lesion area
0.10
0.08
0.06
0.04
0.02
0.00
Control
fHTK
c
CD8
CD8+ cells per lesion area
0.05
0.04
0.03
0.02
0.01
0.00
Control
fHTK
d
Olig2 CC1
% of Olig2+ cells CC1+
0.6
0.4
0.2
0.0
Control
fHTK
e
NF CD11b
axons/lesion area (um^2)
0.0010
0.0008
0.0006
0.0004
0.0002
0.0000
Control
fHTK
Healthy
Blebbed
Total

Figure 2.S6: ECM proteins differentially regulate OPC properties *in vitro*
a. Representative images of Olig2 (green) and PDGFRa (red) staining with EdU labeling (cyan) in rat OPC cultures on PLL, laminin, fibronectin, or collagen I after 2 hour incubation in 10 uM EdU. b, Quantification of EdU+ cells over OPCs (Olig2+PDGFRa+) for cultures represented in a. c. Representative images of MBP (red) staining in rat OPC cultures on PLL, laminin, fibronectin, or collagen I three days after removal of PDGF-AA. Cell nuclei detected with DAPI (blue). d. Quantification of MBP+ cells over total cells (DAPI+) for cultures represented in c. e. Representative images of PDGFRa (green) staining with DAPI in rat OPC cultures that had migrated through transwells coated with PLL, laminin, fibronectin, or collagen I following a 24 hour incubation. f, Quantification of PDGFRa+ cells on the underside of each transwell for the cultures represented in e. Data displayed represent 3 biological replicates with 3 technical replicates and are presented as mean + SEM. Comparisons were performed using one-way ANOVA with Sidak's post hoc tests, ****$p<0.0001$, ***$p<0.001$, *$p<0.05$.

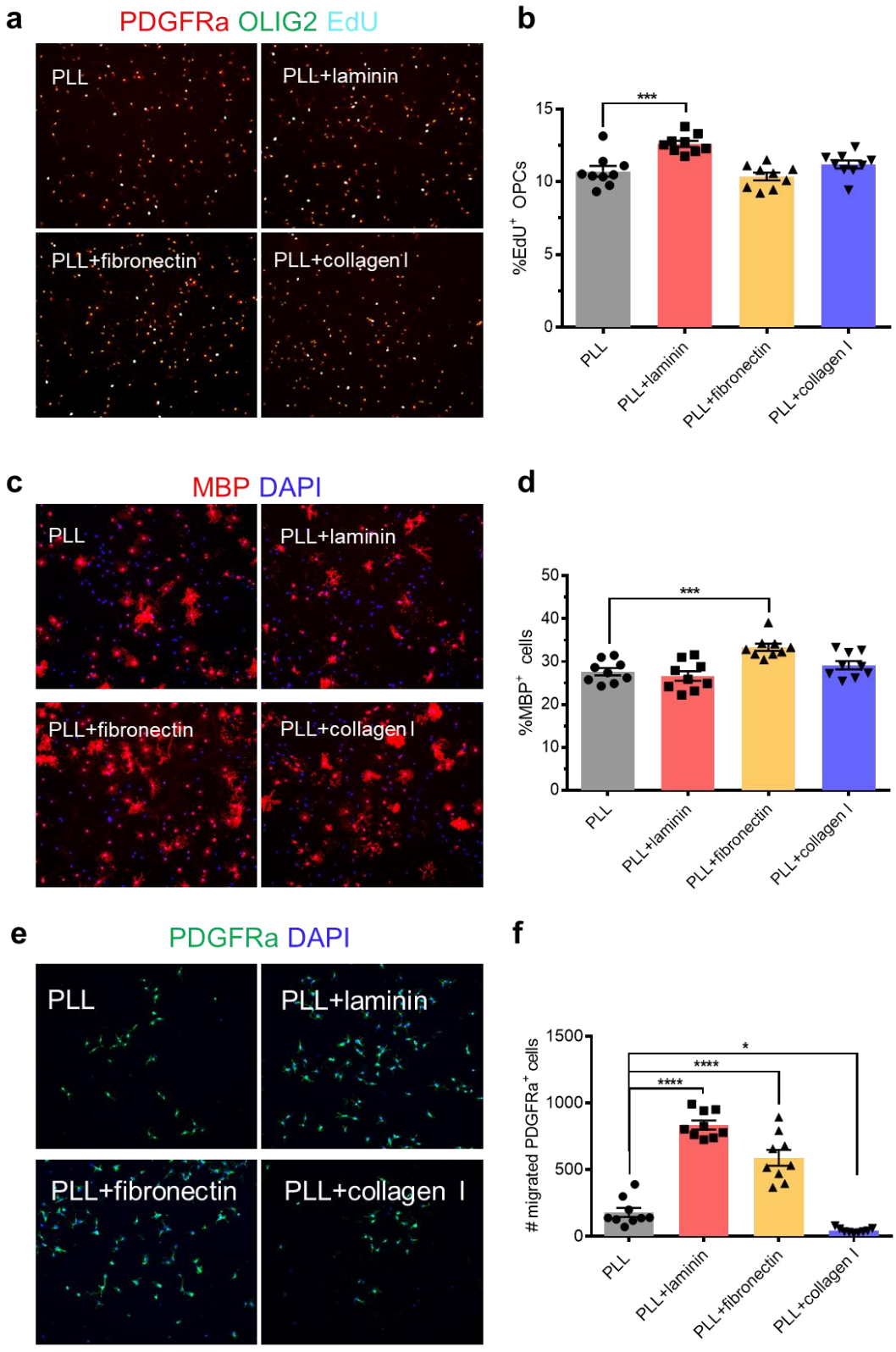
a
PDGFRa OLIG2 EdU
PLL
PLL+laminin
PLL+fibronectin
PLL+collagen I
b
%EdU+ OPCs
***
15
10
5
0
PLL
PLL+laminin
PLL+fibronectin
PLL+collagen I
c
MBP DAPI
PLL
PLL+laminin
PLL+fibronectin
PLL+collagen I
d
%MBP+ cells
***
50
40
30
20
10
0
PLL
PLL+laminin
PLL+fibronectin
PLL+collagen I
e
PDGFRa DAPI
PLL
PLL+laminin
PLL+fibronectin
PLL+collagen I
f
migrated PDGFRa+ cells
*
****
****
1500
1000
500
0
PLL
PLL+laminin
PLL+fibronectin
PLL+collagen I

Figure 2.S7: Bulk RNA sequencing analysis of CNS fibroblasts in health and EAE

a-c. MA plots comparing the transcriptome of CNS fibroblasts in health with whole spinal cord tissue (a), CNS fibroblasts in health with CNS fibroblasts EAE D5 (b) or D10 (c) PSO with red dots signifying genes with FDR < 0.1. d. Pathway analysis using DAVID Bioinformatics Resources 6.8, NIAID/NIH, GOTERM_BP_DIRECT for genes with a log2 fold change greater than 2 for CNS fibroblasts EAE D5 PSO compared to CNS fibroblasts in health. e. CPM of collagen genes from the bulk sequencing of whole spinal cord tissue (Whole SC), CNS fibroblasts from health (CNS Fibro Health) CNS fibroblasts 5 days PSO (CNS Fibro EAE D5) and 10 days PSO (CNS Fibro EAE D10), *FDR < 0.05, **FDR < 0.01 to Whole SC, #FDR < 0.05, ##FDR < 0.01 to CNS Fibro Health. f. Heat map of the expression levels of the top genes differentially expressed in CNS Fibro Health (each expressed at least 1 CPM in each control sample) compared to the whole spinal cord by FDR.

a

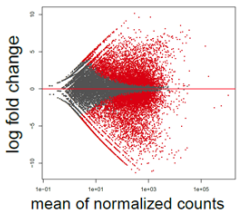

b

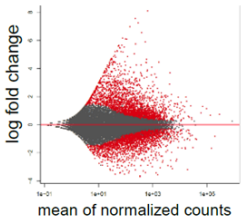

c

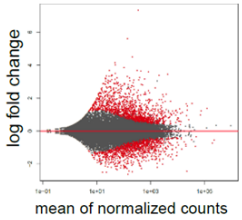

d

Pathways enriched in fibroblasts in disease

GO term	FDR
immune system process	2.09E-31
immune response	4.39E-28
inflammatory response	3.38E-19
cellular response to interferon-beta	8.05E-17
positive regulation of T cell proliferation	1.84E-15
chemotaxis	4.45E-15
adaptive immune response	2.03E-13
innate immune response	3.79E-13
response to lipopolysaccharide	7.27E-11
mitotic nuclear division	1.12E-09
cell division	4.68E-09
cell cycle	4.96E-09
positive regulation of interferon-gamma production	7.30E-09
response to virus	3.54E-08
T cell receptor signaling pathway	6.61E-08
T cell differentiation	7.54E-08
cellular response to cytokine stimulus	1.19E-07
chemokine-mediated signaling pathway	1.51E-07
T cell activation	1.59E-07
cellular response to interferon-gamma	1.76E-07
response to interferon-gamma	2.17E-07
cytokine-mediated signaling pathway	2.90E-07
defense response	3.70E-07
cellular response to lipopolysaccharide	6.59E-07
lymph node development	7.41E-07

e

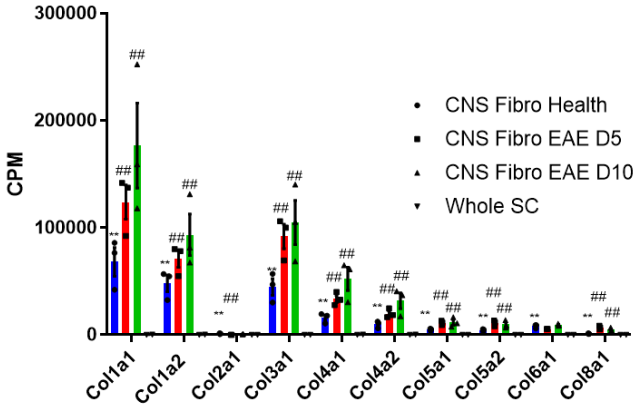

f

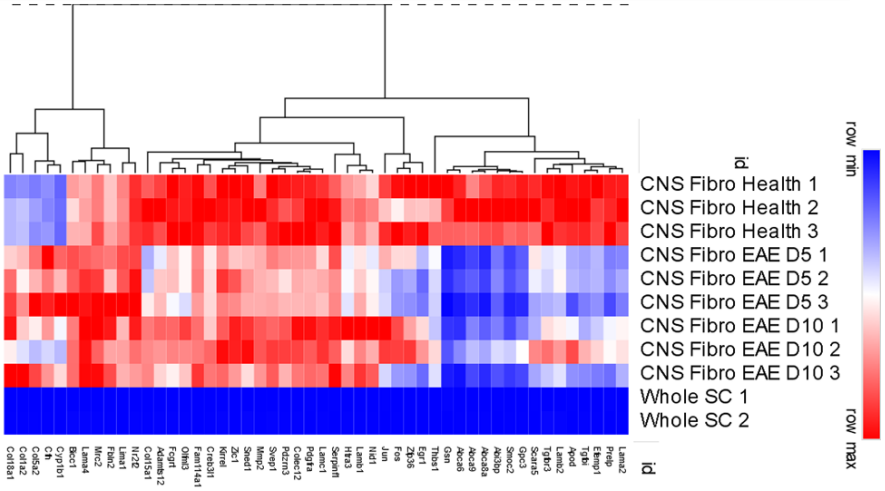

MATERIALS AND METHODS

Experimental subject details

Col1a1GFP mice from David Brenner (C57BL/6 background) were used to label Col1 producing cells for imaging and FACS sorting analysis. Rosa-lsl-tdTomato mice, Charles River Laboratories 007909 (C57BL/6 background), were crossed to Col1a2CreER^{T} mice, Jackson Labs 029567 (C57BL/6 background), Ng2CreER^{TM} mice, Jackson Labs 008538 (C57BL/6 background), or aSMACreER^{T2} mice (previously described)(Wendling et al., 2009)[49] for lineage tracing analysis. B6;129S7-*Hprt1*$^{tm2(Pgk1\text{-}Pac/Tk)Brd}$/Mmucd, MMRRC 010860-UCD (C57BL/6Try c-Brd mixed background), (lox-stop-lox-HTK) mice were crossed to Col1a2CreER^{T} for the fibroblast ablation experiments. Ifngr1$^{fl/fl}$ mice, Jackson Labs 025394 (C57BL/6 background), were crossed to Col1a2CreER^{T} mice for the IFN mechanistic studies. UBC-GFP (004353) reporter mice and CD45.1 (002014) mice used in bone marrow transplant (BMT) experiments were purchased from Jackson Labs. GFAP/tTA mice on the C57BL/6 background were mated with TRE/IFN-γ on the C57BL/6 background to produce GFAP/tTA;TRE/IFN-γ double transgenic mice and were maintained in the Popko lab for cuprizone studies. Animal protocols were approved by IACUC at UCSD, UCSF and Northwestern and we have followed all ethical regulations in the use of mice for this study. All mice used in this study were 3-4 months of age unless otherwise noted in the method details.

EAE

EAE was induced through 2 subcutaneous injections of myelin oligodendrocyte glycoprotein (MOG) in Freud's adjuvant and an IP injection of pertussis toxin (PTX) (Hooke Laboratories EK-2110). 24 hours after the initial injections a second IP injection of PTX was administered. 120-160 ng PTX was used for each dose based on manufacturer's instructions for

the PTX lot. Mice were induced at 10-12 weeks of age unless notified otherwise. The following EAE score system was used to assess motor outcomes:

0.5 – tip of tail limp

1 – whole tail limp

2 – mouse does not instantly turn over when flipped

2.5 – wobbly gait

3 – mouse dragging backside

3.5 – paralysis of one hind limb

4 – paralysis of both hind limbs

5 – moribund

Mice were scored every day following the induction of EAE and until tissue was collected.

FTY720 injections

Col1a1GFP mice were injected with either saline or 2 mg/kg FTY720 I.P. starting on the day of EAE induction and continuing daily until tissue was collected on day 8-10 post symptom onset for the saline mice.

Cuprizone model of demyelination

GFAP/tTA;TRE/IFN-γ double transgenic mice were maintained on 0.05 mg/ml doxycycline (Sigma, #D9891) in drinking water from conception. At six weeks of age doxycycline was discontinued in half the mice to induce CNS expression of IFN-γ, and all mice were administered a 0.2% cuprizone diet (Envigo, #TD.160049). Cuprizone feeding lasted for 5 weeks and then mice were placed back to a normal diet for up to 3 weeks to allow remyelination to occur. Mice were then perfused and brains were removed, post-fixed with 4% PFA and cryopreserved in 30% sucrose. The tissue were then embedded in OCT for sectioning.

LPC model of demyelination

Demyelinated lesions were produced in the ventrolateral or dorsal spinal cord white matter of 8- to 10-week-old female C57bl6 WT mice as previously described (Niu et al., 2019). Anesthesia was induced and maintained with inhalational isoflurane and oxygen supplemented with 0.05 ml of buprenorphine (Vetergesic; 0.05 mg/ml) given subcutaneously. Having exposed the spinal vertebrae at the level of T12/T13, tissue was cleared overlying the intervertebral space, and the dura was pierced with a dental needle just lateral to midline. A Hamilton needle was advanced through the pierced dura at an angle of 45°, and 0.5 µl 1% lysolecithin (L-α-lysophosphatidylcholine; Sigma L4129) was injected into the ventrolateral white matter. Mice were perfused transcardially at 5 days post lesioning (5dpl), 7dpl, or 14dpl with 4% paraformaldehyde, postfixed for 4 hours, and cryoprotected overnight in 30% sucrose. Spinal cords were frozen in OCT for storage and cryostat sections cut at 15 micrometer thickness.

Tissue slice collection and staining

Mice were anesthetized through an intraperitoneal injection of a ketamine/xylene cocktail and then perfused transcardially with D-PBS followed by 4% paraformaldehyde (Electron Microscopy Sciences 15714-S) using a Dynamax peristaltic pump. Spinal cords were dissected and placed in 30% sucrose until frozen in 1:2 30% sucrose:OCT and sectioned into 10 uM slices. Sections were blocked with 5% Normal Goat Serum and permeabilized in 0.2% Triton X-100 in D-PBS followed by an overnight incubation at 4ºC with the following primary antibodies in antibody buffer (NaCl 150 mM, Tris Base 50 mM, 1% BSA, L-Lysine 100 mM, 0.02% Sodium azide in water). Primary antibodies used were: Col1 abcam ab21286 1:750, CD11b Bio-Rad MCA711 1:1000, CD45 Bio-Rad MCA1031 1:1000, GFAP abcam ab7260 1:500, CD31 BD Biosciences 553370 1:1000, PDGFRb eBioscience 14-1402-82 clone APB5 1:500, PDGFRa BD

Biosciences 558774 clone APA5 1:500, Sox9 abcam ab185966 1:500, Iba1 Wako 019-19741 1:500, Olig2 EMD Millipore AB9610 1:500, NG2 EMD Millipore MAB5384 1:500, CD4 eBioscience 16-0041081 1:1000, Col3 abcam ab7778 1:500, Periostin R&D Systems MAB3548 clone 345613, ER-TR7 Novus NB100-64932 1:1000, CD8 clone 53-6.7 eBioscience 14-0081-82 1:1000, Actin, α-smooth muscle Sigma-Aldrich A2547 1:500., Neurofilament heavy polypeptide abcam ab8135 1:1000, Desmin abcam ab8592 1:1000, CC1 Calbiochem OP80 1:500, CXCL10 abcam ab9938 1:1000. Slides were then washed with D-PBS and incubated at room temperature for 1.5 hours with the following secondary antibodies, all 1:1000 in D-PBS: Goat-anti-Rabbit-Alexa 488 (ThermoFisher A11034), Goat-anti-Rat-Alexa 488 (ThermoFisher A11006), Goat-anti-Rabbit-Alexa 594 (ThermoFisher R37117), Goat-anti-Rat-Alexa 594 (ThermoFisher A11007). Following secondary incubation slides were washed and DAPI Fluoromount-G (SouthernBiotech, 0100-20) was added. Images were taken with an Axio Imager D2 (Carl Zeiss) and digital camera (Axiocam HRm, Carl Zeiss) using the AxioVision software and contrasted using Adobe Photoshop. For light sheet microscopy images, mice were perfused with 100 µL of a tomato lectin (Vector Laboratories DL-1177) in dPBS prior to paraformaldehyde and spinal cord tissue was dissected and incubated overnight with 4% PFA followed by a PBS wash. Cords were then cleared in a solution of 8% SDS, 10% N-butyldiethanolamine, 3% 1-Thioglycerol in PBS for 72 hours and then imaged on a Ziess Z.1 light sheet microscope at the UCSD School of Medicine Microscopy Core. For confocal images, Col1a1GFP+ mouse spinal cords stained with CD31 were imaged on a Leica SP8 Confocal microscope at the UCSD School of Medicine Microscopy Core.

Lineage Tracing

All mice received intraperitoneal (IP) injections of 2 mg tamoxifen in sterile corn oil for 3 consecutive days at 6 weeks of age to induce tdTomato expression. EAE was induced at 12 weeks of age as described above. Mice were scored based on the EAE scoring system described above and tissue was collected 10 days post symptom onset and stained for collagen I. The total collagen area per section was traced using Image J and the number of tdTomato+ reporter cells within this area was quantified and compared between groups. This number was normalized to the average of the number of reporter cells per white matter area for each of the reporters in age-matched healthy mice. For Col1a2CreER^{T} analysis n=7 health and n=9 EAE. For the NG2CreER^{TM} analysis n=10 health and n=13 EAE. For aSmaCreER^{T2} analysis n=4 health and n=7 EAE. Males and females were used in all groups.

Bone Marrow Transplantation

Female 12-week-old Col1a1GFP or UBC-GFP mice were used as bone marrow donors. UBC-GFP mice express enhanced GFP under the direction of the human ubiqutin C promoter. GFP is expressed in all tissues examined, is uniform within cell lineages and remains constant throughout development and in injury paradigms (JAX: 004353). Female CD45.1 mice were used as recipients for cell transplantation. This strain carries the CD45.1 pan-leukocyte marker to distinguish donor-derived cells from recipient CD45.2 cells. Recipient mice were irradiated with 900 rads, split dose, 3 hours apart using a cesium source. Purified donor cells (4×10^6) from bone marrow were injected intravenously with 200,000 spleen helper cells, and hematopoietic reconstitution was monitored in the peripheral blood based on either GFP or CD45.1 expression. Recipients with ≥99% donor chimerism were considered reconstituted. Note that no GFP+ cells were observed in the blood from Col1GFP recipients. Transplanted mice were kept on antibiotic-

containing food for 2 weeks. All mice were maintained at UCSF in accordance with IACUC approved protocols.

Tissue Dissociation and FACS Sorting

To obtain single cell suspensions of CNS fibroblasts, spinal cords from Col1a1GFP mice were dissected, chopped with a #10 blade, and enzymatically dissociated with papain (Worthington Biochemical, LK003176, 1 vial per sample) containing DNase (125 U/ml, Worthington LS002007) for 1.5 hours at 35°C. This was followed by mechanical trituration in a solution containing ovomucoid (2 mg/ml, Roche 109878) and DNase (125 U/ml) and a second enzymatic digestion with 1.0 mg/ml Collagenase Type 2 (Worthington Biochemical, LS004176) and 0.4 mg/ml Neutral Protease (Worthington Biochemical, LS02104) at 35°C for 30 minutes. Next, myelin was removed with myelin removal beads (MACS Miltenyi Biotec 130-096-433) and LS columns (MACS Miltenyi Biotec 130-042-401) on a MidiMACS separator (MACS Miltenyi Biotec 130-042-302). Samples were then blocked with Rat IgG 1/100 (Sigma Aldrich I8015) for 25 minutes on ice. Cell suspensions were re-suspended in buffer containing DAPI, and live, CNS fibroblasts were FACS sorted into Trizol (Invitrogen 15596026) based on GFP fluorescence using an ARIA II sorter at the Flow Cytometry Core at the VA Hospital in La Jolla, CA. Forward scatter and side scatter analysis were also used as gates to limit the sorting to single live cells.

Single-cell sequencing

Tissue was dissociated and FACS sorted as described above into PBS + 0.05% BSA. 3 samples were collected of the Col1a1GFP+ cells in health group, each containing 2-3 spinal cords of Col1a1GFP females. For the Col1a1GFP+ cells in EAE group 2 samples each containing 2 spinal cords from Col1a1GFP mice 5 and 7 days after EAE symptom onset were

combined. For the whole spinal cord in EAE 1 spinal cord from a wild type mouse with EAE 4 days after symptom onset was used. Following FACS sorting the single cell suspension was brought to the UCSD IGM core, run through the 10X Genomics pipeline (v2) and sequenced on an Illumnia HiSeq4000 or NovaSeq 6000. The sequencing files were run through the 10X CellRanger 2.1.1 pipeline to generate gene counts data, and then analyzed using Seurat v3. We used the sctransform pipeline to analyze individual datasets, and the integration pipeline to integrate the healthy and EAE samples (Hafemeister and Satija, 2019; Stuart et al., 2019). In all analyses a 200 non-zero genes cut-off was used. We next filtered out Col1a1 negative cell types by identifying clusters where the majority of cells do not express Col1a1 or Col1a2. This strategy removed 463 total cells. Following stringent criteria, 6,509 cells (93.4% of total cells) were analyzed using unsupervised clustering. Following the filtering, the counts were reanalyzed. Resolution parameter of clustering was set to 0.5. Wilcox method was used for differential expression analysis, with min.pct = 0.25 and logfc.threshold = 0.25. SingleR was used to annotate single cells using the Immgen reference dataset.

CNS fibroblast ablation and interferon gamma receptor deletion

All mice received intraperitoneal (IP) injections of 2 mg tamoxifen in sterile corn oil for 3 consecutive days at 6 weeks of age to induce cre expression. EAE was induced at 12 weeks of age as described above. Administration of GCV (Sigma Y0001129) began on day 8 post EAE induction through a subcutaneous injection at a concentration of 25 mg/kg in dPBS and occurred each following day until tissue was collected. For the HTK experiment males were used as the HTK gene is X-linked, n = 22 control and 19 fHTK. One of the control mice died during the course of EAE so it was not included in the histology quantifications. For the IFNγ deletion

experiments, tamoxifen and EAE were administered in males and females. Mice were collected 30 days after EAE induction. n= 14 control, 15 fIFNγ.

Electron Microscopy

Control and fHTK mice at day 30 post EAE induction and C57/bl6 mice were anesthetized through an intraperitoneal injection of a ketamine/xylene cocktail and then perfused transcardially with D-PBS followed by 2% paraformaldehyde and 2.5% glutaraldehyde in a 0.15M sodium cacodylate buffer. 1mm^3 spinal cord sections were dissected and placed in the fixing solution until processed at the CMM UCSD Electron Microscopy Core. Samples were then placed in 1% osmium in 0.15M sodium cacodylate for 1-2 hours on ice, washed 5x10 min in 0.15M sodium cacodylate buffer and rinsed in ddH2O on ice. Samples were incubated in 2% uranyl acetate for 1 to 2 hrs at 4C, dehydrated at increasing concentrations of ethanol on ice and then dry acetone for 15 min at room temperature, placed in 50:50 ethanol: Durcupan for 1hr at room temperature and then incubated in 100% Durcupan overnight. Tissue was embedded in Durcupan in 60C oven for 36 to 48hrs. Ultrathin sections (60nm) were cut on a Leica microtome with a Diamond knife followed by post staining with both uranyl acetate and lead. Images were captured on FEI Spirit Tecnai TEM at 80KV with Eagle 4kx4k camera. Images at 3000x were used for analysis in which all myelinated axons per frame were counted for each of the different conditions.

Oligodendrocyte precursor cell (OPC) cultures

Primary rat OPCs were isolated from cortical hemispheres of postnatal day 7 rat brains as previously described (Mei et al., 2014). Briefly, rat cortices were minced and dissociated in papain (Worthington) for 75 min at 37°C with periodic shaking. Following trituration, the suspension was immersed in 0.2% BSA at room temperature and subjected to sequential

immunopanning consisting of two 30 min incubations in negative selection plates (Ran-2 and Gal-C) and one 45 min incubation for positive selection (O4). Selection plates were prepared by incubating dishes overnight at room temperature with goat IgG and IgM secondary antibodies (Jackson ImmunoResearch) in 50 mM Tris-HCl. Antibodies Ran-2, Gal-C, or O4 were added after washing with DPBS (Invitrogen). OPCs were dissociated from the positive selection dish with 0.05% Trypsin-EDTA (Invitrogen) and purified OPCs subsequently seeded onto 12mm coverslips coated with poly-L-lysine (PLL, Sigma-Aldrich), or PLL with 10 ug/mL of: laminin (EMD Millipore CC095), fibronectin (Sigma-Aldrich F0635), or collagen I (Aviva Systems Biology OPED00033). OPCs were seeded at a density of 15,000 cells per coverslip in DMEM (Invitrogen) supplemented with B27 (Invitrogen), N2 (Invitrogen), N-acetylcysteine (Sigma-Aldrich), forskolin (Sigma-Aldrich), penicillin-streptomycin (Invitrogen), and PDGF-AA (Peprotech) and cultured overnight at 37°C, 5% CO2. The following day, OPCs were either incubated in 10 uM EdU with PDGF-AA for 2 hours, or cultured for 3 days following the removal of PDGF-AA from media with or without the addition of 50 nM T3 (Sigma-Aldrich). Immunohistochemistry: Cultures were fixed in 4% (w/v) paraformaldehyde (PFA) in DPBS for 15 minutes and dehydrated. Cultures were blocked and permeabilized in 10% goat serum in DPBS containing 0.1% (v/v) Triton X-100 for 1 h at room temperature. Primary antibodies were diluted in 10% goat serum and incubated overnight at 4°C. Secondary antibodies were diluted in 10% goat serum with DAPI and incubated for 1 h at room temperature. The following primary antibodies were used: rat monoclonal anti-PDGFRa (BD Biosciences, 558774, 1:200); rabbit polyclonal anti-Olig2 (EMD Millipore AB9610, 1:1000); rat monoclonal anti-MBP (Bio-Rad/Serotec, MCA409S, 1:500). Alexa Fluor 488 and Alexa Fluor 594 IgG secondary antibodies (rat, rabbit, 1:1000) were used to detect fluorescence. The incorporation of EdU by proliferating

cells was detected via the Click-iT EdU Cell Proliferation Kit (Invitrogen C10340) after incubation in primary and secondary antibodies. Images were obtained on a Zeiss Axio Imager Z1 microscope. Cells were quantified from randomly selected fields of view per coverslip under 10x magnification.

For migration experiments, transwell membranes (Corning, 8.0 μm pore polycarbonate membrane insert) were coated on both sides with PLL and 10ug/ml laminin, fibronectin, or collagen I was added to the top of the membrane. OPCs were seeded onto the membranes in DMEM + B27, N2, N-acetylcysteine, forskolin, and pen/strep. DMEM + B27, N2, N-acetylcysteine, forskolin, and pen/strep + 10ng/ml PDGF-AA was added to the bottom of the well. Cells were scraped off the top of the membrane 24 hours after initial seeding and fixed with 4% PFA in DPBS for 15 minutes. Cells were then blocked and permeabilized in 10% goat serum with 0.1% Triton, incubated in rabbit monoclonal anti-PDGFRa antibody (1:500, gift from WB Stallcup) overnight at 4°C and then incubated in secondary antibody & DAPI for 1 hour at room temperature (goat anti-rabbit Alexa Fluor 488 1:1000). The transwell membranes were then cut out and mounted for imaging, and the number of cells on the bottom of the transwell were counted. For all *in vitro* experiments 3 biological replicates, each with 3 technical replicates, were used. Statistics were calculated using Prism with a one-way ANOVA with Sidak's.

Bulk RNA sequencing

For bulk RNA sequencing of CNS fibroblasts we collected and analyzed 3 samples each for the control, EAE 5 days PSO and EAE 10 days PSO groups. 2-3 spinal cords from Col1a1GFP females of 3-4 months of age were combined for each sample. 2 samples were collected for the whole spinal cord homogenate, each consisting of 1 spinal cord of a Col1a1GFP female at 3 months of age. RNA was purified from the FACS-sorted fibroblasts using the Qiagen

RNA Isolation Microkit. The RNA was then tested for quality and concentration at the UCSD IGM Core using an Agilent Bioanalyzer. Stranded, cDNA libraries were made using the SMARTer Stranded Total RNA-Seq Kit - Pico Input Mammalian (Clontech) and then the samples were sequenced on an Illumnia HiSeq4000, 100 cycles, paired ends. Sequence reads were aligned to Ensembl mm9 v67 mouse whole genome using Tophat v 2.0.11 and Bowtie 2 v 2.2.1 using parameters –m 2 –a 5 –p 7. The resulting files were then sorted using SAMtools v.0.1.19 and count tables generated using HTSeq-0.6.1. Differential expression analysis and statistical analysis including p values and FDR was performed using DESeq2**.** Heat maps were prepared using the Morpheus software (https://software.broadinstitute.org/morpheus) and clustered using hierarchical clustering with a metric of one minus the pearson correlation.

EAE time course quantifications

To calculate the number of Col1a1GFP+ cells per lesion over time, tissue sections from Col1a1GFP mice with EAE were stained for CD45. CD45 areas were traced using Image J and the number of Col1a1GFP+ cells within this area were counted at different time points throughout EAE. To calculate the number of pericytes and T cells in EAE lesions over time, tissue sections from Co1la1GFP or c57/Bl6 mice induced with EAE and collected at different time points post symptom onset were stained with Desmin, CD4, or CD8. DAPI was then administered to all slides and used to determine the lesion location due to increased cell density. The number of Desmin, CD4 or CD8+ cells within the lesion were counted for each mouse using Image J. 3-6 mice were quantified per group with at least 4 spinal cord sections (two thoracic and two lumbar) analyzed from each mouse.

fHTK quantifications

To determine the extent of fibrotic scar tissue reduction, tissue was collected as described above and stained for collagen I and CD11b. The total area of both stains was traced using Image J and the total Col1+ area/CD11b+ area was reported. To quantify the % myelination per group tissue sections were stained with FluoroMyelin (Thermo Fisher F34652) 1:300 in dPBS at room temperature. The total white matter area was traced using Image J and compared to the total area of the myelin stain. To calculate the number of Olig2+ cells per lesion tissue sections were stained for Olig2 and CD11b. CD11b areas were traced using Image J and the number of Olig2+ cells within this area were counted and compared between groups. To calculate the percentage of Olig2+ cells that were CC1+, sections were stained with Olig2 and CC1 using the Vector Labs Mouse on Mouse Basic Kit (BMK-2202). DAPI was then administered to all slides and used to determine the lesion location due to increased cell density. The percentage of Olig2+ cells also positive for CC1 within the lesion were counted for each mouse using Image J. To calculate the number of CD4+ and CD8+ cells per lesion, tissue sections were stained for CD4 or CD8. Lesion areas were traced using DAPI in Image J and the number of CD4 or 8+ cells within this area were counted and compared between groups. To calculate the number of axons in the lesions of control and fHTK mice, tissue sections were stained for CD11b and neurofilament heavy polypeptide. Quantifications were done using Cell Profiler. For all quantifications at least 6 spinal cord sections (3 thoracic and 3 lumbar) were analyzed from each mouse.

Col1a1GFP regional analysis

Brains and spinal cords of 4 adult, male, Col1a1GFP mice were collected, sectioned and stained for CD31 in red and smooth muscle actin in far red. The length of the total vasculature and smooth muscle actin positive vasculature and the number of GFP+ cells associated with the vasculature for the different brain regions were quantified using Image J.

Col1a1GFP; Col1a2CreER^{T} overlap analysis

All mice were injected with tamoxifen, induced with EAE and tissue was collected and sectioned in the same way as the lineage training mice. 6 spinal cord cross sections per mouse were imaged and the percentage of Col1a1GFP+ cells that were also positive for the tdTomato reporter was calculated using Image J. n=5 health and n=4 EAE.

Statistics

The statistics and *n* values used for each experiment are described in the figure legends. All error bars presented are ± standard error of the mean and n refers to the number of animals used in the experiment in every case.

Data Availability

All RNA sequencing and single-cell sequencing raw and processed data files have been uploaded to GEO and will be made public before the time of publication. Reviewer access codes can be provided if requested.

ACKNOWLEDGEMENTS

We would like to thank Kristen Jepsen and the UCSD Institute of Genomic Medicine Genomics center, Tara Lambardo and the UCSD Veterans Hospital Flow Cytometry Core, Ying Jones and the CMM UCSD Electron Microscopy Core and Jennifer Santini and Marcy Erb at the UCSD Microscopy Core. We would like to thank David Brenner for kindly supplying the Col1GFP mice.

Chapter 2, in part, has been submitted for publication of the material as it may appear in Nature Neuroscience, 2020, Dorrier CE, Aran D, Haenelt EA, Sheehy RN, Hoi KK, Pintarić L,

Chen Y, Lizama CO, Cautivo KM, Weiner GA, Popko B, Fancy SPJ, Arnold T, Daneman R.

The dissertation author was the primary investigator and author of this paper.

CHAPTER THREE:

Mechanisms of CNS fibrosis

INTRODUCTION

Understanding the mechanisms that lead to scar formation is essential to develop therapeutics that can prevent or reduce fibrosis in the CNS. Unfortunately, as of now very little is known about the pathways that lead to CNS fibrosis. Previous studies that have blocked scar formation in the CNS have done so using manipulations that are not cell specific and therefore difficult to target (Dias et al., 2018). The herpes thymidine kinase cell ablation paradigm used to reduce fibrosis in the previous chapter requires fibroblast genetic manipulation and is not a viable treatment for human patients. The interferon gamma studies from the previous chapter suggest that interferon gamma signaling regulates the amplitude of CNS fibrosis following inflammation, but blocking interferon gamma signaling in fibroblasts does not reduce fibrosis enough to result in changes in motor symptoms. We set out to test a series of molecular pathways to determine whether they are required for CNS fibrosis and impact overall disease severity. The pathways were chosen based on known pathways that regulate peripheral fibrosis, as well as pathways identified as enriched in CNS fibroblasts, or upregulated during EAE in CNS fibroblasts using RNA-seq.

The PDGFR signaling pathway plays roles in processes such as cellular proliferation and differentiation, pericyte recruitment, tumor growth, and fibrosis (Buhl et al., 2020; Daneman et al., 2010; Hoch and Soriano, 2003; Klinkhammer et al., 2018). PDGFRα and PDGFRβ are receptor tyrosine kinases that form homo (PDGFRα/α, PDGFRβ/β) or heterodimers (PDGFRα/β) upon ligand binding. The receptor dimers then transphophorylate tyrosine residues on opposite subunits leading to conformational changes and further activation of kinase activity whereby the receptors can phosphorylate a variety of substrates including Ras, PI3K, and Jak kinases that drive signaling and gene expression (Klinkhammer et al., 2018; Ying et al., 2017). PDGFR

signaling is a potential target for modulating fibrosis as PDGFR signaling through Ras and MEK/ERK in fibroblasts plays a key role in the migration of these fibrotic cells to the site of injury/inflammation in solid organ fibrosis (Donovan et al., 2013; Gao et al., 2005; Klinkhammer et al., 2018; Ying et al., 2017). Interestingly, the PDGFR inhibitor Imatinib attenuates neurologic inflammation and associated neurologic symptoms in a rat EAE model (Adzemovic et al., 2013), and the PDGFR inhibitor masatinib demonstrated therapeutic benefit to patients with multiple sclerosis in a pilot study (Vermersch et al., 2012), however the mechanism of action remains unknown. It has also been shown that reducing PDGFR signaling following rodent models of traumatic brain injury and stroke reduces fibrotic scar formation and in the case of stroke, increases the size of the infarct (Makihara et al., 2015; Pei et al., 2017). It is unknown in both cases how this reduction in scar formation impacts in overall tissue repair or symptom recovery. Here we aim to further understand how the PDGFR pathway contributes to CNS scar formation and disease recovery on a molecular level.

Other pathways known to be involved in fibrosis in the periphery include the Wnt pathway and LPA signaling pathway. We found using RNA sequencing of CNS fibroblasts in health and EAE that *Wnt5a* and *Enpp2*, genes involved in these pathways, are strongly expressed in CNS fibroblasts and decided to further investigate their role along with the PDGFR pathway in CNS fibrosis using *in vitro* and *in vivo* model systems.

Wnt5a is a ligand for the Wnt pathway, and has been shown to be highly expressed in fibrotic tissue of the lung and liver and positively regulate fibrosis in the kidney by promoting macrophage polarization (Feng et al., 2018; Newman et al., 2016; Rashid et al., 2012). More general roles of the Wnt pathway throughout the body include cell fate specification, proliferation and migration (Komiya and Habas, 2008). Wnt ligands can either activate canonical

Wnt signaling, which is characterized by the nuclear translocation of the intracellular signaling molecule β catenin, or noncanonical signaling which does not rely on β catenin translocation. While most of the common cell functions attributed to Wnt signaling occur due to canonical pathway activation, Wnt5a mainly activates the noncanonical pathway through interactions with Fzd2 and ROR1/2. (Zhou et al., 2017). Noncanonical pathway signaling has been implicated in cell polarity and differentiation, and specifically noncanonical pathway signaling by Wnt5a has been shown to promote inflammation (Pashirzad et al., 2017).

Enpp2 encodes for the protein Autotaxin (Atx), which is an enzyme that catalyzes the conversion of LPC to LPA, a bioactive lipid that can signal via G protein coupled receptors. This process occurs outside of the cell, allowing the newly-formed LPA to signal through LPA transmembrane receptors on the cell surface. LPA pathway signaling has been linked to fibrosis in the periphery, and pharmacologically targeting autotaxin itself has been shown to reverse fibrosis in the lung (Ikeda et al., 1998; Ninou et al., 2018; Ongenaert et al., 2016; Tager et al., 2008). In the brain, LPA signaling has also been linked to myelination, progenitor cell function, synaptic transmission, brain immune responses, and neurovascular function (Yung et al., 2015). We hypothesized that autotaxin secretion by fibroblasts promotes LPA signaling to sustain fibrotic responses by fibroblasts.

RESULTS

Wnt5a and Autotaxin from CNS fibroblasts do not regulate fibrotic scarring

In our RNA sequencing dataset we found that fibroblasts are highly enriched for *Wnt5a* as well as the Frizzled receptor that Wnt5a uses to activate the non-canonical branch of Wnt

signaling, *Fzd2* (Figure 3.1a). Because Wnt5a is secreted from the cell and been shown to promote inflammation, it is possible that Wnt5a release from fibroblasts acts on nearby cell types such as macrophages to sustain inflammatory signaling in EAE lesions. It is also possible that Wnt5a acts on fibroblasts themselves to promote fibrosis.

To test if Wnt5a expression by fibroblasts is necessary for inflammation and scarring in EAE, we selectively deleted *Wnt5a* from fibroblasts prior to EAE induction. Mice with fibroblast-specific *Wnt5a* deletion (Wnt5af/f;Col1a2CreERT) and littermate controls (Wnt5af/f) were injected with tamoxifen at 6 weeks of age, induced with EAE at 12 weeks of age and tissue was collected 30 days post EAE induction and analyzed for the extent of fibrotic scar formation. Both groups had robust scar formation and similar EAE score curves, so we determined that fibroblast-derived Wnt5a is not required for scar formation or inflammation in EAE (Figure 3.1b,c). It is possible that Wnt5a does play a role in CNS fibrotic scarring, but there is redundancy with other Wnt pathway members.

CNS fibroblasts also highly express the gene encoding for autotaxin, *Enpp2* (Figure 3.2a). To test whether Autotaxin expression by fibroblasts is necessary for inflammation and scarring in EAE, we selectively deleted *Enpp2* from fibroblasts prior to EAE induction. Mice with fibroblast-specific Atx deletion (Atxf/f;Col1a2CreERT) and littermate controls (Atxf/f) were injected with tamoxifen at 6 weeks of age, induced with EAE at 12 weeks of age and tissue was collected 30 days post EAE induction. Both groups had robust scar formation and motor symptoms equivalent to control mice, so we determined that fibroblast-derived Atx is also not required for scar formation or inflammation in EAE (Figure 3.2b,c). Other cell types could contribute to Atx secretion and LPA production such that an Atx deletion from fibroblasts would not significantly affect LPA signaling.

PDGFR signaling regulates fibroblast development and migration *in vitro*

Another pathway of interest is the PDGFR signaling pathway, as PDGFRα and PDGFRβ are both highly expressed in CNS fibroblasts (Figure 3.3a). To test whether PDGFRβ signaling is required for the development of CNS fibroblasts, we quantified the extent of vascular collagen I expression as a proxy for fibroblast presence in mice with knockouts of *PDGFRβ*. We collected *PDGFRβ*+/+, *PDGFRβ*+/- and *PDGFRβ*-/- embryos at e16.5 as the full knockout mice die at birth (Hoch and Soriano, 2003). We found that *PDGFRβ*-/- embryos had significantly less collagen expression surrounding blood vessels, suggesting that there are less collagen-forming cells in these mice (Figure 3.3b). To test whether PDGFR signaling is required for fibroblast maintenance in adulthood, we analyzed fibroblast numbers in adult Col1a1GFP mice with mutations in the *PDGFRβ* gene, deemed F7 mice, that have diminished PDGFR signaling but remain viable into adulthood (Winkler et al., 2010). We found less ER-TR7 staining, a marker for fibroblasts, around the vasculature in adult mice with less functional PDGFRβ signaling in the striatum (Figure 3.3c,d).

To determine whether PDGFR signaling is necessary and/or sufficient for fibroblast proliferation, migration and collagen production, we generated an *in vitro* model of CNS fibroblasts. To culture CNS fibroblasts we dissect and dissociate the meninges of Col1a1GFP+ mice pups at p2-3 and plate the resulting single cell suspension on a culture dish. Fibroblasts are the predominant cell type to adhere to the dish without the addition of any sort of cell adhesion additive, and they grow rapidly when cultured in 10% serum. To determine if PDGFR signaling is necessary for fibroblast proliferation we added 10uM AG1296, a nonspecific PDGFR inhibitor, to the fibroblast cultures and measured the number of cells 48 hours later using the alamarBlue proliferation reagent. To test if PDGFR signaling is necessary for collagen

production we measured the GFP fluorescence of the cells, as GFP is produced under the collagen promoter and is therefore an indirect measurement of collagen synthesis, following the same experiment. We then divided the GFP fluorescence by the alamarBlue measurements to calculate the collagen production per cell. We found no differences in proliferation or collagen production between cells treated with AG1296 or a buffer, indicating that PDGFR signaling is not necessary for fibroblast proliferation or collagen production. To test if PDGFR signaling is sufficient for these properties we added PDGF-BB, a PDGFR ligand, to the cultures at 20ng/uL and repeated the same experiment. We found that addition of PDGF-BB had no impact on fibroblast proliferation or collagen production and therefore PDGFR signaling is not sufficient to induce these properties.

To test whether PDGFR signaling is necessary and/or sufficient for fibroblast migration we plated fibroblasts on transwells with 8 uM pores and placed the transwells in 24 well culture dishes. Fibroblasts migrate through these transwells to serum if the transwell chamber does not contain serum. To test whether PDGFR signaling is necessary for migration we added AG1296 or a buffer to the transwell chamber with the fibroblasts and placed media with serum in the cell culture well. We found that significantly fewer fibroblasts migrated to the serum if they were exposed to AG1296. To test whether PDGFR signaling is sufficient for migration we added PDGF-BB or buffer to media in the culture well without serum. Significantly more fibroblasts migrated to PDGF-BB than to a buffer in the absence of serum. Together these experiments show that PDGFR pathway activation is both necessary and sufficient for fibroblast migration.

To test whether PDGFRα and PDGFRβ expression by fibroblasts are necessary for inflammation and scarring in EAE we selectively deleted *PDGFRα*, *PDGFRβ* or both from fibroblasts prior to EAE induction. Mice with fibroblast-specific PDGFR deletions (PDGFRαf/f;

and/or PDGFRβf/f;Col1a2CreERT) and littermate controls (PDGFRαf/f, PDGFRβf/f, PDGFRαf/fβf/f) were injected with tamoxifen at 6 weeks of age, induced with EAE at 12 weeks of age and tissue was collected 30 days post EAE induction. There were no significant differences in the EAE score or fibrotic scar formation between the groups, suggesting that PDGFR signaling does not affect scarring at a chronic time point (Figure 3.4b).

DISCUSSION

Together this data highlights that no single pathway that we have tested is necessary or sufficient for promoting CNS fibrotic scar formation. Instead, a pathway we have not tested yet, or different combinations of activated signaling pathways are likely necessary for CNS fibroblast proliferation, migration and collagen deposition which together promote CNS fibrosis.

As discussed in the previous chapter, we found that interferon gamma signaling in fibroblasts significantly impacts the amplitude of scar formation. However, deletion of *Ifngr1* from fibroblasts did not block scar formation to the same extent as a genetic ablation of fibroblast proliferation, suggesting that other signaling pathways are important for scar formation. This data inspired us to find these other pathways based on our RNA sequencing dataset of CNS fibroblasts in health and EAE, known contributors to fibrosis in the periphery and histological analyses of EAE lesions, and to test their role in CNS scar formation.

It is clear from the data presented here that Autotaxin and Wnt5a secretion from fibroblasts are not required for CNS fibrotic scar formation following inflammation, as mice with fibroblast-specific deletions of these genes do not have reductions in collagen deposition in EAE lesions. As Wnt5a is a secreted ligand that could be affecting the inflammatory environment of the EAE lesions, we were interested to see if deleting this gene from fibroblasts impacted the

overall EAE score. Although our n was small, we saw no changes in EAE score or lesion size after a fibroblast-specific *Wnt5a* deletion. While it is possible that the proportion of various immune cells differs in this model, we believe that due to the lack of EAE motor score differences that this paradigm did not warrant future study.

The overall role for PDGFR signaling in CNS fibrosis is less clear. In development, PDGFR signaling impacts the number of collagen-secreting cells surrounding the vasculature. Whether these cells are indeed fibroblasts remains unknown as it is possible that pericytes could secrete collagen in development, and reductions in PDGFR signaling also impact pericyte levels. In adulthood, when pericytes do not express Col1, our data suggests a region-specific role for PDGFR signaling in CNS perivascular fibroblast maintenance, as there are fewer ER-TR7+ vessels in the striatum but not the cortex in mice that had reductions in PDGFRβ signaling. It is unknown whether or not there is extensive perivascular fibroblast heterogeneity in the brain, but single-cell sequencing of Col1a1GFP+ cells in different adult brain regions could provide insights into this question. It is also unclear whether reductions in PDGFR signaling affect fibroblasts directly, or if pericyte signaling to fibroblasts plays a greater role in fibroblast maintenance.

Due to these developmental effects, we decided to use an *in vitro* model to investigate whether PDGFR signaling affects fibroblast proliferation, collagen production, and/or migration. While we did not find any evidence that PDGFR signaling affects fibroblast proliferation or collagen production, we saw striking a migration phenotype where fibroblasts migrate to PDGF-BB and AG1296, a PDGFR inhibitor, blocks fibroblast migration to serum. We hypothesize that PDGF-BB secretion from endothelial cells serves as a migratory cue for CNS fibroblasts.

Expression of PDGFR ligands by other cell types in the EAE lesion could be the driving factor for fibroblast migration away from blood vessels in EAE, a critical early step for fibrosis.

When we deleted the PDGF receptors from fibroblasts and induced EAE we saw no significant effects on scar formation at day 30 post induction. It is possible that mice with impaired PDGFR signaling in fibroblasts do have a delay in scar formation due to migration defects of the cells, but to test this hypothesis tissue would have to be collected at earlier time points post EAE induction. It should also be noted that the control levels of fibrosis for this experiment were lower than reported for other similar experiments (scarring was present in around 50 % of the lesion area in the control mice for the PDGFR experiment compared to around 85 % in the HTK experiment). This could be because the mice strain used for these experiments was not on a pure C57/bl6 background like many of the other mouse strains reported here. The particular EAE kit that we used is optimized for mice of this background stain, so back-crossing this line into a pure C57/bl6 background could lead to higher total levels of scarring in control mice and enable us to see stronger differences between the different receptor knockouts.

An additional pathway that we hypothesize is involved in CNS scar formation is the TGFβ pathway, which has shown to be critical for fibrosis in tissues such as the lung and kidney (Biernacka et al., 2011; Meng et al., 2016; Meng et al., 2015). Previous studies have shown that CNS fibroblasts express TGFβ receptors following traumatic brain injury, and that inhibiting TGFβ signaling following brain injuries in rodents reduced fibrotic scarring and promoted neuronal regeneration (Komuta et al., 2010; Logan et al., 1994; Yoshioka et al., 2011). We have an ongoing collaboration with Tom Arnold at UCSF to investigate the role of this pathway in CNS fibrosis, which will illuminate whether this pathway also contributes to CNS fibrotic

scarring. It is possible that the combination of TGFβ, IFNGR and PDGFR signaling are required for a robust fibrotic response, and further studies knocking out these pathways from fibroblasts in combination are recommended to understand the complete profile of fibroblast activation and fibrosis.

FIGURES

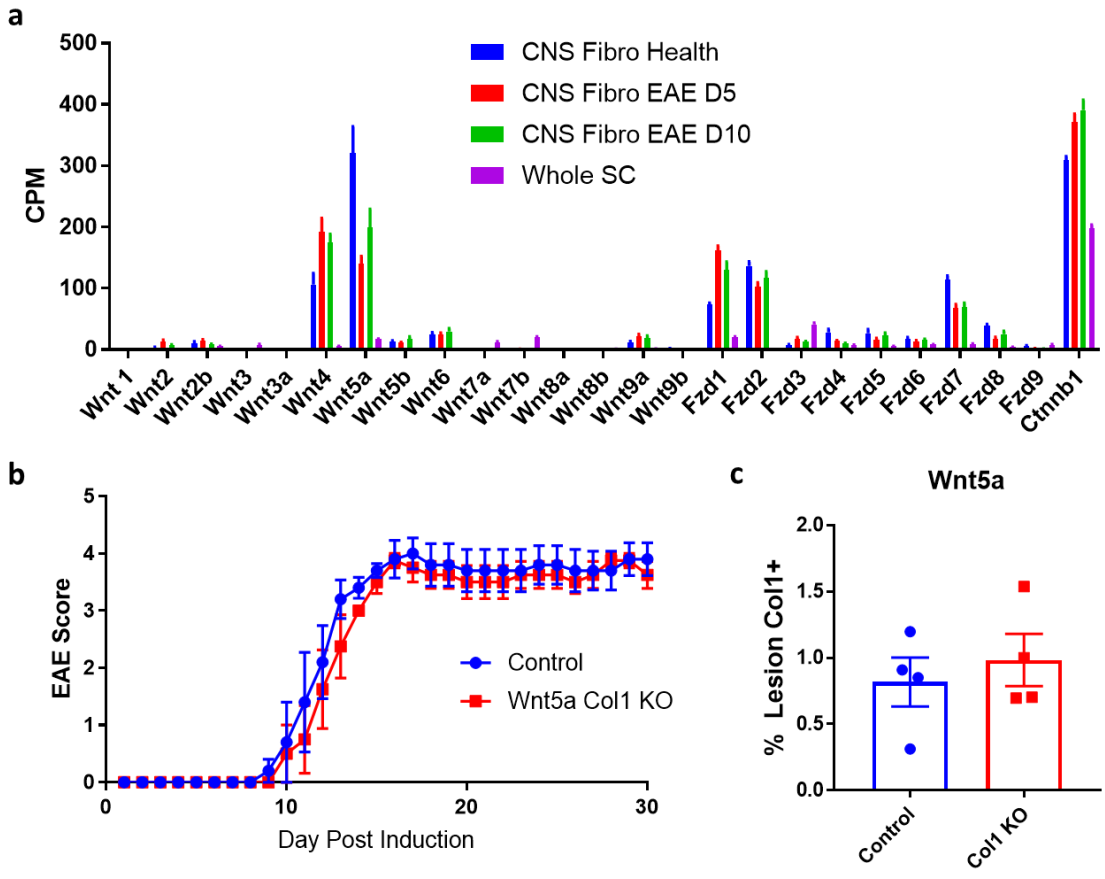

Figure 3.1: Wnt5a is highly expressed by CNS fibroblasts but does not contribute to CNS scar formation. a. mRNA levels in counts per million (CPM) of Wnt pathway genes from the sequencing of whole spinal cord tissue (Whole SC) and CNS Fibro Health, CNS Fibro EAE D5 and CNS Fibro EAE D10. b. EAE score for the control and Wnt5a Col1 KO mice up to 30 days post EAE induction. c. Quantification of the percentage of the area of immune infiltration (denoted by CD11b) that is Col1+, n= 4 per condition.

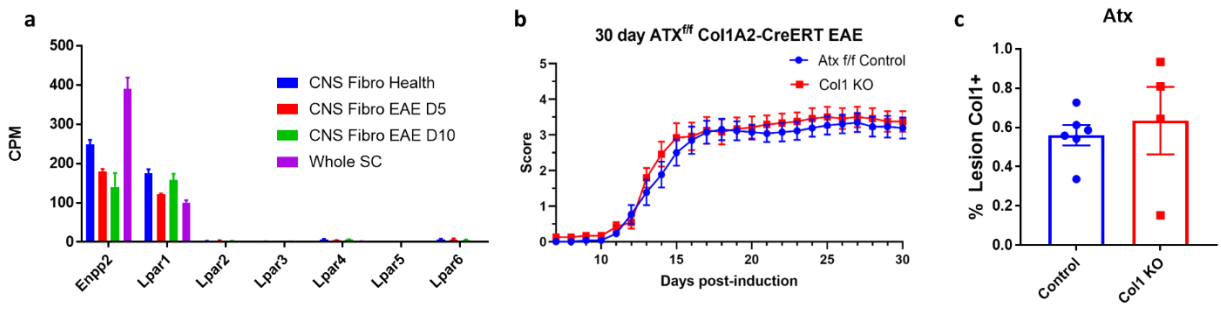

Figure 3.2: Autotaxin is highly expressed by CNS fibroblasts but does not contribute to CNS scar formation. a. mRNA levels in counts per million (CPM) of LPA signaling pathway genes from the sequencing of whole spinal cord tissue (Whole SC) and CNS Fibro Health, CNS Fibro EAE D5 and CNS Fibro EAE D10. b. EAE score for the control and Atx Col1 KO mice up to 30 days post EAE induction. c. Quantification of the percentage of the area of immune infiltration (denoted by CD11b) that is Col1+, n=4 or 6 per condition.

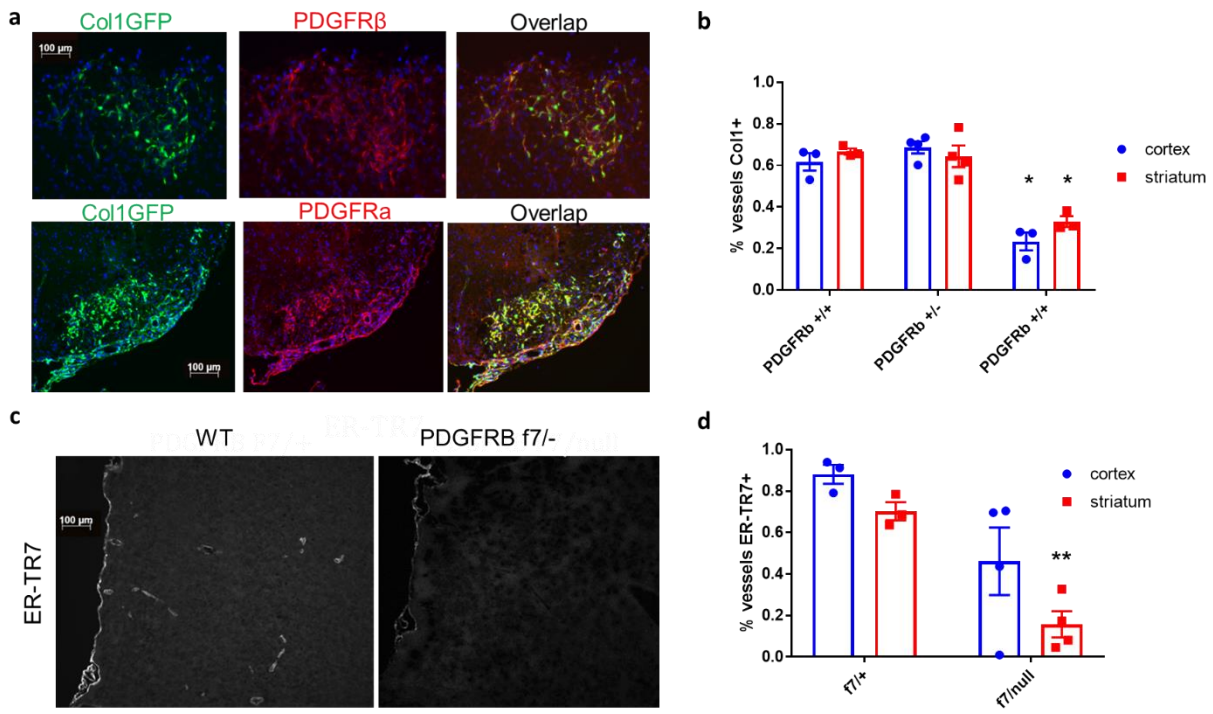

Figure 3.3: PDGFRβ signaling plays a role in CNS fibroblast development. a. Spinal cord sections from mice with chronic EAE were stained for Col1 (green) and PDGFRβ (red, top) or PDGFRα (red, bottom). Col1a1-GFP+ cells express both PDGFRα and PDGFRβ. b. Brain tissue sections of embryonic *PDGFRβ* null mutants, heterozygotes and wild type mice were stained for Col1 and the percent vascular length that was Col1+ was measured. n=3-4 per condition, *p<0.05. c,d. Brains tissue sections from adult PDGFRβ f7/null and PDGFRβ f7/+ mice were stained for the fibroblast marker ER-TR7 (c) and the percent vascular length positive was measured in the cortex and striatum (d). n=3-4 per condition, **p<0.01.

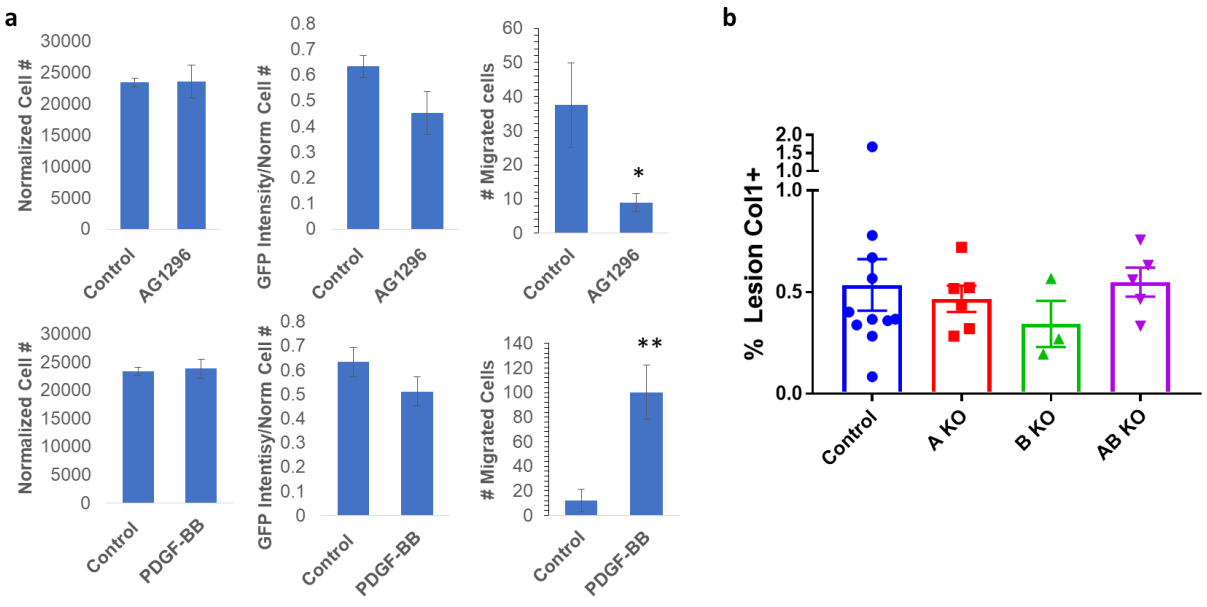

Figure 3.4: PDGFRβ signaling enhances CNS fibroblast migration *in vitro* but not collagen production *in vivo*. a. Cell proliferation, Col1a1-GFP reporter expression per cell and migration assays were performed in media with either a PDGFR inhibitor (AG1296), a recombinant PDGF-BB ligand or vehicle. The PDGFR inhibitor decreased the migration, but not proliferation or Col1 expression of CNS fibroblasts, and PDGF-BB increased migration, but not proliferation or Col1 expression. n=3 per condition, *p<0.05, **p<0.001. b. Quantification of the percentage of the area of immune infiltration (denoted by CD11b) that is Col1+ for mice with fibroblast-specific knockouts of the different PDGFR receptor combinations, n=3-10 per condition.

MATERIALS AND METHODS

RNA sequencing

RNA sequencing plots were generated from the RNA sequencing dataset described in Chapter 2.

Mice and EAE

EAE was induced through 2 subcutaneous injections of myelin oligodendrocyte glycoprotein (MOG) in Freud's adjuvant and an IP injection of pertussis toxin (PTX) (Hooke Laboratories EK-2110). 24 hours after the initial injections a second IP injection of PTX was administered. 120-160 ng PTX was used for each dose based on manufacturer's instructions for the PTX lot. Mice were scored in the manner described in Chapter 2 (see page --- for details) Mice strains used include: Wnt5a f/f (Jackson Labs 026626), Autotaxin f/f from Wouter Meelenaar through Jason Cyster, Col1a2CreERT (Jackson Labs 029567), PDGFRaf/fbf/f mice obtained from Philip Soriano, and PDGFRBnull/F7 from Philippe Soriano.

Histological Analysis and Staining

Mice were anesthetized through an intraperitoneal injection of a ketamine/xylene cocktail and then perfused transcardially with D-PBS followed by 4% paraformaldehyde (Electron Microscopy Sciences 15714-S) using a Dynamax peristaltic pump. Spinal cords were dissected and placed in 30% sucrose until frozen in 1:2 30% sucrose:OCT and sectioned into 10 uM slices. Sections were blocked with 5% Normal Goat Serum and permeabilized in 0.2% Triton X-100 in D-PBS followed by an overnight incubation at 4ºC with the following primary antibodies in antibody buffer (NaCl 150 mM, Tris Base 50 mM, 1% BSA, L-Lysine 100 mM, 0.02% Sodium azide in water). Primary antibodies used were: Col1 abcam ab21286 1:750, CD11b Bio-Rad MCA711 1:1000, PDGFRb eBioscience 14-1402-82 clone APB5 1:500, PDGFRa BD

Biosciences 558774 clone APA5 1:500, ER-TR7 Novus NB100-64932 1:1000, Actin, α-smooth muscle Sigma A5228. Slides were then washed with D-PBS and incubated at room temperature for 1.5 hours with the following secondary antibodies, all 1:1000 in D-PBS: Goat-anti-Rabbit-Alexa 488 (ThermoFisher A11034), Goat-anti-Rat-Alexa 594 (ThermoFisher A11007), Goat-anti-Mouse-Alexa 594 (ThermoFisher A11005). Following secondary incubation slides were washed and DAPI Fluoromount-G (SouthernBiotech, 0100-20) was added. Images were taken with an Axio Imager D2 (Carl Zeiss) and digital camera (Axiocam HRm, Carl Zeiss) using the AxioVision software and contrasted using Adobe Photoshop.

PDGFRβ developmental experiments

Pregnant mothers from *PDGFRβ*+/-; *PDGFRβ*+/- matings were monitored for plug formation and sacrificed when the pups were p16.5. Brains were dissected and placed straight into 4% PFA for 4-5 hours after which they were washed, incubated in 30% sucrose, and then frozen in blocks containing 1:2 30% sucrose:OCT. Brain tissue sections of embryonic *PDGFRβ* null mutants, heterozygotes and wild type mice were stained for Col1 and the percent vascular length that was Col1+ was measured using Image J. To study how PDGFRβ levels in adulthood affect perivascular fibrotic protein levels, brain tissue sections from adult *PDGFRβ* f7/- and *PDGFRβ* f7/+ mice were stained for the fibroblast marker ER-TR7 and the vascular smooth muscle marker α smooth muscle actin (as a proxy for large blood vessels) and the percent vascular length positive for ER-TR7 was measured in the cortex and striatum using Image J.

PDGFR *in vitro* experiments

The brain meninges from p2-3 Col1a1GFP mice were dissected and digested with papain for 1 hour at 37^{C}. Following a light mechanical digestion and spin in an ovomucoid solution, the resulting pellet was resuspended in a DMEM-based culture media and plated on 96 well plates

with 10% fetal bovine serum for proliferation and collagen production studies and transwell inserts for migration studies. For the PDGF-BB migration experiments the upper chamber contained DMEM with 0% serum and the lower chamber contained this solution with 20 ng/uL recombinant PDGF-BB or vehicle alone (Sigma srp3229). For the AG1296 experiments the upper chamber contained DMEM with 0% serum and 10 uM AG1296 (abcam ab141170) or vehicle and the lower chamber contained DMEM with 10% serum. After 24 hours the cells on the top of the transwell were scraped, the cells on the bottom were fixed and the number of GFP+ cells on the bottom of the transwell were counted using a fluorescent microscope. To measure collagen production, GFP fluorescence of the cultures with 10% serum and the same concentrations of PDGF-BB, AG1296 or a vehicle was measured with a spectrophotometer as GFP is produced under the control of the collagen promoter. The number of cells was determined by adding 10 uL of the the alamarBlue proliferation reagent (ThermoFisher DAL1025) to each well, incubating the cells for 3 hours and then measuring the fluorescence with an excitation wavelength of 540 nm and emission wavelength of 590 nm.

CHAPTER FOUR:

Generation and characterization of a model of preretinal fibrotic scarring

INTRODUCTION

Fibrosis, or the pathological deposition of extracellular matrix proteins, occurs as a consequence of many common ischemic retinal vasculopathies, including retinopathy of prematurity (ROP) and end-stage proliferative diabetic retinopathy (Friedlander, 2007). Ischemic retinal diseases are characterized by areas of non-perfused retina, leading to aberrant neovascularization and blood vessels that lack the properties of the blood-retinal barrier (Sapieha et al., 2010). Neovascularization occurs on the retinal surface and grows into and along the posterior vitreous cortex (Campochiaro, 2013). These vessels are friable, often resulting in vitreous hemorrhage, and form pre-retinal fibrotic membranes mainly composed of fibrillar collagens (Snead et al., 2008). The fibrovascular membranes have contractile properties, resulting in traction on the underlying retina, which can ultimately result in retinal detachment and blindness (Snead et al., 2008). Although fibrosis is a common cause of visual morbidity, intervention is limited to invasive surgery (El Rayes et al., 2008; Gilbert et al., 1996; Gupta et al., 2012; Meleth and Carvounis, 2014; Mintz-Hittner et al., 1997; Newman, 2010; Repka et al., 2011; Storey et al., 2018; Trese and Droste, 1998). Identifying therapeutic targets to limit pre-retinal fibrosis would be of enormous clinical value and potentially reduce vision loss in many retinal diseases.

The cell type responsible for retinal scar tissue formation is unclear. Some evidence suggests that retinal fibrotic scars originate from retinal pigment epithelial (RPE) cells, which adopt macrophage-like or fibroblast-like functions in response to retinal disease; these cells then migrate to the site of injury and form a scar by producing collagen (Hiscott et al., 1999; Machemer et al., 1978). Although this may contribute to the scarring of proliferative vitreoretinopathy following rhegmatogenous retinal detachment, it is unclear how RPE cells would migrate through the intact retina in the absence of retinal breaks, as is the case in most ischemic retinal diseases.

Other studies suggest that Müller glia cells are activated as a consequence of neovascularization; upon activation, glial cells are thought to proliferate and extend processes to aid in the development of proliferative blood vessels (Friedlander, 2007). These processes are thought to consequently extend to the vitreous where the glial cells produce a scar (referred to as gliosis and a gliotic scar), causing traction and retinal detachment (Friedlander, 2007). In cases of brain and spinal cord injury, a scar of two parts forms in the injury site: an inner fibrotic scar characterized by the deposition of extracellular matrix, and an outer glial scar made of reactive astrocytes (Kawano et al., 2012; O'Shea et al., 2017). This fibrotic layer is paramount as it prevents blood, debris, and toxins from entering the CNS parenchyma, however, it also prevents proper repair since axons cannot grow past the deposited ECM proteins (Fernández-Klett and Priller, 2014b), (Sofroniew, 2009b). It is possible that similar distinct scar layers form in the retina, and that Müller glia are responsible for glial scarring while another cell type forms the fibrotic scar. In these cases of brain and spinal cord injury, pericytes have been shown to upregulate collagen following injury and form the fibrotic scar (Dias et al., 2018; Göritz et al., 2011). However, resident CNS fibroblasts associated with the meninges and large vessels were found in a single-cell sequencing study of the CNS vasculature, and have also been suggested to contribute to fibrotic scar formation (Soderblom et al., 2013; Vanlandewijck et al., 2018). It is unclear whether resident fibroblasts are found in the retina. In an original single-cell sequencing study of the retina, fibroblasts were picked up in a couple of samples, but were described as contamination (Macosko et al., 2015).

In order to study pre-retinal fibrosis, a reproducible disease model in mice that reliably produces scarring is needed. One common model of ischemic vasculopathy, including ROP, is oxygen-induced Retinopathy (OIR) in rodents (Smith et al., 1994). To mimic the high oxygen environment given to premature babies, neonatal mice are exposed to 75% oxygen in an enclosed

chamber from postnatal day 7 (P7) until P12, when they are returned to room air (21% oxygen). The hyperoxia results in vaso-obliteration that recapitulates avascular retina in ischemic retinal vasculopathies. Once returned to room air, these avascular areas experience relative hypoxia which leads to pathological neovascularization. However, in OIR the neovascularization regresses and a functional capillary bed forms in the areas of vaso-obliteration. Hence, this traditional mouse model of OIR does not result in the clinically-severe pathological pre-retinal fibrotic scarring that occurs in humans (Gupta et al., 2012; Lajko et al., 2016b; Selvam et al., 2018; Trese and Droste, 1998). It is well known that earlier pre-term birth and longer duration of oxygen supplemented are risk factors for progressive ROP (Aiello et al., 1995; Cayabyab et al., 2016; Hellström et al., 2009; Lajko et al., 2016b; Selvam et al., 2018). Therefore, we hypothesized that in mice exposed to hypoxia earlier and longer than in the standard mouse model of OIR, the phenotype may be more severe and result in persistent neovascularization, and subsequent pre-retinal fibrosis.

Here, we designed specific exposure conditions to reliably reproduce fibrotic scars in the retina based on the OIR model, which we refer to as long OIR, or l-OIR. Using this model, we performed single-cell sequencing of the scar forming cells to implicate that that pericytes are the main scar-forming cells in a model of ischemic retinal disease.

RESULTS

Col1a1GFP expression drops throughout development in healthy mouse retinas

To determine the extent of collagen expression in the retina throughout development we collected fixed retinas from Col1a1GFP mice at various postnatal time points and characterized GFP expression. GFP expression increased until P7, then declined precipitously in non-disease retinas (Fig 1). GFP expression also became concentrated in specific layers over time, such as the

inner nuclear layer (INL) and nerve fiber layer (NFL), suggesting cells in these layers have the highest potential for fibrotic scar formation. By P14, GFP expression in the retina was limited to the INL and NFL and decreased in intensity as the mice age.

l-OIR mice display robust neovascularization at P30

To investigate the effect of l-OIR on vascular development in the mouse retina, we performed l-OIR on Col1a1GFP+ mice and compared their vascular pathology to Cola1GFP+ mice with traditional OIR and Col1a1GFP+ mice in a normoxic environment. For l-OIR experiments mice were placed in 75% oxygen from p2 to p16 to mimic the conditions of a pre-term birth (Fig 2A). In both P25 OIR and normoxic P25 and P30 control retinas, deep, intermediate and superficial blood vessels spanned full retinal area. As expected, P25 OIR retinas did not contain areas of vasoobliteration or neovascularization (Connor et al., 2009; Lajko et al., 2016a; Selvam et al., 2018; Smith et al., 1994). In P30 l-OIR retinas, however, abundant neovascular buds continued to persist at P30 and the vascular layers were disrupted (Fig 2B,C). Together, these observations indicate that the l-OIR model causes more severe pathology that is sustained at later developmental time points than OIR in mouse retinas.

Scar production and increased Col1a1GFP expression are present in l-OIR mouse retinas

To determine if the l-OIR model leads to pre-retinal fibrotic scarring, we analyzed both whole retina eyecups and sections for the presence of collagen protein and Col1a1GFP+ cells. In retinal eyecups from l-OIR mice, an extensive collagen-positive fibrotic plaque spanned the majority of the retinal surface (Fig 3C). In retinal tissue sections from l-OIR mice, we saw collagen 1 deposition in the NFL surrounding Col1a1GFP+ cells that were absent in the control mice (Fig 3B). GFP expression significantly increased in both the NFL and the INL in l-OIR retina sections

relative to age matched normoxic controls (Figure 3D), demonstrating induction of collagen 1 protein production and fibrotic scarring in response to l-OIR.

Pericyte, Fibroblast and Müller glia markers colocalize with GFP+ cells in l-OIR retinas

To determine the identity of the Col1a1GFP+ cells in l-OIR, we immunostained control and l-OIR retina tissue sections for markers of pericytes (NG2), fibroblasts and pericytes (PDGFRβ), Müller glia (SOX9), and retinal pigment epithelium (Stra6), as past studies suggest both retinal pigment epithelial cells and Müller glia produce scar tissue in the retina(Friedlander, 2007; Hiscott et al., 1999; Machemer et al., 1978), and that pericytes and/or fibroblasts play roles in fibrosis in other CNS locations (Dias et al., 2018; Göritz et al., 2011; Soderblom et al., 2013). The majority of inner nuclear layer Col1a1GFP+ cells colocalized with the Müller glia marker Sox9, and the majority of NFL Col1a1GFP+ cells colocalized with the pericyte and fibroblast marker PDGFRβ and to a lesser extent the pericyte marker NG2 (Fig 4). Hence, the collage 1 fibrotic tissue deposition at the NFL may originate from fibroblast or pericytes.

Single-cell sequencing of the retina in health and l-OIR reveals collagen-expressing cells express pericyte marker genes

To further characterize the identity of the cell types expressing collagen in l-OIR, we performed single-cell sequencing on Col1a1GFP+ cells from healthy and l-OIR retinas and analyzed all clusters exhibiting collagen I expression. The healthy and l-OIR retinas displayed significant overlap (Figure 5A). Comparison to other transcriptomic databases of the retina and CNS vasculature were used to define the likely cell type of each of the clusters, revealing the presence of pericytes, various neuron populations, and Müller glia (Macosko et al., 2015; Roesch et al., 2008; Vanlandewijck et al., 2018) (Figure 5B-H, S1). Interestingly, we did not observe perivascular fibroblasts present in the retina in health or following l-OIR. In general, the Müller

glia clusters decreased in proportion of total cells from control to l-OIR while the neuron and pericyte clusters increased in total proportion (Figure 6A). Collagen expression was restricted mainly to the cells in cluster i, the cluster expressing mainly pericyte and some smooth muscle markers. Further analysis of this cluster identified distinct regions corresponding to pericytes and smooth muscle cells. *Col1a1* expression was restricted to pericytes while *Col1a2* expression was found in both cell types but higher in proportion in pericytes (Figure S2). Sporadic collagen expression was found throughout the Müller glia and neuronal cell clusters, indicating that while the cells had enough reporter expression to be sorted by FACS, collagen I mRNA was expressed at very low levels (Figure 5C, S1). This suggests that the cells actively secreting extracellular matrix proteins have a transcriptomic profile of pericytes.

DISCUSSION

We developed the l-OIR model to generate a more severe model of ROP than traditional OIR that mimics earlier term pregnancies and the severe, chronic pathology of the disease. We chose to expose mice pups to high oxygen levels at P2 both to model a premature birth and because our data showed that during the first 6 weeks of development, the overall area of the retina that is Col1a1GFP+ decreases. This decrease in retinal collagen expression may indicate that younger pups are more vulnerable to robust scarring, consistent with clinical experience in humans (Hellström et al., 1991). This would be in contrast to many peripheral tissues where the likelihood of fibrotic scarring increases with age (Murtha et al., 2019).

l-OIR retinas exhibit extensive and persistent neovascular budding, followed by the presence of a plaque-like scar on the surface of the retina at postnatal day 30. Therefore, the l-OIR model more closely resembles the phenotype of ischemic retinal diseases in humans, such as

advanced ROP and DR, and could be used to evaluate therapeutic targets to reduce retinal fibrotic scarring. The exact time point during l-OIR where fibrotic scarring begins, and whether or not the fibrotic scarring persists past P30 remain unknown.

Potential candidates for the origin of the pre-retinal fibrotic scar include fibroblasts, pericytes, Müller glia and RPE cells. Here, we analyzed l-OIR tissue for overlap of Col1a1GFP+ cells with markers specific to these cell types. Interestingly, we saw colocalization of different cell-specific markers in different retinal layers. In the NFL, where we see the most collagen protein expression, we mainly see colocalization of the Col1a1GFP with PDGFRβ and to a lesser extent NG2, both pericyte markers, suggesting that pericytes could be responsible for scar production in the retina. Because fibroblasts also express PDGFRβ, they may also be contributing to scar formation.

In the INL, however, we mainly see colocalization of the Müller glia marker Sox9 with the Col1a1GFP reporter, suggesting that Müller glia cell bodies express collagen 1. Previous studies imply that Müller cells play a role in scar formation in the retina, commonly referred to as gliosis (Bringmann et al., 2009; Bringmann et al., 2006). These studies suggest that Müller glia undergo hypertrophic growth in disease and extend their glial processes on the surface of the retina. In the brain and spinal cord fibrosis and gliosis are two separate processes, with an inner fibrotic scar in the injury core surrounded by a glial scar made up of reactive astrocytes (Kawano et al., 2012; O'Shea et al., 2017). Müller glia may extend processes to the surface of the retina to form a glial scar in l-OIR, and these processes could also secrete collagen proteins to contribute to the fibrotic scar.

Single-cell sequencing of Col1a1GFP+ cells from healthy and l-OIR retinas revealed that cells that highly express collagen genes also express pericyte-specific markers. The pericyte cluster

also increased in proportion from health to l-OIR, which could suggest either pericyte proliferation or collagen reporter upregulation following hyperoxia. Müller glia and neuronal-like cells were FACS sorted as GFP+ but did not express many detectable copies of the *Col1a1* or *Col1a2* genes, suggesting they express collagen at low enough levels to turn on the reporter, but likely not levels that significantly contribute to scarring. While Müller glia could be playing a small role in fibrotic, and more likely glial, scar formation, our data suggests that pericytes are the major drivers of pre-retinal fibrosis. It remains possible that another cell population has trans-differentiated following l-OIR into pericyte-like cells. Future genetic lineage tracing studies could confirm the pericyte origin of retinal scar tissue.

We were surprised that our dataset did not contain perivascular fibroblasts, as these cells have been implicated in fibrotic scar formation in the brain and spinal cord (Kelly et al., 2016; Soderblom et al., 2013). It is possible that modeling fibrotic scarring in the mouse retina has traditionally been difficult due to the lack of these cells, and that perivascular fibroblasts are found in the retinas of species more prone to scarring, such as humans. This could be tested through a single-cell sequencing study of human postmortem retinas.

FIGURES

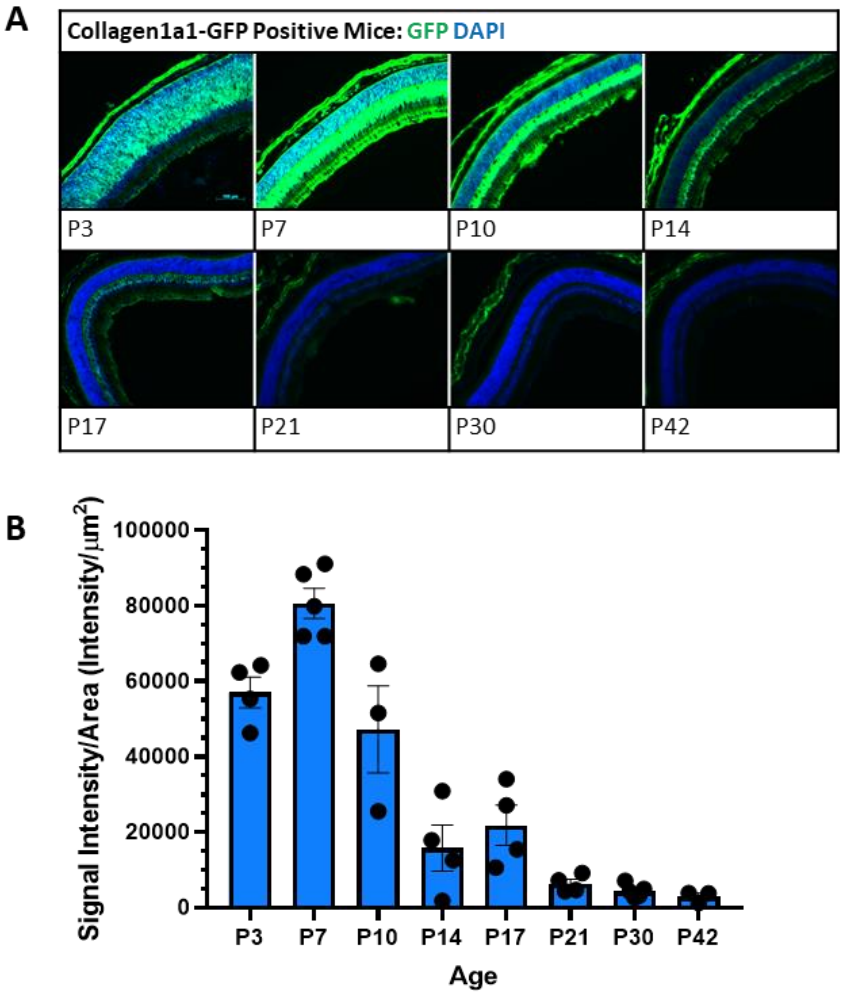

Figure 4.1: Collagen1a1-GFP expression in the retina throughout development. A. Col1a1GFP+ mouse retinas were sectioned into 10μm slices, stained for DAPI and imaged for DAPI and GFP fluorescence at a fixed exposure time. B. GFP expression per total retina section was quantified and increases from P3 to P7, then decreases with time. Scale bar is 100μm. Error bars represent SEM. n = 3-4 per time point.

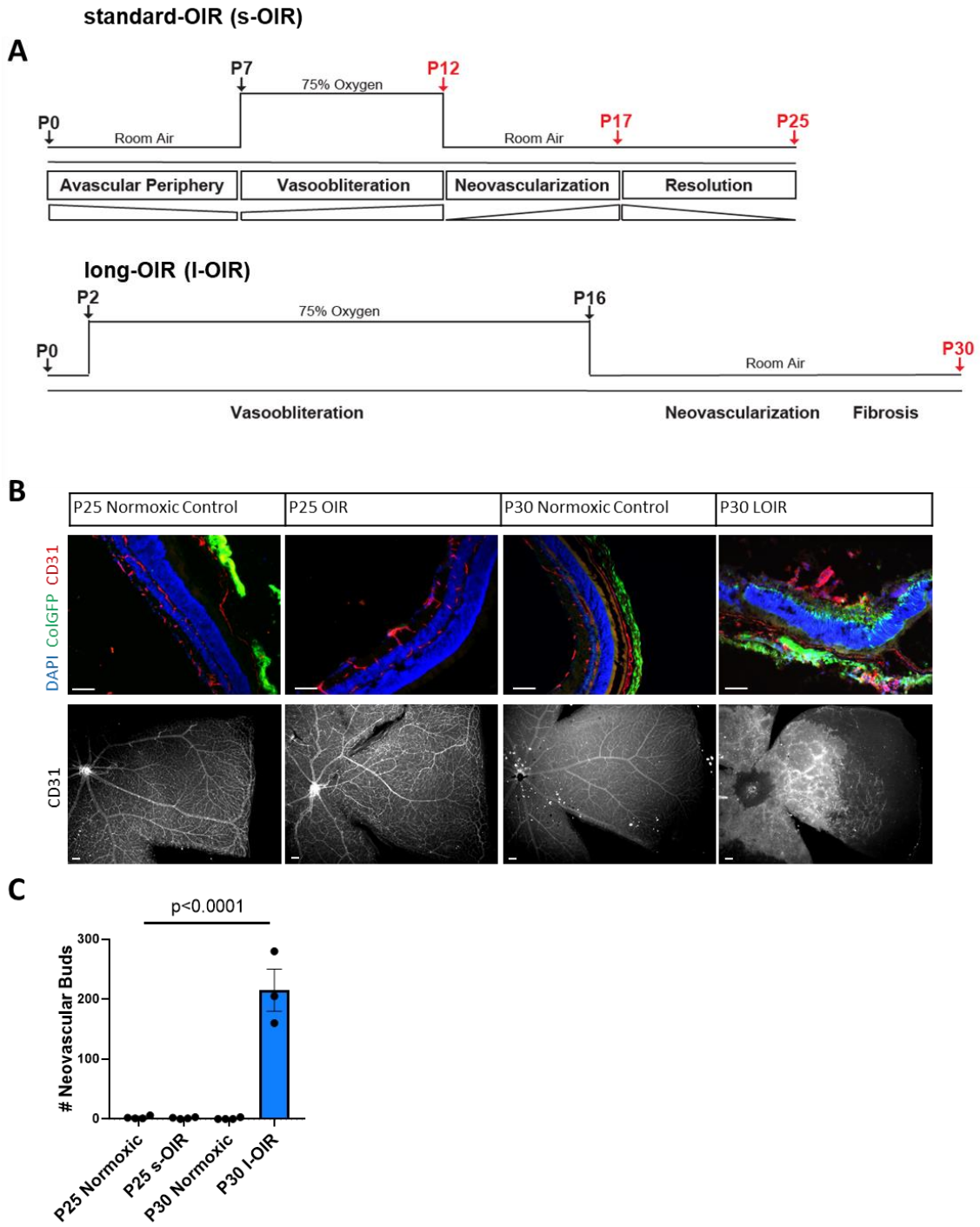

Figure 4.2: Vascular pathology in l-OIR retinas. A. Protocol for OIR and l-OIR. The standard tissue collection points for s-OIR and the tissue collection point used here for l-OIR are labeled in red. The stages of retinal pathology for s-OIR are boxed below the s-OIR timeline and the hypothesized stages of pathology for l-OIR are labeled below the l-OIR timeline. B. s-OIR, l-OIR and control retina sections from Col1a1GFP mice (top) or flatmounted retinas (bottom) were stained for CD31 to demonstrate the formation of neovascular buds in l-OIR but not control retinas, quantified per leaflet in (C). Error bars signify SEM, scale bar is 100µm. n = 3-4 per time point.

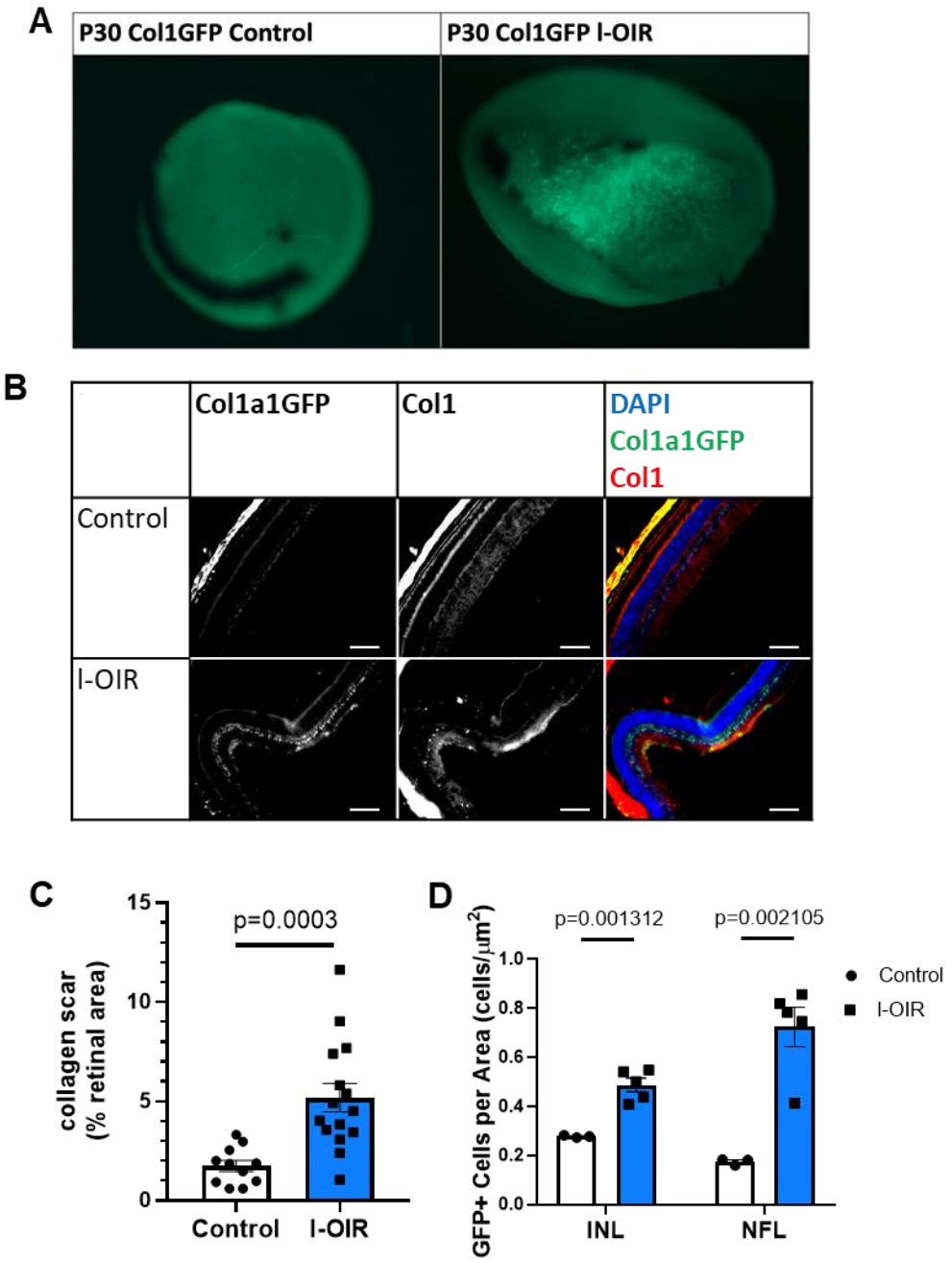

Figure 4.3: Collagen scar pathology in l-OIR retinas. A. Fixed and dissected Col1a1GFP+ retinas were imaged under a dissecting microscope to visualize GFP+ cells. B. Control and l-OIR retina sections from Col1a1GFP+ mice were stained for collagen in red, and the percentage of the collagen scar relative to the retinal area is quantified in (C), n = 12 control and 15 l-OIR. D. l-OIR and control retinas were sectioned and quantified for GFP+ cells in the INL and NFL, n = 3-5 per condition. Error bars signify SEM, scale bars are 100μm.

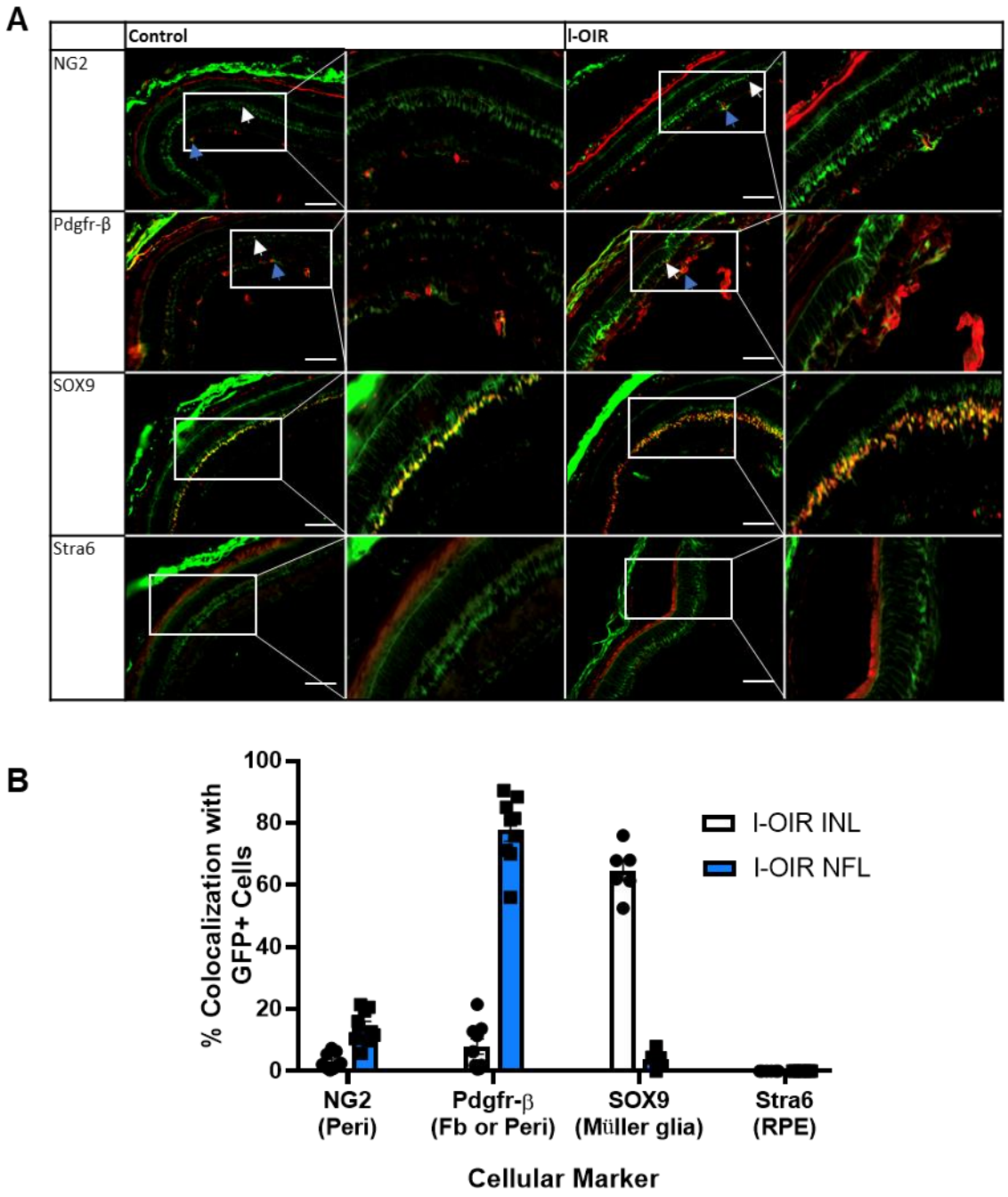

Figure 4.4: Colocalization of cellular markers with Col1a1GFP+ cells in l-OIR retinal sections. A. Control and l-OIR retinal sections from Col1a1GFP mice were stained for a pericyte marker (NG2), a fibroblast and pericyte marker (PDGFRβ), a Müller glia marker (SOX9), and a retinal pigment epithelium marker (Stra6) in red with the GFP reporter in green. In the top 2 rows the NFL is marked by blue arrows and the INL with white arrows. B. Quantification of colocalization in the images from (A), we see the majority of GFP positive cells in the INL are SOX9 positive, however, the majority of NFL GFP positive cells colocalize with PDGFRβ or NG2. Error bars signify SEM, scale bar is 100µm, n = 3-9 per condition.

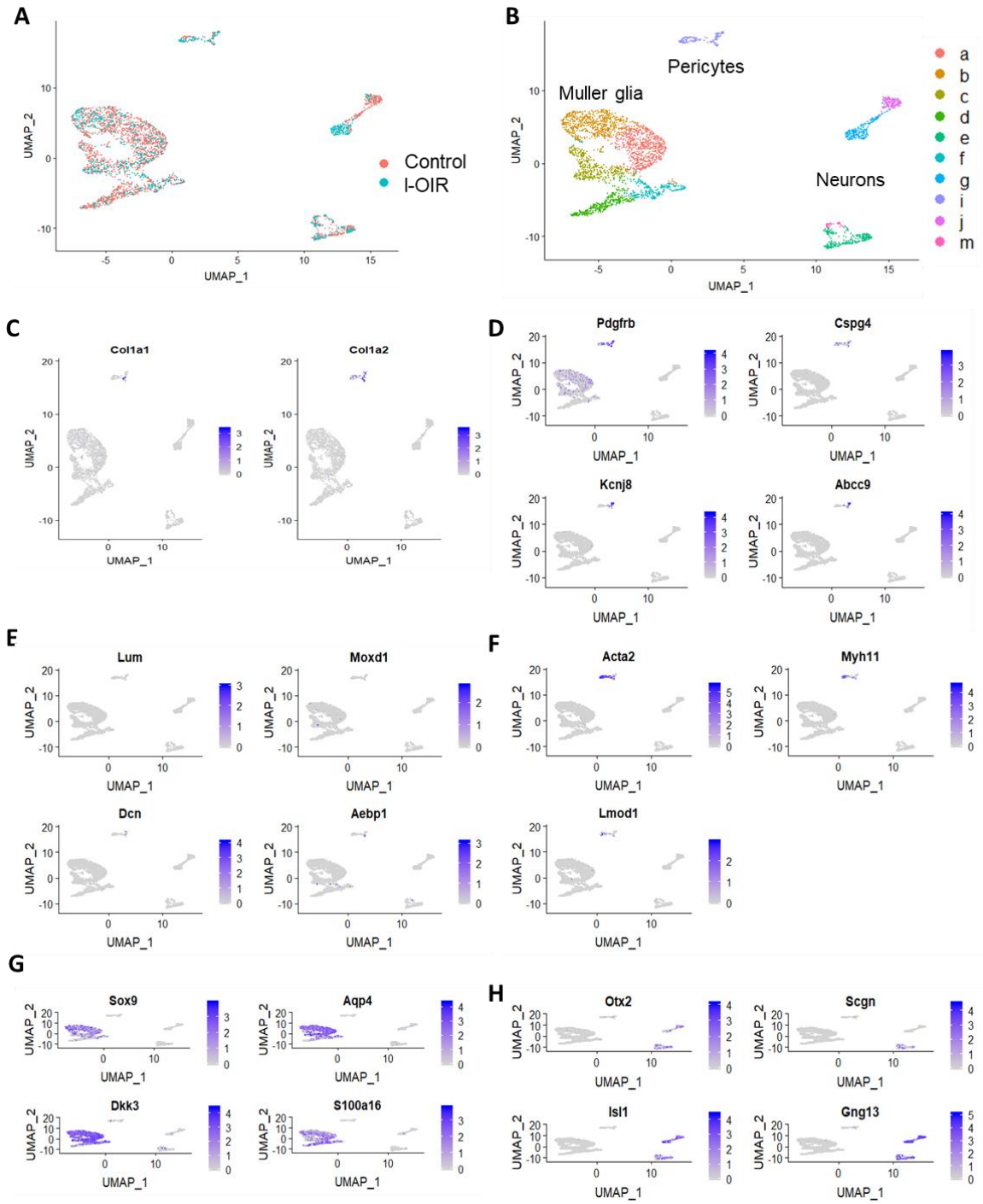

Figure 4.5: Single-cell sequencing of Col1a1GFP+ cells from control and l-OIR retinas suggests that pericytes are the scar-forming cells. A. UMAP plot of Col1a1GFP+ cells sorted from control and l-OIR retinas showing overlap of the 2 samples. B. UMAP plot of the cells colored by the different cluster and labeled with the cell type identity of each cluster. C-E. Feature plots of the expression levels of collagen I genes (C), pericyte-specific genes (D), fibroblast-specific genes (E), smooth muscle-specific genes (F), Müller glia-specific genes (G), and retinal neuronal-specific genes (H).

A

Cluster	Control cell #	% Control	LOIR cell #	% LOIR	Identity
a	568	25.5	161	16.6	MG
b	435	19.5	181	18.6	MG
c	278	12.5	101	10.4	MG
d	290	13.0	58	6.0	MG
e	174	7.8	99	10.2	Neuron
f	160	7.2	96	9.9	MG
g	91	4.1	150	15.4	Neuron
i	69	3.1	89	9.2	Pericyte
j	138	6.2	18	1.9	Neuron
m	28	1.3	18	1.9	Neuron

B

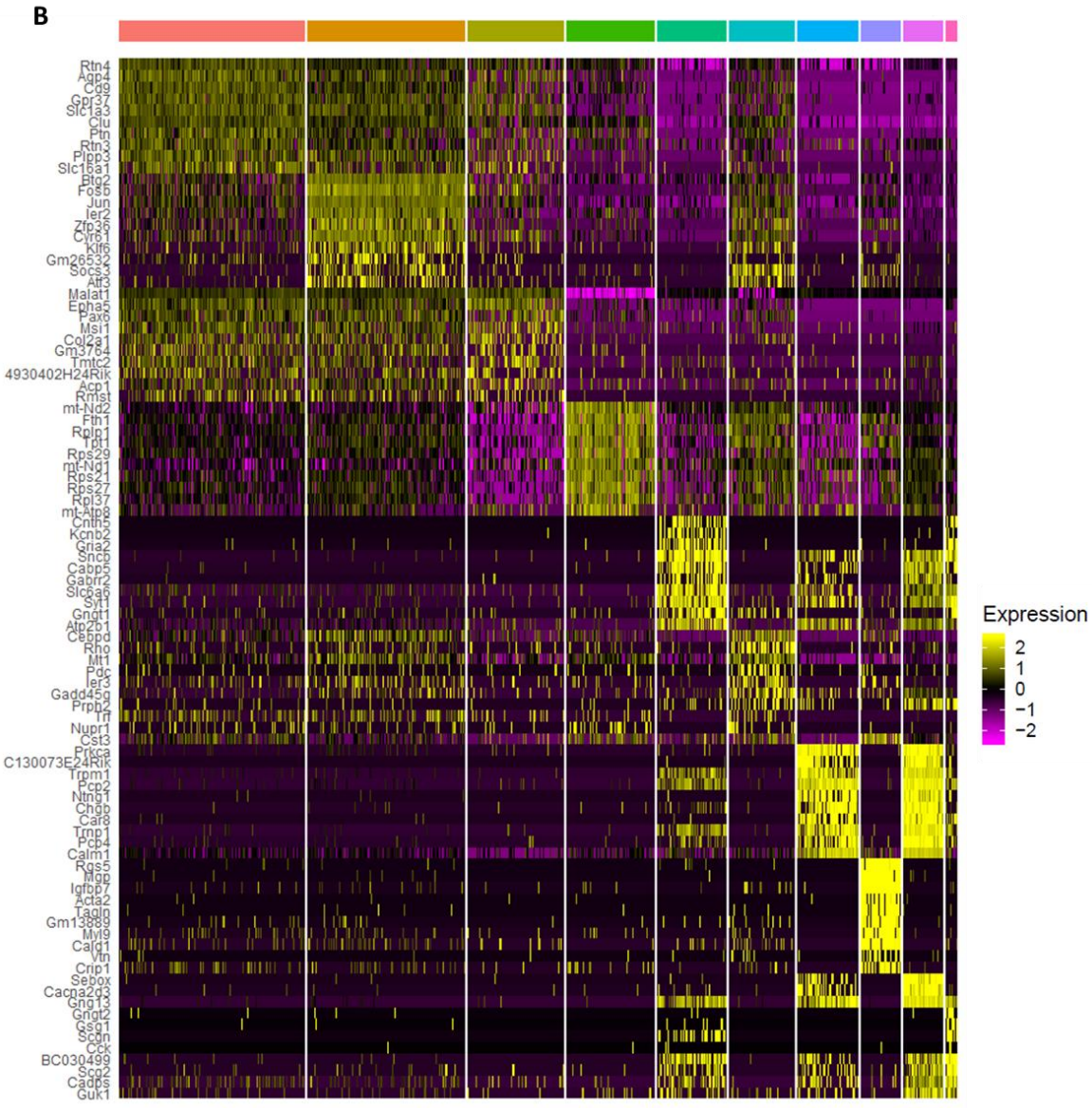

Figure 4.6: Single-cell sequencing cluster analysis. A. Table of the number of cells per cluster, the percentage of the total number of cells for health and l-OIR that corresponds to each cluster, and the identity of each cluster (MG = Müller glia). B. Heat map depicting the top 10 differentially expressed genes per cluster.

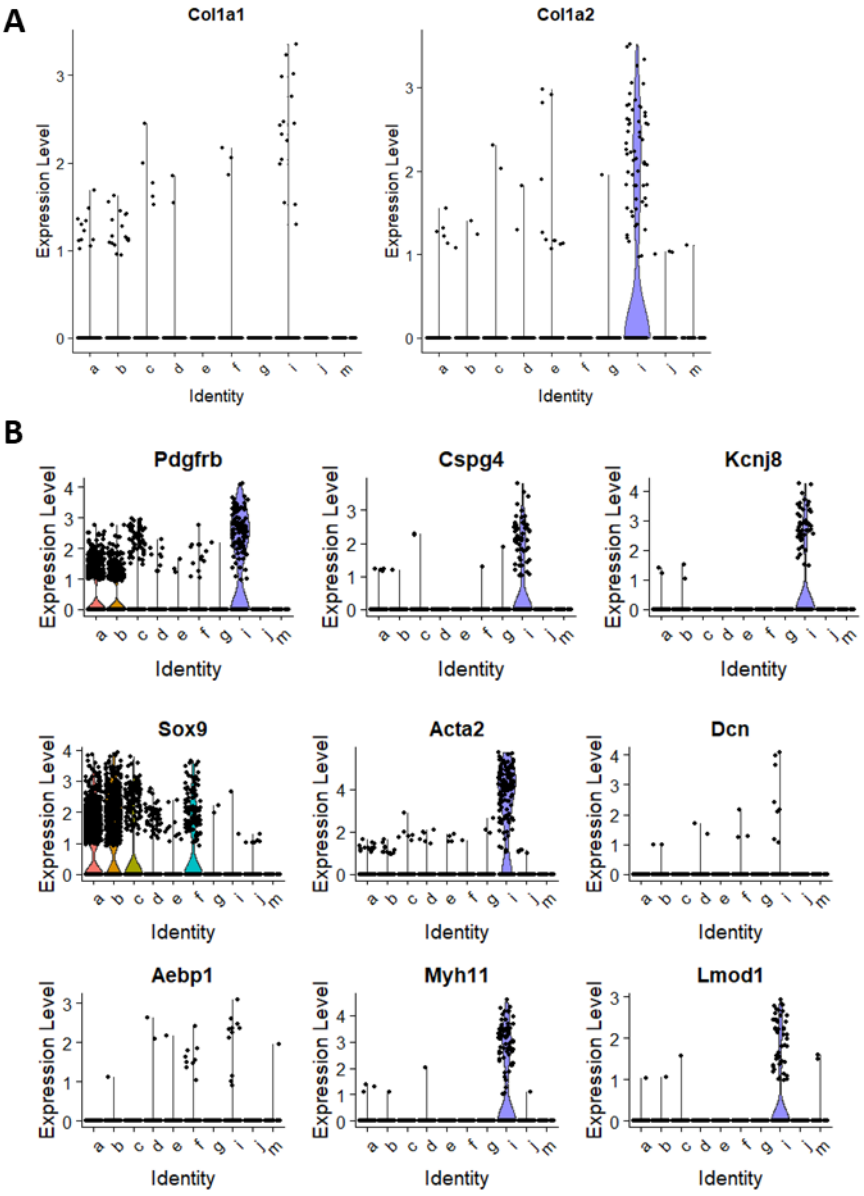

Figure 4.S1: Cell-specific marker expression in the single-cell sequencing dataset. Violin plots of the expression levels and probability densities of collagen I genes (A) and genes specific for pericytes (*Cspg4, Kcnj8*), Müller glia (*Sox9*), vSMCs (*Myh11, Lmod1, Acta2*) and fibroblasts (*Dcn, Aebp1*) (B).

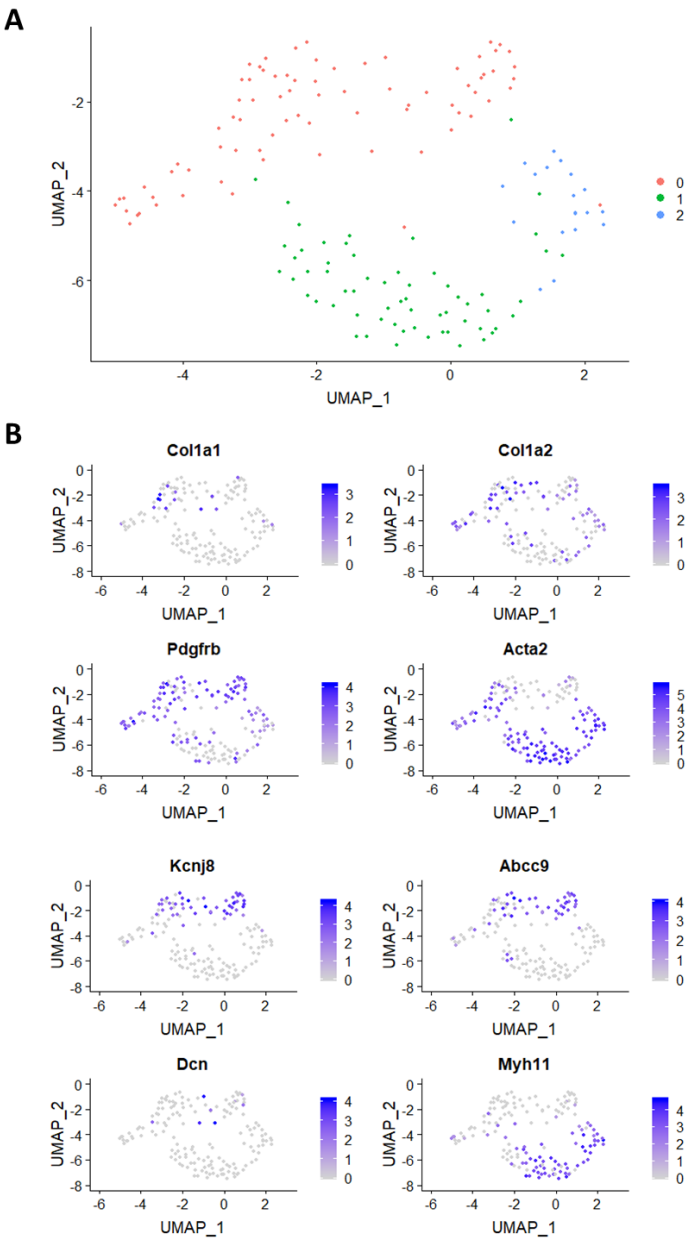

Figure 4.S2: Detailed analysis of cluster i. A. UMAP plot of the re-clustering of original cluster i. B. Feature plots depicting the expression levels of collagen I genes and genes specific for pericytes (*Kcnj8*, *Abcc9*), vSMCs (*Acta2*, *Myh11*), and fibroblasts (*Dcn*) throughout cluster i.

MATERIALS AND METHODS

Animals

Col1a1GFP+ mice were obtained from David Brenner and maintained in the UCSD BSB animal facility. These mice have a C57/Bl6 background and express GFP under control of the collagen promoter.

Reagents

1xDPBS used in the following experiments is Ca^{2+} and Mg^{2+}- free (Thermo Fisher Scientific, Waltham, MA, USA), unless specified otherwise.

4% PFA for tissue fixation was prepared from 32% PFA (Electron Microscopy Sciences, Hatfield, PA, USA) diluted in DPBS and kept at 4°C for maximum one week. Used PFA was disposed of in accordance to the Environment Health and Services (EH&S) guidelines.

Permeabilizing-blocking solution (Perm-Block) was prepared by dissolving 0.2% of bovine serum albumin powder (BSA – Sigma-Aldrich, St Louis, MO, USA), 0.3% of Triton X-100 (Thermo Fisher Scientific, Waltham, MA, USA) and 5% of normal goat serum (NGS) (Life Technologies, Carlsbad, CA, USA) in DPBS.

Ketamine-Xylazine anesthesia solution was prepared by combining Ketamine (MWI/Vetone, Boise, ID, USAbrand) and Xylazine (MWI/Vetone, Boise, ID, USA) to a final concentration of 4mg/mL Ketamine and 0.6mg/mL Xylazine in sterile clinical-grade saline solution (MWI/Vetone, Boise, ID, USA).

30% Sucrose solution was prepared by dissolving sucrose (Sigma Aldrich, St. Louis, MO, USA) in 1xPBS.

Mouse model of Oxygen Induced Retinopathy (OIR)

The mouse OIR model was performed as described (Smith et al., 1994). Briefly, pups and their nursing mothers were placed in a sealed 75% oxygen chamber (Biospherix, Parish, NY, USA) at postnatal day 7 (P7) and monitored daily. The mice were removed from the chamber at postnatal day 12 (P12) and placed in room air until tissue was collected.

Mouse model of Long Oxygen Induced Retinopathy (l-OIR)

Pups and their nursing mothers were placed in a sealed 75% oxygen chamber (Biospherix, Parish, NY, USA) at postnatal day 2 (P2) and monitored daily. Every two days, the nursing mother mouse would be switched with a normoxic nursing mother mouse to minimize oxygen toxicity. The mice were removed from the chamber at postnatal day 16 (P16) and placed in room air until tissue was collected.

Perfusion

Pups were anesthetized with 1 ml of Ketamine-Xylazine (4mg/mL Ketamine and 0.6mg/mL Xylazine) 10 minutes before perfusion. The thoracic cavity of the mice was opened and the right atrium was clipped. The animals were then perfused through the left ventricle of the heart with sterile DPBS for 2 minutes, at a speed of 4.5 ml/min, using the Dynamax RP-1 peristaltic pump (Mettler Toledo-Rainin, Oakland, CA), followed by perfusion with 4% PFA for 8 minutes at the same speed. Finally, the mice were washed with DPBS for 1 minute. The globes were then enucleated and post-fixed for 10 minutes in 4% PFA. One globe from each mouse was placed in DPBS for retina dissection, and the other globe was placed in a 30% sucrose solution for sectioning.

Fluorescent dyes and Antibodies

The following fluorescent dyes and antibodies were used for immunostaining: Col1 abcam ab21286, CD31 BD Biosciences 553370, PDGFRb eBioscience 14-1402-82 clone APB5, Sox9

R&D Systems AF3075, NG2 EMD Millipore MAB5384, Stra6 Abgent AP9433b, Goat-anti-Rabbit-Alexa 594 ThermoFisher R37117, Goat-anti-Rat-Alexa 594 ThermoFisher A11007, Donkey-anti-Goat-Alexa 594 ThermoFisher A11058. All antibodies were used at a dilution of 1:500.

Retinal flat mounts and immunostaining

Following fixation, globes were rinsed once in DPBS. The whole retina was dissected in a 35x10mm petri dish (Becton Dickinson Labware, Franklin Lakes, NJ, USA) filled with DPBS under a dissecting microscope using two #5 forceps (FST by Dumont, Switzerland) and a 27G needle (BD Biosciences, San Jose, CA, USA). To generate flatmounts, four short radial incisions were made using Vannas Spring Scissors (Fine Science Tools, Inc., Foster City, CA, USA). Once opened, one retina was placed per well in a 24-well plate (Corning, Corning, NY, USA) wrapped in an aluminum foil to prevent fluorescence decay, and blocked for 1 hour in Perm-Block (200µl/well) at room temperature on an orbital shaker. Next, the retinas were placed in 200µl/well of fresh DPBS with primary antibodies added at 4°C on a shaker overnight. The retinas were then washed 4 x 10 minutes, and placed in 200µl/well of DPBS with secondary antibodies at 4°C overnight. After the secondary antibody staining, retinas were washed 4 x 15 minutes and laid flat on a 25x75x1mm microscopy slide (VWR, Randor, PA, USA), with the inner side of the retina facing up. Retinas were mounted using the Vectashield mounting medium with DAPI (Vector Laboratories Inc., Burlingame, CA, USA), and covered with a thin glass coverslip (VWR, Randor, PA, USA). The slides were dried for 10 minutes in the dark, then sealed using nail polish (Electron Microscopy Sciences, Hatfield, PA, USA), and imaged using a Zeiss Imager D2 fluorescence microscope (Carl Zeiss AG, Oberkochen, Germany) equipped with the AxioVision software (Carl Zeiss AG, Oberkochen, Germany).

Retinal Sectioning and immunostaining

Whole globes from the 30% sucrose solution were frozen in Optimal Cutting Temperature (OCT) Compound (Sakura Finetek USA, Inc., Torrance, CA, USA) and sectioned into 10μm sections using a croyostat. These sections were placed on a 25x75x1mm microscopy slide (VWR, Randor, PA, USA) for immunostaining. The sectioned retinas were circumscribed with an ImmEdge pen (Vector Laboratories, Inc. Burlingame, CA, USA) and were placed in Perm-Block for 30 minutes at room temperature, with the exception of slides stained with Sox9 which were blocked in a solution of 0.2% Triton-X 100, 10% Normal Donkely Serum in DPBS. Perm-Block was removed with a vacuum, and the retinas were placed in Perm-Block with primary antibodies overnight at 4℃. The next day, the Perm-Block with primary antibodies were removed with a vacuum and the retinas were washed three times for 10 minutes each was with 0.1% Triton-X 100 in DPBS. The sections were then placed in 0.1% Triton-X 100 in DPBS with secondary antibodies added and left overnight to stain at 4℃. After the secondary antibody staining, retinas were rinsed four times for 15 minutes, twice with 0.1% Triton-X 100 in DPBS, then twice with just DPBS. Sections were mounted using the Vectashield mounting medium with DAPI (Vector Laboratories Inc., Burlingame, CA, USA), and covered with a thin glass coverslip (VWR, Randor, PA, USA). The slides were dried for 10 minutes in the dark, sealed using nail polish (Electron Microscopy Sciences, Hatfield, PA, USA) and imaged using a Zeiss Imager D2 fluorescence microscope (Carl Zeiss AG, Oberkochen, Germany) equipped with the AxioVision software (Carl Zeiss AG, Oberkochen, Germany).

ImageStudioLite Analysis

Retinal sections for the development time course study were analyzed in ImageStudioLite by circumscribing the entire retinal tissue with the freehand drawing tool using DAPI as a guideline

and using a green color filter to analyze the GFP fluorescence intensity (images taken at the same exposure time were used for this analysis). The intensity was then normalized by the total area for each retina analyzed.

ImageJ Analysis of l-OIR Tissue Sections

Retinal sections were analyzed in ImageJ for the l-OIR analyses. To determine the percentage of the retina that was affected by a collagen scar, the entire retina would be outlined using DAPI as a guideline. Collagen in the NFL was then outlined and the collagen+ area was divided by the area of the total retina. To determine the number of GFP+ cells per retinal layer, freehand selections were used to circumscribe the INL and NFL using DAPI to obtain the total area of these layers. The multipoint tool was used to count the number of GFP positive cells in each layer, which was then normalized to the area of that layer. The normalized counts were averaged in RStudio. A two-tailed T-test was performed comparing the significance between each layer analyzed. To determine the colocalization of the GFP marker with other cellular markers, images stained for these markers were uploaded into Image J and the total number of GFP+ cells in the INL and NFL were counted as described above. Then, the number of GFP+ cells in each layer positive for the different cellular markers was counted and divided by the total number of GFP+ cells in that layer.

Tissue Dissociation and FACS Sorting

To obtain single cell suspensions of collagen-producing cells in the retina, retinas from p30 Col1a1GFP normoxic mice, or mice exposed to l-OIR, were dissected, grossly chopped with a #10 blade and enzymatically dissociated with papain (Worthington Cat no. LS003127, 100 uL per sample) containing DNase (125 U/ml, Worthington LS002007) for 1 hour in a cell culture incubator at 35°C. Following the incubation the samples were mechanically triturated in a solution

containing ovomucoid (2 mg/ml, Roche 109878) and DNase (125 U/ml). The samples were spun down and re-suspended in buffer containing DAPI, and live, Col1-expressing cells were FACS sorted into dPBS + 0.05% BSA based on GFP fluorescence using an ARIA II sorter at the Flow Cytometry Core at the VA Hospital in La Jolla, CA. Forward scatter and side scatter gating was used to limit the sorting to single live cells.

Single-cell sequencing

Tissue was dissociated and FACS sorted as described above. 1 sample was collected of each of the p30 control and l-OIR group, each containing both retinas from 4 mice. Following FACS sorting, the single cell suspension was run through the 10X Genomics pipeline (v3) at the UCSD IGM Core and sequenced on an Illumnia HiSeq4000. The sequencing files were run through the 10X CellRanger 3.0.2 pipeline to align the data to a reference genome and generate counts files, and then analyzed using Seurat v3. Both samples were merged tougher and in all analyses a 200 non-zero genes cut-off was used. We next filtered out 3 clusters with no Col1a1 or Col1a2 expression and the remaining cells were analyzed using unbiased clustering where the resolution parameter of clustering was set to 0.5. The Wilcox method was used for differential expression analysis where the min.pct = 0.25 and logfc.threshold = 0.25.

Statistics

The *n* values used for each experiment are described in the figure legends. T-tests were used for statistical analyses unless otherwise noted and all error bars presented are ± standard error of the mean.

Data Availability

The single-cell sequencing raw data files have been uploaded to SRA and will be made public before the time of publication. Reviewer access codes can be provided if requested.

ACKNOWLEDGEMENTS

Chapter 4, in part, is currently being prepared for submission for publication of the material. Miller J, Dorrier CE, Daneman R, Nudleman E. The dissertation author was the primary investigator and author of this material.

CHAPTER FIVE:

Scientific discussion on the roles and functions of CNS fibrosis and fibroblasts

While only found in small numbers in the CNS parenchyma, CNS fibroblasts have been shown to contribute in important ways to CNS development and disease pathology, progression and recovery. Their role in contributing to CNS fibrosis makes them important drug targets for neurological diseases and conditions.

CNS fibroblasts form a fibrotic scar in response to neuroinflammation

We have shown that a robust fibrotic scar forms following neuroinflammation. In the EAE model of neuroinflammation we illustrated using lineage tracing studies that the fibrotic scar arises from the proliferation of CNS fibroblasts and not pericytes or bone marrow-derived cells, although the relative contribution of fibroblasts in the meninges and perivascular spaces remains unknown. This is an especially intriguing question in inflammation where there may not be physical damage to the pial/glial barrier, as opposed to physical injury, where meningeal barriers could be damaged and provide meningeal fibroblasts easy access to injury sites. This data is in contrast to studies that suggest that pericytes are responsible for CNS fibrotic scar formation, and has important implications for the treatment of CNS disorders with fibrotic scarring.

It is possible that different cell types form the fibrotic scar following different triggers, where different signaling mechanisms are upregulated in the perivascular spaces. We have shown here that fibroblasts are the predominant origin of the scar following neuroinflammation, but a different cell type such as pericytes, or combinations of fibroblasts and pericytes, could be activated to upregulate collagens following hypoxia or an injury. It is also a possibility that CNS fibroblasts form the fibrotic scar following all triggers in tissues where they are present. We hypothesize that this scenario is more likely as the Type A pericytes that have been identified as the scar-forming cells in spinal cord injury have never been identified by single-cell sequencing

studies, and may actually be CNS fibroblasts. They were identified as pericytes by the expression of PDGFRβ and their location in the perivascular space, but fibroblasts also share these characteristics. Either way, the lineage tracing experiments here should be repeated under cases of CNS injury and hypoxia.

We next demonstrated that reducing fibroblast proliferation and therefore scar formation in EAE using a fibroblast-specific expression of the herpes thymidine kinase led to a modest EAE motor symptom decrease and an increase in oligodendrocyte lineage cells in inflammatory, demyelinating lesions. We saw no overall changes in myelination as there were severe reductions in healthy axon numbers in our EAE model, but hypothesize that in a less severe inflammatory demyelinating model that the increase in oligodendrocyte availability in lesions caused by reducing scar formation would lead to higher levels of remyelination and even greater changes in disease recovery. Our method of reducing scar formation was not perfect, and many of the remaining collagen protein in our model was located around blood vessels. It is possible that this perivascular fibrosis is especially detrimental as it could hinder blood flow and deprive local neurons of necessary nutrients. The impact of perivascular fibrosis specifically should continue to be studied *in vitro* and *in vivo*, and methods for reducing perivascular fibrosis should be tested in a variety of CNS disease models.

Additionally, we showed that interferon gamma signaling contributes to CNS scar formation, although blocking this signaling in fibroblasts does not disrupt scar formation to an extent that leads to significant changes in EAE motor scores. To attempt to discover a mechanism that is required for CNS scar formation and impacts disease outcomes, we also tested the roles of numerous other signaling pathways in CNS fibrosis following EAE through fibroblast-specific knockouts of *Wnt5a*, *Enpp2*, *PDGFRα* and *PDGFRβ*. We found that none of

these additional pathways alone are required for scar formation following EAE. While PDGFRβ signaling is important for fibroblast development and migration, specifically deleting the PDGFRβ receptor from CNS fibroblasts did not impact overall fibrotic scar formation. Although we did not discover a potential therapeutic target to reduce fibrosis following inflammation, we believe that the advances we have made will be important to understand CNS fibrosis following other triggers such as physical injury, and that the RNA sequencing dataset we have generated will be useful in identifying other potential mechanisms of fibrosis.

Fibrosis in the retina can be modeled through l-OIR and arises from pericytes

In the retina, fibrosis is a devastating component of many vascular retinopathies and yet almost nothing is known about its origin. It has been difficult to answer questions about the source and mechanisms of retinal scarring as the current mouse models of retinopathies do not exhibit fibrotic pathology. We showed that fibrotic scarring can be modeled in the mouse through an extended OIR procedure termed l-OIR. This model will advance the study of retinopathies by providing a framework to test for potential therapeutics that could reduce the harmful pathologies found in these diseases.

Early characterization of this model revealed that this scar is likely formed by cells of pericyte origin. This is intriguing as it differs from our discovery that CNS fibroblasts, and not pericytes, are the primary drivers of fibrosis in the spinal cord following EAE. Single-cell sequencing studies of the mouse retina in health and following l-OIR were devoid of fibroblasts completely, suggesting that the mouse retina, unlike the brain and spinal cord, may not contain CNS fibroblasts. We hypothesize that producing scarring in the mouse retina is so difficult because there are no CNS fibroblasts present, and pericytes are activated to form the scar although they have less potential to produce robust scarring. We further hypothesize that there

are fibroblasts in the human retina, where scarring is far more prevalent and severe. Single-cell sequencing studies in the human retina that target perivascular cell populations would reveal whether fibroblasts are present and to what extent.

CNS fibroblast unanswered questions

Many unanswered questions remain about the functions of CNS fibroblasts in health and disease that will need to be answered to fully understand how they can be best targeted to promote disease recovery. First, it is unknown whether there are significant transcriptional and functional differences between fibroblasts in the meninges and perivascular spaces, and if fibroblasts in these different locations respond differently to disease. Techniques such as two-photon microscopy can be utilized to further probe their location-specific responses. Additionally, other than structural support largely in the meninges, it is unknown how these cells contribute to the healthy, adult CNS.

We propose that CNS perivascular fibroblasts may play a role in sensing changes in their environment, specifically blood flow and tissue stiffness, via mechanotransduction. Fibroblasts are known to respond to mechanical stress through membrane receptors such as integrins and respond by remodeling local tissue through secretions of extracellular matrix proteins (Camelliti et al., 2005; Herum et al., 2017). Blood flow throughout the body is sensitive to environmental factors, and fibroblasts in the CNS could be responding to these changes over time by subtly remodeling their environments and signaling to nearby smooth muscle and endothelial cells. The exact responses and consequences of this fibroblast mechanical sensing should be confirmed as these cells sit in critical sites where they can monitor both the periphery and CNS. It is unknown whether CNS fibroblasts play a role in maintaining perivascular basement membrane tissue and stiffness over time, but it is possible due to their high expression of ECM proteins.

While the role of CNS fibroblasts in fibrotic scar formation has been the most widely studied function of these cells in disease, there are still many open questions about this response such as whether there is fibrosis following neurodegenerative diseases and infections, the role of fibroblast proliferation and fibrosis in repair from stroke, and the full profile of signaling mechanisms that lead to scar formation. While PDGFR, TFGβ and IFNG signaling in fibroblasts have been shown to impact CNS fibrosis, the effect on manipulating these pathways was incomplete and other pathways and/or combinations of these pathways are likely contributing to scar formation.

It is also unknown whether CNS fibroblasts contribute to diseases in other ways than secreting fibrotic matrices and supporting reticular networks. In the periphery, fibroblasts have been shown to be key players in inflammatory signaling. They can attract immune cells to sites of injury by releasing chemokines such as monocyte chemoattractant protein 1, influence leukocyte transendothelial migration and promote immune survival through reductions in apoptosis (Van Linthout et al., 2014). The RNA sequencing data from CNS fibroblasts presented here illustrates that fibroblasts upregulate the expression of many cytokines in disease, and it has also been revealed that fibroblasts are a source of retinoic acid following stroke (Kelly et al., 2016). These studies suggest that CNS fibroblasts could play important roles in recruiting and eliciting damage responses from other cells in injury sites. As current studies have shown that fibrotic scarring impedes axon regeneration, it will be interesting to learn whether other contributions of fibroblasts to CNS disease have only negative outcomes for recovery. Ways of preventing collagen expression in fibroblasts without influencing their proliferation or signaling could delineate other roles for these intriguing cells in disease.

Finally, to appreciate how CNS fibroblasts impact human disease, further characterization of human tissue from different CNS pathologies is needed to understand how the responses of CNS fibroblasts compare between humans and mice. While fibroblasts in the human meninges have been well documented, less is known about the presence of perivascular fibroblasts associated with parenchymal vessels. It is well known that there is fibrotic scarring following human pathologies such as spinal cord injury, but unknown if fibroblasts contribute in different ways than we have presented here in the mouse.

REFERENCES

Adzemovic, M.V., Zeitelhofer, M., Eriksson, U., Olsson, T., and Nilsson, I. (2013). Imatinib ameliorates neuroinflammation in a rat model of multiple sclerosis by enhancing blood-brain barrier integrity and by modulating the peripheral immune response. PLoS One *8*, e56586.

Aiello, L.P., Pierce, E.A., Foley, E.D., Takagi, H., Chen, H., Riddle, L., Ferrara, N., King, G.L., and Smith, L.E. (1995). Suppression of retinal neovascularization in vivo by inhibition of vascular endothelial growth factor (VEGF) using soluble VEGF-receptor chimeric proteins. Proc Natl Acad Sci U S A *92*, 10457-10461.

Aktas, O., Küry, P., Kieseier, B., and Hartung, H.P. (2010). Fingolimod is a potential novel therapy for multiple sclerosis. Nat Rev Neurol *6*, 373-382.

Alberts, B., Johnson, A., Lewis, J., Raff, M., Roberts, K., Walter, P. (2002). Fibroblasts and Their Transformations: The Connective-Tissue Cell Family. 4th edn (New York: Garland Science).

Alcolado, R., Weller, R.O., Parrish, E.P., and Garrod, D. (1988). The cranial arachnoid and pia mater in man: anatomical and ultrastructural observations. Neuropathol Appl Neurobiol *14*, 1-17.

Aldea, R., Weller, R.O., Wilcock, D.M., Carare, R.O., and Richardson, G. (2019). Cerebrovascular Smooth Muscle Cells as the Drivers of Intramural Periarterial Drainage of the Brain. Front Aging Neurosci *11*, 1-1.

Aldrich, A., and Kielian, T. (2011). Central nervous system fibrosis is associated with fibrocyte-like infiltrates. American Journal of Pathology.

Aloisi, F., and Pujol-Borrell, R. (2006). Lymphoid neogenesis in chronic inflammatory diseases. Nature Reviews Immunology *6*, 205-217.

Anderson, M.A., Burda, J.E., Ren, Y., Ao, Y., O'Shea, T.M., Kawaguchi, R., Coppola, G., Khakh, B.S., Deming, T.J., and Sofroniew, M.V. (2016). Astrocyte scar formation aids central nervous system axon regeneration. Nature *532*, 195-200.

Angelov, D.N., and Vasilev, V.A. (1989). Morphogenesis of rat cranial meninges. A light- and electron-microscopic study. Cell Tissue Res *257*, 207-216.

Aran, D., Looney, A.P., Liu, L., Wu, E., Fong, V., Hsu, A., Chak, S., Naikawadi, R.P., Wolters, P.J., Abate, A.R., Butte, A.J., and Bhattacharya, M. (2019). Reference-based analysis of lung single-cell sequencing reveals a transitional profibrotic macrophage. Nature Immunology *20*, 163-172.

Armulik, A., Genové, G., and Betsholtz, C. (2011). Pericytes: Developmental, Physiological, and Pathological Perspectives, Problems, and Promises. Developmental Cell *21*, 193-215.

Armulik, A., Genové, G., Mäe, M., Nisancioglu, M.H., Wallgard, E., Niaudet, C., He, L., Norlin, J., Lindblom, P., Strittmatter, K., Johansson, B.R., and Betsholtz, C. (2010). Pericytes regulate the blood–brain barrier. Nature *468*, 557-561.

Attwell, D., Mishra, A., Hall, C.N., O'Farrell, F.M., and Dalkara, T. (2016). What is a pericyte? Journal of cerebral blood flow and metabolism : official journal of the International Society of Cerebral Blood Flow and Metabolism *36*, 451-455.

Bajénoff, M., Egen, J.G., Koo, L.Y., Laugier, Jean P., Brau, F., Glaichenhaus, N., and Germain, R.N. (2006). Stromal Cell Networks Regulate Lymphocyte Entry, Migration, and Territoriality in Lymph Nodes. Immunity.

Bataller, R., and Brenner, D.A. (2005). Liver fibrosis. The Journal of clinical investigation *115*, 209-218.

Bergers, G., and Song, S. (2005). The role of pericytes in blood-vessel formation and maintenance. Neuro Oncol *7*, 452-464.

Biernacka, A., Dobaczewski, M., and Frangogiannis, N.G. (2011). TGF-β signaling in fibrosis. Growth factors (Chur, Switzerland) *29*, 196-202.

Birbrair, A., Zhang, T., Files, D.C., Mannava, S., Smith, T., Wang, Z.-M., Messi, M.L., Mintz, A., and Delbono, O. (2014). Type-1 pericytes accumulate after tissue injury and produce collagen in an organ-dependent manner. Stem cell research & therapy *5*, 122-122.

Bondjers, C., He, L., Takemoto, M., Norlin, J., Asker, N., Hellström, M., Lindahl, P., and Betsholtz, C. (2006). Microarray analysis of blood microvessels from PDGF-B and PDGF-Rbeta mutant mice identifies novel markers for brain pericytes. FASEB journal : official publication of the Federation of American Societies for Experimental Biology *20*, 1703-1705.

Brazda, N., and Müller, H.W. (2009). Pharmacological modification of the extracellular matrix to promote regeneration of the injured brain and spinal cord. Progress in Brain Research *175*, 269-281.

Bringmann, A., Iandiev, I., Pannicke, T., Wurm, A., Hollborn, M., Wiedemann, P., Osborne, N.N., and Reichenbach, A. (2009). Cellular signaling and factors involved in Müller cell gliosis: neuroprotective and detrimental effects. Prog Retin Eye Res *28*, 423-451.

Bringmann, A., Pannicke, T., Grosche, J., Francke, M., Wiedemann, P., Skatchkov, S.N., Osborne, N.N., and Reichenbach, A. (2006). Müller cells in the healthy and diseased retina. Prog Retin Eye Res *25*, 397-424.

Buhl, E.M., Djudjaj, S., Klinkhammer, B.M., Ermert, K., Puelles, V.G., Lindenmeyer, M.T., Cohen, C.D., He, C., Borkham-Kamphorst, E., Weiskirchen, R., Denecke, B., Trairatphisan, P., Saez-Rodriguez, J., Huber, T.B., Olson, L.E., Floege, J., and Boor, P. (2020). Dysregulated mesenchymal PDGFR-β drives kidney fibrosis. EMBO Molecular Medicine *12*, e11021.

Burda, J.E., and Sofroniew, M.V. (2014). Reactive gliosis and the multicellular response to CNS damage and disease. Neuron *81*, 229-248.

Burgy, O., and Königshoff, M. (2018). The WNT signaling pathways in wound healing and fibrosis. Matrix Biology *68-69*, 67-80.

Camelliti, P., Borg, T.K., and Kohl, P. (2005). Structural and functional characterisation of cardiac fibroblasts. Cardiovascular Research *65*, 40-51.

Campochiaro, P.A. (2013). Ocular neovascularization. Journal of molecular medicine (Berlin, Germany) *91*, 311-321.

Cayabyab, R., Arora, V., Wertheimer, F., Durand, M., and Ramanathan, R. (2016). Graded oxygen saturation targets and retinopathy of prematurity in extremely preterm infants. Pediatr Res *80*, 401-406.

Chang, J.E., and Turley, S.J. (2015). Stromal infrastructure of the lymph node and coordination of immunity. Trends Immunol *36*, 30-39.

Chen, E.S., Greenlee, B.M., Wills-Karp, M., and Moller, D.R. (2001). Attenuation of lung inflammation and fibrosis in interferon-gamma-deficient mice after intratracheal bleomycin. Am J Respir Cell Mol Biol *24*, 545-555.

Chen, Y.-T., Levasseur, R., Vaishnav, S., Karsenty, G., and Bradley, A. (2004). Bigenic Cre/loxP, puDeltatk conditional genetic ablation. Nucleic acids research *32*, e161-e161.

Chun, J., and Hartung, H.-P. (2010). Mechanism of action of oral fingolimod (FTY720) in multiple sclerosis. Clinical neuropharmacology *33*, 91-101.

Connor, K.M., Krah, N.M., Dennison, R.J., Aderman, C.M., Chen, J., Guerin, K.I., Sapieha, P., Stahl, A., Willett, K.L., and Smith, L.E. (2009). Quantification of oxygen-induced retinopathy in the mouse: a model of vessel loss, vessel regrowth and pathological angiogenesis. Nat Protoc *4*, 1565-1573.

Cregg, J.M., DePaul, M.A., Filous, A.R., Lang, B.T., Tran, A., and Silver, J. (2014). Functional regeneration beyond the glial scar. Experimental neurology *253*, 197-207.

Cupovic, J., Onder, L., Gil-Cruz, C., Weiler, E., Caviezel-Firner, S., Perez-Shibayama, C., Rülicke, T., Bechmann, I., and Ludewig, B. (2016). Central Nervous System Stromal Cells Control Local CD8+ T Cell Responses during Virus-Induced Neuroinflammation. Immunity.

Daneman, R., Zhou, L., Kebede, A.A., and Barres, B.A. (2010). Pericytes are required for blood-brain barrier integrity during embryogenesis. Nature *468*, 562-566.

Dasgupta, K., and Jeong, J. (2019). Developmental biology of the meninges. Genesis *57*, e23288.

De La Fuente, A.G., Lange, S., Silva, M.E., Gonzalez, G.A., Tempfer, H., van Wijngaarden, P., Zhao, C., Di Canio, L., Trost, A., Bieler, L., Zaunmair, P., Rotheneichner, P., O'Sullivan, A., Couillard-Despres, S., Errea, O., Mäe, M.A., Andrae, J., He, L., Keller, A., Bátiz, L.F., Betsholtz, C., Aigner, L., Franklin, R.J.M., and Rivera, F.J. (2017). Pericytes Stimulate Oligodendrocyte Progenitor Cell Differentiation during CNS Remyelination. Cell Reports *20*, 1755-1764.

DeSisto, J., O'Rourke, R., Jones, H.E., Pawlikowski, B., Malek, A.D., Bonney, S., Guimiot, F., Jones, K.L., and Siegenthaler, J.A. (2020). Single-Cell Transcriptomic Analyses of the Developing Meninges Reveal Meningeal Fibroblast Diversity and Function. Dev Cell *54*, 43-59.e44.

Dias, D.O., and Göritz, C. (2018). Fibrotic scarring following lesions to the central nervous system. Matrix Biology.

Dias, D.O., Kim, H., Holl, D., Werne Solnestam, B., Lundeberg, J., Carlén, M., Göritz, C., and Frisén, J. (2018). Reducing Pericyte-Derived Scarring Promotes Recovery after Spinal Cord Injury. Cell *173*, 153-165.e122.

Donovan, J., Shiwen, X., Norman, J., and Abraham, D. (2013). Platelet-derived growth factor alpha and beta receptors have overlapping functional activities towards fibroblasts. Fibrogenesis & Tissue Repair *6*, 10-10.

Dore-Duffy, P. (2008). Pericytes: pluripotent cells of the blood brain barrier. Curr Pharm Des *14*, 1581-1593.

Douillet, C.D., Velarde, V., Christopher, J.T., Mayfield, R.K., Trojanowska, M.E., and Jaffa, A.A. (2000). Mechanisms by which bradykinin promotes fibrosis in vascular smooth muscle cells: role of TGF-beta and MAPK. Am J Physiol Heart Circ Physiol *279*, H2829-2837.

El Rayes, E.N., Vinekar, A., and Capone, A., Jr. (2008). Three-year anatomic and visual outcomes after vitrectomy for stage 4B retinopathy of prematurity. Retina *28*, 568-572.

Faraco, G., Park, L., Anrather, J., and Iadecola, C. (2017). Brain perivascular macrophages: characterization and functional roles in health and disease. Journal of molecular medicine (Berlin, Germany) *95*, 1143-1152.

Faulkner, J.R., Herrmann, J.E., Woo, M.J., Tansey, K.E., Doan, N.B., and Sofroniew, M.V. (2004). Reactive astrocytes protect tissue and preserve function after spinal cord injury. The Journal of neuroscience : the official journal of the Society for Neuroscience *24*, 2143-2155.

Feng, Y., Liang, Y., Zhu, X., Wang, M., Gui, Y., Lu, Q., Gu, M., Xue, X., Sun, X., He, W., Yang, J., Johnson, R.L., and Dai, C. (2018). The signaling protein Wnt5a promotes TGFβ1-mediated macrophage polarization and kidney fibrosis by inducing the transcriptional regulators Yap/Taz. The Journal of biological chemistry *293*, 19290-19302.

Fernández-Klett, F., Offenhauser, N., Dirnagl, U., Priller, J., and Lindauer, U. (2010). Pericytes in capillaries are contractile in vivo, but arterioles mediate functional hyperemia in the mouse brain. Proceedings of the National Academy of Sciences of the United States of America *107*, 22290-22295.

Fernández-Klett, F., Potas, J.R., Hilpert, D., Blazej, K., Radke, J., Huck, J., Engel, O., Stenzel, W., Genové, G., and Priller, J. (2013). Early Loss of Pericytes and Perivascular Stromal Cell-Induced Scar Formation after Stroke. Journal of Cerebral Blood Flow & Metabolism *33*, 428-439.

Fernández-Klett, F., and Priller, J. (2014a). The Fibrotic Scar in Neurological Disorders. Brain Pathology *24*, 404-413.

Fernández-Klett, F., and Priller, J. (2014b). The fibrotic scar in neurological disorders. Brain Pathology Zurich Switz *24*, 404-413.

Friedlander, M. (2007). Fibrosis and diseases of the eye. The Journal of clinical investigation *117*, 576-586.

Gao, Z., Sasaoka, T., Fujimori, T., Oya, T., Ishii, Y., Sabit, H., Kawaguchi, M., Kurotaki, Y., Naito, M., Wada, T., Ishizawa, S., Kobayashi, M., Nabeshima, Y.-I., and Sasahara, M. (2005). Deletion of the PDGFR-beta gene affects key fibroblast functions important for wound healing. The Journal of biological chemistry *280*, 9375-9389.

Gilbert, W.S., Quinn, G.E., Dobson, V., Reynolds, J., Hardy, R.J., and Palmer, E.A. (1996). Partial retinal detachment at 3 months after threshold retinopathy of prematurity. Long-term structural and functional outcome. Multicenter Trial of Cryotherapy for Retinopathy of Prematurity Cooperative Group. Arch Ophthalmol *114*, 1085-1091.

Göritz, C., Dias, D.O., Tomilin, N., Barbacid, M., Shupliakov, O., and Frisén, J. (2011). A Pericyte Origin of Spinal Cord Scar Tissue. Science *333*.

Gray, D.H.D., Tull, D., Ueno, T., Seach, N., Classon, B.J., Chidgey, A., McConville, M.J., and Boyd, R.L. (2007). A Unique Thymic Fibroblast Population Revealed by the Monoclonal Antibody MTS-15. The Journal of Immunology *178*, 4956.

Guimarães-Camboa, N., Cattaneo, P., Sun, Y., Moore-Morris, T., Gu, Y., Dalton, N.D., Rockenstein, E., Masliah, E., Peterson, K.L., Stallcup, W.B., Chen, J., Evans, S.M., Alvarez-Dolado, M., Pardal, R., Garcia-Verdugo, J.M., Fike, J.R., Lee, H.O., Pfeffer, K., Lois, C., Morrison, S.J., Alvarez-Buylla, A., Armulik, A., Genové, G., Betsholtz, C., Ben-David, U., Benvenisty, N., Bohnenpoll, T., Bettenhausen, E., Weiss, A.C., Foik, A.B., Trowe, M.O., Blank, P., Airik, R., Kispert, A., Buckingham, M.E., Meilhac, S.M., Bussen, M., Petry, M., Schuster-Gossler, K., Leitges, M., Gossler, A., Kispert, A., Cai, C.L., Martin, J.C., Sun, Y., Cui, L., Wang, L., Ouyang, K., Yang, L., Bu, L., Liang, X., Zhang, X., al, e., Chen, W.C., Baily, J.E., Corselli, M., Díaz, M.E., Sun, B., Xiang, G., Gray, G.A., Huard, J., Péault, B., Crisan, M., Yap, S., Casteilla, L., Chen, C.W., Corselli, M., Park, T.S., Andriolo, G., Sun, B., Zheng, B., Zhang, L.,

al, e., Dellavalle, A., Sampaolesi, M., Tonlorenzi, R., Tagliafico, E., Sacchetti, B., Perani, L., Innocenzi, A., Galvez, B.G., Messina, G., Morosetti, R., al, e., Dellavalle, A., Maroli, G., Covarello, D., Azzoni, E., Innocenzi, A., Perani, L., Antonini, S., Sambasivan, R., Brunelli, S., Tajbakhsh, S., Cossu, G., Dore-Duffy, P., Katychev, A., Wang, X., Buren, E.V., Foo, S.S., Turner, C.J., Adams, S., Compagni, A., Aubyn, D., Kogata, N., Lindblom, P., Shani, M., Zicha, D., Adams, R.H., Fuchs, E., Tumbar, T., Guasch, G., Göritz, C., Dias, D.O., Tomilin, N., Barbacid, M., Shupliakov, O., Frisén, J., Greenhalgh, S.N., Iredale, J.P., Henderson, N.C., Kapoor, N., Liang, W., Marbán, E., Cho, H.C., Kisanuki, Y.Y., Hammer, R.E., Miyazaki, J., Williams, S.C., Richardson, J.A., Yanagisawa, M., Kraus, F., Haenig, B., Kispert, A., Krautler, N.J., Kana, V., Kranich, J., Tian, Y., Perera, D., Lemm, D., Schwarz, P., Armulik, A., Browning, J.L., Tallquist, M., al, e., Long, J.Z., Svensson, K.J., Tsai, L., Zeng, X., Roh, H.C., Kong, X., Rao, R.R., Lou, J., Lokurkar, I., Baur, W., al, e., Madisen, L., Zwingman, T.A., Sunkin, S.M., Oh, S.W., Zariwala, H.A., Gu, H., Ng, L.L., Palmiter, R.D., Hawrylycz, M.J., Jones, A.R., al, e., Moore-Morris, T., Guimarães-Camboa, N., Banerjee, I., Zambon, A.C., Kisseleva, T., Velayoudon, A., Stallcup, W.B., Gu, Y., Dalton, N.D., Cedenilla, M., al, e., Nakagomi, T., Nakano-Doi, A., Kawamura, M., Matsuyama, T., Paul, G., Özen, I., Christophersen, N.S., Reinbothe, T., Bengzon, J., Visse, E., Jansson, K., Dannaeus, K., Henriques-Oliveira, C., Roybon, L., al, e., Raymond, C.S., Soriano, P., Rockman, H.A., Ross, R.S., Harris, A.N., Knowlton, K.U., Steinhelper, M.E., Field, L.J., Ross, J., Chien, K.R., Sakuma, R., Kawahara, M., Nakano-Doi, A., Takahashi, A., Tanaka, Y., Narita, A., Kuwahara-Otani, S., Hayakawa, T., Yagi, H., Matsuyama, T., Nakagomi, T., Sancho-Martinez, I., Baek, S.H., Belmonte, J.C.I., Senyo, S.E., Steinhauser, M.L., Pizzimenti, C.L., Yang, V.K., Cai, L., Wang, M., Wu, T.D., Guerquin-Kern, J.L., Lechene, C.P., Lee, R.T., Silver, J., Miller, J.H., Snippert, H.J., Clevers, H., Tang, W., Zeve, D., Suh, J.M., Bosnakovski, D., Kyba, M., Hammer, R.E., Tallquist, M.D., Graff, J.M., Berlo, J.H.v., Kanisicak, O., Maillet, M., Vagnozzi, R.J., Karch, J., Lin, S.C., Middleton, R.C., Marbán, E., Molkentin, J.D., Wiese, C., Grieskamp, T., Airik, R., Mommersteeg, M.T., Gardiwal, A., Vries, C.d.G.-d., Schuster-Gossler, K., Moorman, A.F., Kispert, A., Christoffels, V.M., Yata, Y., Scanga, A., Gillan, A., Yang, L., Reif, S., Breindl, M., Brenner, D.A., and Rippe, R.A. (2017). Pericytes of Multiple Organs Do Not Behave as Mesenchymal Stem Cells In Vivo. Cell stem cell *0*, 968-973.

Gupta, B., Sivaprasad, S., Wong, R., Laidlaw, A., Jackson, T.L., McHugh, D., and Williamson, T.H. (2012). Visual and anatomical outcomes following vitrectomy for complications of diabetic retinopathy: the DRIVE UK study. Eye (Lond) *26*, 510-516.

Hafemeister, C., and Satija, R. (2019). Normalization and variance stabilization of single-cell RNA-seq data using regularized negative binomial regression. bioRxiv, 576827.

Haines, D.E., Harkey, H.L., and Al-Mefty, O. (1993). The “subdural” space: A new look at an outdated concept. Neurosurgery.

Halfter, W., Dong, S., Yip, Y.-P., Willem, M., and Mayer, U. (2002). A Critical Function of the Pial Basement Membrane in Cortical Histogenesis. The Journal of Neuroscience *22*, 6029.

Hall, C.N., Reynell, C., Gesslein, B., Hamilton, N.B., Mishra, A., Sutherland, B.A., O'Farrell, F.M., Buchan, A.M., Lauritzen, M., and Attwell, D. (2014). Capillary pericytes regulate cerebral blood flow in health and disease. Nature *508*, 55-60.

Hellal, F., Hurtado, A., Ruschel, J., Flynn, K.C., Laskowski, C.J., Umlauf, M., Kapitein, L.C., Strikis, D., Lemmon, V., Bixby, J., Hoogenraad, C.C., and Bradke, F. (2011). Microtubule stabilization reduces scarring and causes axon regeneration after spinal cord injury. Science (New York, NY) *331*, 928-931.

Hellström, A., Hård, A.L., Engström, E., Niklasson, A., Andersson, E., Smith, L., and Löfqvist, C. (2009). Early weight gain predicts retinopathy in preterm infants: new, simple, efficient approach to screening. Pediatrics *123*, e638-645.

Hellström, A., Smith, L.E.H., and Dammann, O. (1991). Retinopathy of prematurity. Lancet (London, England) *337*, 83-84.

Herum, K.M., Lunde, I.G., McCulloch, A.D., and Christensen, G. (2017). The Soft- and Hard-Heartedness of Cardiac Fibroblasts: Mechanotransduction Signaling Pathways in Fibrosis of the Heart. J Clin Med *6*, 53.

Hill, Robert A., Tong, L., Yuan, P., Murikinati, S., Gupta, S., Grutzendler, J., Armstrong, J.J., Larina, I.V., Dickinson, M.E., Zimmer, W.E., Hirschi, K.K., Armulik, A., Genové, G., Mäe, M., Nisancioglu, M.H., Wallgard, E., Niaudet, C., He, L., Norlin, J., Lindblom, P., Strittmatter, K., al, e., Armulik, A., Genové, G., Betsholtz, C., Attwell, D., Iadecola, C., Bell, R.D., Winkler, E.A., Sagare, A.P., Singh, I., LaRue, B., Deane, R., Zlokovic, B.V., Blinder, P., Tsai, P.S., Kaufhold, J.P., Knutsen, P.M., Suhl, H., Kleinfeld, D., Borysova, L., Wray, S., Eisner, D.A., Burdyga, T., Brian, J.E., Faraci, F.M., Feuerstein, G., Chaigneau, E., Oheim, M., Audinat, E., Charpak, S., Cuevas, P., Gutierrez-Diaz, J.A., Reimers, D., Dujovny, M., Diaz, F.G., Ausman, J.I., Daneman, R., Zhou, L., Kebede, A.A., Barres, B.A., Zoppo, G.J.d., Schmid-Schönbein, G.W., Mori, E., Copeland, B.R., Chang, C.M., Devor, A., Tian, P., Nishimura, N., Teng, I.C., Hillman, E.M.C., Narayanan, S.N., Ulbert, I., Boas, D.A., Kleinfeld, D., Dale, A.M., Drew, P.J., Shih, A.Y., Kleinfeld, D., Duan, X., Krishnaswamy, A., Huerta, I.D.l., Sanes, J.R., Faraci, F.M., Farkas, E., Luiten, P.G., Fernández-Klett, F., Offenhauser, N., Dirnagl, U., Priller, J., Lindauer, U., Grinvald, A., Lieke, E., Frostig, R.D., Gilbert, C.D., Wiesel, T.N., Grutzendler, J., Murikinati, S., Hiner, B., Ji, L., Lam, C.K., Yoo, T., Gupta, S., Hafler, B.P., Adelman, R.A., Yuan, P., Rodriguez, G., Hall, C.N., Reynell, C., Gesslein, B., Hamilton, N.B., Mishra, A., Sutherland, B.A., O'Farrell, F.M., Buchan, A.M., Lauritzen, M., Attwell, D., Hamel, E., Hamilton, N.B., Attwell, D., Hall, C.N., Harb, R., Whiteus, C., Freitas, C., Grutzendler, J., Haydon, P.G., Carmignoto, G., Hill, R.A., Grutzendler, J., Hill, R.A., Patel, K.D., Goncalves, C.M., Grutzendler, J., Nishiyama, A., Iadecola, C., Iadecola, C., Nedergaard, M., Iadecola, C., Yang, G., Ebner, T.J., Chen, G., Itoh, Y., Suzuki, N., Kety, S.S., Schmidt, C.F., Kornfield, T.E., Newman, E.A., Krueger, M., Bechmann, I., Lam, C.K., Yoo, T., Hiner, B., Liu, Z., Grutzendler, J., Leao, A.A.P., Logothetis, N.K., Wandell, B.A., Logothetis, N.K., Pauls, J., Augath, M., Trinath, T., Oeltermann, A., Madisen, L., Mao, T., Koch, H., Zhuo, J.M., Berenyi, A., Fujisawa, S., Hsu, Y.W.A., Garcia, A.J., Gu, X., Zanella, S., al, e., Motoike, T., Loughna, S., Perens, E., Roman, B.L., Liao, W., Chau, T.C., Richardson, C.D., Kawate, T., Kuno, J., Weinstein, B.M., al,

e., Muzumdar, M.D., Tasic, B., Miyamichi, K., Li, L., Luo, L., Nakayama, A., Nakayama, M., Turner, C.J., Höing, S., Lepore, J.J., Adams, R.H., Nishiyama, A., Suzuki, R., Zhu, X., Noguchi, H., Gompper, G., Novak, A., Guo, C., Yang, W., Nagy, A., Lobe, C.G., O'Farrell, F.M., Attwell, D., Ogawa, S., Lee, T.M., Kay, A.R., Tank, D.W., Oku, H., Kodama, T., Sakagami, K., Puro, D.G., Pawlik, G., Rackl, A., Bing, R.J., Peppiatt, C.M., Howarth, C., Mobbs, P., Attwell, D., Puro, D.G., Raichle, M.E., Mintun, M.A., Rezkalla, S.H., Kloner, R.A., Rouget, C., Roy, C.S., Sherrington, C.S., Sagare, A.P., Bell, R.D., Zhao, Z., Ma, Q., Winkler, E.A., Ramanathan, A., Zlokovic, B.V., Sakagami, K., Wu, D.M., Puro, D.G., Schain, A.J., Hill, R.A., Grutzendler, J., Shen, Z., Lu, Z., Chhatbar, P.Y., O'Herron, P., Kara, P., Simard, M., Arcuino, G., Takano, T., Liu, Q.S., Nedergaard, M., Skalak, R., Branemark, P.I., Snippert, H.J., Flier, L.G.v.d., Sato, T., Es, J.H.v., Born, M.v.d., Kroon-Veenboer, C., Barker, N., Klein, A.M., Rheenen, J.v., Simons, B.D., Clevers, H., Somjen, G.G., Uemura, A., Ogawa, M., Hirashima, M., Fujiwara, T., Koyama, S., Takagi, H., Honda, Y., Wiegand, S.J., Yancopoulos, G.D., Nishikawa, S., Vanzetta, I., Hildesheim, R., Grinvald, A., Vates, G.E., Takano, T., Zlokovic, B., Nedergaard, M., Wendling, O., Bornert, J.M., Chambon, P., Metzger, D., Winkler, E.A., Bell, R.D., Zlokovic, B.V., Winkler, E.A., Sagare, A.P., Zlokovic, B.V., Yemisci, M., Gursoy-Ozdemir, Y., Vural, A., Can, A., Topalkara, K., Dalkara, T., Zariwala, H.A., Borghuis, B.G., Hoogland, T.M., Madisen, L., Tian, L., Zeeuw, C.I.D., Zeng, H., Looger, L.L., Svoboda, K., Chen, T.W., Zhu, X., Bergles, D.E., Nishiyama, A., Zhu, X., Hill, R.A., Dietrich, D., Komitova, M., Suzuki, R., and Nishiyama, A. (2015). Regional Blood Flow in the Normal and Ischemic Brain Is Controlled by Arteriolar Smooth Muscle Cell Contractility and Not by Capillary Pericytes. Neuron *87*, 95-110.
Hiscott, P., Sheridan, C., Magee, R.M., and Grierson, I. (1999). Matrix and the retinal pigment epithelium in proliferative retinal disease. Prog Retin Eye Res *18*, 167-190.
Hoch, R.V., and Soriano, P. (2003). Roles of PDGF in animal development. Development *130*, 4769.

Hu, D., Yin, C., Luo, S., Habenicht, A.J.R., and Mohanta, S.K. (2019). Vascular Smooth Muscle Cells Contribute to Atherosclerosis Immunity. Frontiers in Immunology *10*.

Ikeda, H., Yatomi, Y., Yanase, M., Satoh, H., Nishihara, A., Kawabata, M., and Fujiwara, K. (1998). Effects of lysophosphatidic acid on proliferation of stellate cells and hepatocytes in culture. Biochem Biophys Res Commun *248*, 436-440.

Junt, T., Scandella, E., and Ludewig, B. (2008). Form follows function: lymphoid tissue microarchitecture in antimicrobial immune defence. Nat Rev Immunol *8*, 764-775.

Kawano, H., Kimura-Kuroda, J., Komuta, Y., Yoshioka, N., Li, H.P., Kawamura, K., Li, Y., and Raisman, G. (2012). Role of the lesion scar in the response to damage and repair of the central nervous system. Cell Tissue Res *349*, 169-180.

Kelly, K.K., MacPherson, A.M., Grewal, H., Strnad, F., Jones, J.W., Yu, J., Pierzchalski, K., Kane, M.A., Herson, P.S., and Siegenthaler, J.A. (2016). Col1a1+ perivascular cells in the brain are a source of retinoic acid following stroke. BMC neuroscience *17*, 49-49.

Kendall, R.T., and Feghali-Bostwick, C.A. (2014). Fibroblasts in fibrosis: novel roles and mediators. Frontiers in Pharmacology *5*, 123.

Kim, J.H., Kim, H.Y., Kim, S., Chung, J.-H., Park, W.S., and Chung, D.H. (2005). Natural killer T (NKT) cells attenuate bleomycin-induced pulmonary fibrosis by producing interferon-gamma. The American journal of pathology *167*, 1231-1241.

Kim, J.V., Kang, S.S., Dustin, M.L., and McGavern, D.B. (2009). Myelomonocytic cell recruitment causes fatal CNS vascular injury during acute viral meningitis. Nature.

King, T.E., Albera, C., Bradford, W.Z., Costabel, U., Hormel, P., Lancaster, L., Noble, P.W., Sahn, S.A., Szwarcberg, J., Thomeer, M., Valeyre, D., and du Bois, R.M. (2009). Effect of interferon gamma-1b on survival in patients with idiopathic pulmonary fibrosis (INSPIRE): a multicentre, randomised, placebo-controlled trial. The Lancet *374*, 222-228.

Kirmi, O., Sheerin, F., and Patel, N. (2009). Imaging of the meninges and the extra-axial spaces. Semin Ultrasound CT MR *30*, 565-593.

Klapka, N., Hermanns, S., Straten, G., Masanneck, C., Duis, S., Hamers, F.P.T., Müller, D., Zuschratter, W., and Müller, H.W. (2005). Suppression of fibrous scarring in spinal cord injury of rat promotes long-distance regeneration of corticospinal tract axons, rescue of primary motoneurons in somatosensory cortex and significant functional recovery. European Journal of Neuroscience *22*, 3047-3058.

Klinkhammer, B.M., Floege, J., and Boor, P. (2018). PDGF in organ fibrosis. Mol Aspects Med *62*, 44-62.

Komiya, Y., and Habas, R. (2008). Wnt signal transduction pathways. Organogenesis *4*, 68-75.

Komuta, Y., Teng, X., Yanagisawa, H., Sango, K., Kawamura, K., and Kawano, H. (2010). Expression of transforming growth factor-β receptors in meningeal fibroblasts of the injured mouse brain. Cellular and Molecular Neurobiology.

Kyyriäinen, J., Ekolle Ndode-Ekane, X., and Pitkänen, A. (2017). Dynamics of PDGFRβ expression in different cell types after brain injury. GLIA.

Lajko, M., Cardona, H.J., Taylor, J.M., Shah, R.S., Farrow, K.N., and Fawzi, A.A. (2016a). Hyperoxia-Induced Proliferative Retinopathy: Early Interruption of Retinal Vascular Development with Severe and Irreversible Neurovascular Disruption. PLOS ONE *11*, e0166886-e0166886.

Lajko, M., Cardona, H.J., Taylor, J.M., Shah, R.S., Farrow, K.N., and Fawzi, A.A. (2016b). Hyperoxia-Induced Proliferative Retinopathy: Early Interruption of Retinal Vascular Development with Severe and Irreversible Neurovascular Disruption. PLoS One *11*, e0166886.

Lam, M.A., Hemley, S.J., Najafi, E., Vella, N.G.F., Bilston, L.E., and Stoodley, M.A. (2017). The ultrastructure of spinal cord perivascular spaces: Implications for the circulation of cerebrospinal fluid. Scientific Reports.

Lapenna, A., De Palma, M., and Lewis, C.E. (2018). Perivascular macrophages in health and disease. Nature Reviews Immunology *18*, 689-702.

Lederer, D.J., and Martinez, F.J. (2018). Idiopathic Pulmonary Fibrosis. New England Journal of Medicine *378*, 1811-1823.

Lee, S.B., and Kalluri, R. (2010). Mechanistic connection between inflammation and fibrosis. Kidney international Supplement, S22-26.

Lin, W., Kemper, A., Dupree, J.L., Harding, H.P., Ron, D., and Popko, B. (2006). Interferon-gamma inhibits central nervous system remyelination through a process modulated by endoplasmic reticulum stress. Brain *129*, 1306-1318.

Logan, A., Berry, M., Gonzalez, A.M., Frautschy, S.A., Sporn, M.B., and Baird, A. (1994). Effects of Transforming Growth Factor β ₁ , on Scar Production in the Injured Central Nervous System of the Rat. European Journal of Neuroscience *6*, 355-363.

Machemer, R., van Horn, D., and Aaberg, T.M. (1978). Pigment epithelial proliferation in human retinal detachment with massive periretinal proliferation. Am J Ophthalmol *85*, 181-191.

Mack, M. (2018). Inflammation and fibrosis. Matrix Biology *68-69*, 106-121.

Macosko, Evan Z., Basu, A., Satija, R., Nemesh, J., Shekhar, K., Goldman, M., Tirosh, I., Bialas, Allison R., Kamitaki, N., Martersteck, Emily M., Trombetta, John J., Weitz, David A., Sanes, Joshua R., Shalek, Alex K., Regev, A., and McCarroll, Steven A. (2015). Highly Parallel Genome-wide Expression Profiling of Individual Cells Using Nanoliter Droplets. Cell *161*, 1202-1214.

Magliozzi, R., Howell, O., Vora, A., Serafini, B., Nicholas, R., Puopolo, M., Reynolds, R., and Aloisi, F. (2007). Meningeal B-cell follicles in secondary progressive multiple sclerosis associate with early onset of disease and severe cortical pathology. Brain *130*, 1089-1104.

Magliozzi, R., Howell, O.W., Reeves, C., Roncaroli, F., Nicholas, R., Serafini, B., Aloisi, F., and Reynolds, R. (2010). A Gradient of neuronal loss and meningeal inflammation in multiple sclerosis. Ann Neurol *68*, 477-493.

Makihara, N., Arimura, K., Ago, T., Tachibana, M., Nishimura, A., Nakamura, K., Matsuo, R., Wakisaka, Y., Kuroda, J., Sugimori, H., Kamouchi, M., and Kitazono, T. (2015). Involvement of platelet-derived growth factor receptor β in fibrosis through extracellular matrix protein production after ischemic stroke. Experimental Neurology *264*, 127-134.

Mastorakos, P., and McGavern, D. (2019). The anatomy and immunology of vasculature in the central nervous system.

Mei, F., Fancy, S.P.J., Shen, Y.-A.A., Niu, J., Zhao, C., Presley, B., Miao, E., Lee, S., Mayoral, S.R., Redmond, S.A., Etxeberria, A., Xiao, L., Franklin, R.J.M., Green, A., Hauser, S.L., and

Chan, J.R. (2014). Micropillar arrays as a high-throughput screening platform for therapeutics in multiple sclerosis. Nature medicine *20*, 954-960.

Meleth, A.D., and Carvounis, P.E. (2014). Outcomes of vitrectomy for tractional retinal detachment in diabetic retinopathy. Int Ophthalmol Clin *54*, 127-139.

Meng, X.-m., Nikolic-Paterson, D.J., and Lan, H.Y. (2016). TGF-β: the master regulator of fibrosis. Nature Reviews Nephrology *12*, 325-338.

Meng, X.-M., Tang, P.M.-K., Li, J., and Lan, H.Y. (2015). TGF-β/Smad signaling in renal fibrosis. Frontiers in Physiology *6*.

Mescher, A.L. (2017). Macrophages and fibroblasts during inflammation and tissue repair in models of organ regeneration. Regeneration (Oxf) *4*, 39-53.

Mintz-Hittner, H.A., O'Malley, R.E., and Kretzer, F.L. (1997). Long-term form identification vision after early, closed, lensectomy-vitrectomy for stage 5 retinopathy of prematurity. Ophthalmology *104*, 454-459.

Mohan, H., Krumbholz, M., Sharma, R., Eisele, S., Junker, A., Sixt, M., Newcombe, J., Wekerle, H., Hohlfeld, R., Lassmann, H., and Meinl, E. (2010). Extracellular Matrix in Multiple Sclerosis Lesions: Fibrillar Collagens, Biglycan and Decorin are Upregulated and Associated with Infiltrating Immune Cells. Brain Pathology *20*.

Murtha, L.A., Morten, M., Schuliga, M.J., Mabotuwana, N.S., Hardy, S.A., Waters, D.W., Burgess, J.K., Ngo, D.T., Sverdlov, A.L., Knight, D.A., and Boyle, A.J. (2019). The Role of Pathological Aging in Cardiac and Pulmonary Fibrosis. Aging Dis *10*, 419-428.

Newman, A.C., Nakatsu, M.N., Chou, W., Gershon, P.D., and Hughes, C.C.W. (2011). The requirement for fibroblasts in angiogenesis: fibroblast-derived matrix proteins are essential for endothelial cell lumen formation. Molecular Biology of the Cell *22*, 3791-3800.

Newman, D.K. (2010). Surgical management of the late complications of proliferative diabetic retinopathy. Eye (Lond) *24*, 441-449.

Newman, D.R., Sills, W.S., Hanrahan, K., Ziegler, A., Tidd, K.M., Cook, E., and Sannes, P.L. (2016). Expression of WNT5A in Idiopathic Pulmonary Fibrosis and Its Control by TGF-β and WNT7B in Human Lung Fibroblasts. The journal of histochemistry and cytochemistry : official journal of the Histochemistry Society *64*, 99-111.

Ninou, I., Magkrioti, C., and Aidinis, V. (2018). Autotaxin in Pathophysiology and Pulmonary Fibrosis. Frontiers in medicine *5*, 180-180.

Niu, J., Tsai, H.H., Hoi, K.K., Huang, N., Yu, G., Kim, K., Baranzini, S.E., Xiao, L., Chan, J.R., and Fancy, S.P.J. (2019). Aberrant oligodendroglial-vascular interactions disrupt the blood-brain barrier, triggering CNS inflammation. Nat Neurosci *22*, 709-718.

O'Rahilly, R., and Müller, F. (1986). The meninges in human development. J Neuropathol Exp Neurol *45*, 588-608.

O'Shea, T.M., Burda, J.E., and Sofroniew, M.V. (2017). Cell biology of spinal cord injury and repair. The Journal of Clinical Investigation *127*, 3259-3270.

Oldroyd, S.D., Thomas, G.L., Gabbiani, G., and El Nahas, A.M. (1999). Interferon-γ inhibits experimental renal fibrosis. Kidney International *56*, 2116-2127.

Ongenaert, M., Dupont, S., Blanqué, R., Brys, R., van der Aar, E., and Heckmann, B. (2016). Strong reversal of the lung fibrosis disease signature by autotaxin inhibitor GLPG1690 in a mouse model for IPF. European Respiratory Journal *48*, OA4540.

Pashirzad, M., Shafiee, M., Rahmani, F., Behnam-Rassouli, R., Hoseinkhani, F., Ryzhikov, M., Moradi Binabaj, M., Parizadeh, M.R., Avan, A., and Hassanian, S.M. (2017). Role of Wnt5a in the Pathogenesis of Inflammatory Diseases. J Cell Physiol *232*, 1611-1616.

Pei, D., Liu, N., Li, D., Yan, H., Wang, Q.-b., Fang, Y., Xie, L., and Li, H.-P. (2017). Inhibition of platelet-derived growth factor receptor β reduces reactive glia and scar formation after traumatic brain injury in mice. Brain Research Bulletin *134*, 121-127.

Peppiatt, C.M., Howarth, C., Mobbs, P., and Attwell, D. (2006). Bidirectional control of CNS capillary diameter by pericytes. Nature *443*, 700-704.

Philippeos, C., Telerman, S.B., Oulès, B., Pisco, A.O., Shaw, T.J., Elgueta, R., Lombardi, G., Driskell, R.R., Soldin, M., Lynch, M.D., and Watt, F.M. (2018). Spatial and Single-Cell Transcriptional Profiling Identifies Functionally Distinct Human Dermal Fibroblast Subpopulations. J Invest Dermatol *138*, 811-825.

Pikor, Natalia B., Astarita, Jillian L., Summers-Deluca, L., Galicia, G., Qu, J., Ward, Lesley A., Armstrong, S., Dominguez, Claudia X., Malhotra, D., Heiden, B., Kay, R., Castanov, V., Touil, H., Boon, L., O'Connor, P., Bar-Or, A., Prat, A., Ramaglia, V., Ludwin, S., Turley, Shannon J., and Gommerman, Jennifer L. (2015). Integration of Th17- and Lymphotoxin-Derived Signals Initiates Meningeal-Resident Stromal Cell Remodeling to Propagate Neuroinflammation. Immunity *43*, 1160-1173.

Poosti, F., Bansal, R., Yazdani, S., Prakash, J., Post, E., Klok, P., van den Born, J., de Borst, M.H., van Goor, H., Poelstra, K., and Hillebrands, J.-L. (2015). Selective delivery of IFN-γ to renal interstitial myofibroblasts: a novel strategy for the treatment of renal fibrosis. The FASEB Journal *29*, 1029-1042.

Ramachandran, A., Gong, E.M., Pelton, K., Ranpura, S.A., Mulone, M., Seth, A., Gomez, P., 3rd, and Adam, R.M. (2011). FosB regulates stretch-induced expression of extracellular matrix proteins in smooth muscle. The American journal of pathology *179*, 2977-2989.

Rashid, S.T., Humphries, J.D., Byron, A., Dhar, A., Askari, J.A., Selley, J.N., Knight, D., Goldin, R.D., Thursz, M., and Humphries, M.J. (2012). Proteomic analysis of extracellular matrix from the hepatic stellate cell line LX-2 identifies CYR61 and Wnt-5a as novel constituents of fibrotic liver. J Proteome Res *11*, 4052-4064.

Rawlings, J.S., Rosler, K.M., and Harrison, D.A. (2004). The JAK/STAT signaling pathway. Journal of cell science *117*, 1281-1283.

Repka, M.X., Tung, B., Good, W.V., Capone, A., and Shapiro, M.J. (2011). Outcome of Eyes Developing Retinal Detachment During the Early Treatment for Retinopathy of Prematurity Study. Archives of Ophthalmology *129*, 1175-1179.

Rockey, D.C., Bell, P.D., and Hill, J.A. (2015). Fibrosis — A Common Pathway to Organ Injury and Failure. New England Journal of Medicine *372*, 1138-1149.

Roesch, K., Jadhav, A.P., Trimarchi, J.M., Stadler, M.B., Roska, B., Sun, B.B., and Cepko, C.L. (2008). The transcriptome of retinal Müller glial cells. The Journal of comparative neurology *509*, 225-238.

Sagare, A.P., Bell, R.D., Zhao, Z., Ma, Q., Winkler, E.A., Ramanathan, A., and Zlokovic, B.V. (2013). Pericyte loss influences Alzheimer-like neurodegeneration in mice. Nature Communications *4*, 2932-2932.

Saha, B., Jyothi Prasanna, S., Chandrasekar, B., and Nandi, D. (2010). Gene modulation and immunoregulatory roles of Interferonγ. Cytokine *50*, 1-14.

Sapieha, P., Joyal, J.-S., Rivera, J.C., Kermorvant-Duchemin, E., Sennlaub, F., Hardy, P., Lachapelle, P., and Chemtob, S. (2010). Retinopathy of prematurity: understanding ischemic retinal vasculopathies at an extreme of life. The Journal of clinical investigation *120*, 3022-3032.

Schroder, K., Hertzog, P.J., Ravasi, T., and Hume, D.A. (2004). Interferon-gamma: an overview of signals, mechanisms and functions. J Leukoc Biol *75*, 163-189.

Schuliga, M. (2015). Smooth muscle and extracellular matrix interactions in health and disease. Muscle cell and tissue, 359-391.

Selvam, S., Kumar, T., and Fruttiger, M. (2018). Retinal vasculature development in health and disease. Prog Retin Eye Res *63*, 1-19.

Shepro, D., and Morel, N.M.L. (1993). Pericyte physiology. The FASEB Journal *7*, 1031-1038.
Siegenthaler, Julie A., Ashique, Amir M., Zarbalis, K., Patterson, Katelin P., Hecht, Jonathan H., Kane, Maureen A., Folias, Alexandra E., Choe, Y., May, Scott R., Kume, T., Napoli, Joseph L., Peterson, Andrew S., and Pleasure, Samuel J. (2011). Retinoic Acid from the Meninges Regulates Cortical Neuron Generation. Cell *146*, 486.

Siegenthaler, J.A., and Pleasure, S.J. (2011). We have got you 'covered': how the meninges control brain development. Curr Opin Genet Dev *21*, 249-255.

Singhmar, P., Trinh, R.T.P., Ma, J., Huo, X., Peng, B., Heijnen, C.J., and Kavelaars, A. (2020). The fibroblast-derived protein PI16 controls neuropathic pain. Proc Natl Acad Sci U S A *117*, 5463-5471.

Smith, L.E., Wesolowski, E., McLellan, A., Kostyk, S.K., D'Amato, R., Sullivan, R., and D'Amore, P.A. (1994). Oxygen-induced retinopathy in the mouse. Invest Ophthalmol Vis Sci *35*, 101-111.

Smyth, L.C.D., Rustenhoven, J., Scotter, E.L., Schweder, P., Faull, R.L.M., Park, T.I.H., and Dragunow, M. (2018). Markers for human brain pericytes and smooth muscle cells. J Chem Neuroanat *92*, 48-60.

Snead, D.R.J., James, S., and Snead, M.P. (2008). Pathological changes in the vitreoretinal junction 1: epiretinal membrane formation. Eye *22*, 1310-1317.

Soderblom, C., Luo, X., Blumenthal, E., Bray, E., Lyapichev, K., Ramos, J., Krishnan, V., Lai-Hsu, C., Park, K.K., Tsoulfas, P., and Lee, J.K. (2013). Perivascular fibroblasts form the fibrotic scar after contusive spinal cord injury. The Journal of neuroscience : the official journal of the Society for Neuroscience *33*, 13882-13887.

Sofroniew, M.V. (2009a). Molecular dissection of reactive astrogliosis and glial scar formation. Trends in neurosciences *32*, 638-647.

Sofroniew, M.V. (2009b). Molecular dissection of reactive astrogliosis and glial scar formation. Trends Neurosci *32*, 638-647.

Storey, P.P., Ter-Zakarian, A., Philander, S.A., Olmos de Koo, L., George, M., Humayun, M.S., Rodger, D.C., and Ameri, H. (2018). VISUAL AND ANATOMICAL OUTCOMES AFTER DIABETIC TRACTION AND TRACTION-RHEGMATOGENOUS RETINAL DETACHMENT REPAIR. Retina *38*, 1913-1919.

Stuart, T., Butler, A., Hoffman, P., Hafemeister, C., Papalexi, E., Mauck, W.M., 3rd, Hao, Y., Stoeckius, M., Smibert, P., and Satija, R. (2019). Comprehensive Integration of Single-Cell Data. Cell *177*, 1888-1902.e1821.

Sweeney, M.D., Ayyadurai, S., and Zlokovic, B.V. (2016). Pericytes of the neurovascular unit: key functions and signaling pathways. Nat Neurosci *19*, 771-783.

Tager, A.M., LaCamera, P., Shea, B.S., Campanella, G.S., Selman, M., Zhao, Z., Polosukhin, V., Wain, J., Karimi-Shah, B.A., Kim, N.D., Hart, W.K., Pardo, A., Blackwell, T.S., Xu, Y., Chun, J., and Luster, A.D. (2008). The lysophosphatidic acid receptor LPA1 links pulmonary fibrosis to lung injury by mediating fibroblast recruitment and vascular leak. Nature Medicine *14*, 45-54.

Travers, J.G., Kamal, F.A., Robbins, J., Yutzey, K.E., and Blaxall, B.C. (2016). Cardiac Fibrosis: The Fibroblast Awakens. Circulation research *118*, 1021-1040.

Trese, M.T., and Droste, P.J. (1998). Long-term postoperative results of a consecutive series of stages 4 and 5 retinopathy of prematurity. Ophthalmology *105*, 992-997.

Tsai, H.H., Niu, J., Munji, R., Davalos, D., Chang, J., Zhang, H., Tien, A.C., Kuo, C.J., Chan, J.R., Daneman, R., and Fancy, S.P. (2016). Oligodendrocyte precursors migrate along vasculature in the developing nervous system. Science *351*, 379-384.

van Horssen, J., Bö, L., Dijkstra, C.D., and de Vries, H.E. (2006). Extensive extracellular matrix depositions in active multiple sclerosis lesions. Neurobiology of Disease *24*, 484-491.

van Horssen, J., Dijkstra, C.D., and de Vries, H.E. (2007). The extracellular matrix in multiple sclerosis pathology. Journal of Neurochemistry *103*, 1293-1301.

Van Linthout, S., Miteva, K., and Tschöpe, C. (2014). Crosstalk between fibroblasts and inflammatory cells. Cardiovascular Research *102*, 258-269.

Van Vliet, E., Melis, M., Foidart, J.M., and Van Ewijk, W. (1986). Reticular fibroblasts in peripheral lymphoid organs identified by a monoclonal antibody. J Histochem Cytochem *34*, 883-890.

Van Vliet, E., Melis, M., and Van Ewijk, W. (1984). Monoclonal antibodies to stromal cell types of the mouse thymus. Eur J Immunol *14*, 524-529.

Vangansewinkel, T., Lemmens, S., Geurts, N., Quanten, K., Dooley, D., Pejler, G., and Hendrix, S. (2019). Mouse mast cell protease 4 suppresses scar formation after traumatic spinal cord injury. Scientific reports *9*, 3715-3715.

Vanlandewijck, M., He, L., Mäe, M.A., Andrae, J., Ando, K., Del Gaudio, F., Nahar, K., Lebouvier, T., Laviña, B., Gouveia, L., Sun, Y., Raschperger, E., Räsänen, M., Zarb, Y., Mochizuki, N., Keller, A., Lendahl, U., and Betsholtz, C. (2018). A molecular atlas of cell types and zonation in the brain vasculature. Nature.

Vermersch, P., Benrabah, R., Schmidt, N., Zéphir, H., Clavelou, P., Vongsouthi, C., Dubreuil, P., Moussy, A., and Hermine, O. (2012). Masitinib treatment in patients with progressive multiple sclerosis: a randomized pilot study. BMC Neurology *12*, 36.

Vivatbutsiri, P., Ichinose, S., Hytönen, M., Sainio, K., Eto, K., and Iseki, S. (2008). Impaired meningeal development in association with apical expansion of calvarial bone osteogenesis in the Foxc1 mutant. J Anat *212*, 603-611.

Voskuhl, R.R., Peterson, R.S., Song, B., Ao, Y., Morales, L.B.J., Tiwari-Woodruff, S., and Sofroniew, M.V. (2009). Reactive astrocytes form scar-like perivascular barriers to leukocytes

during adaptive immune inflammation of the CNS. The Journal of neuroscience : the official journal of the Society for Neuroscience *29*, 11511-11522.

Wang, L., Li, J., and Li, D. (2015). Losartan reduces myocardial interstitial fibrosis in diabetic cardiomyopathy rats by inhibiting JAK/STAT signaling pathway. Int J Clin Exp Pathol *8*, 466-473.

Watanabe, R., Kakizaki, M., Ikehara, Y., and Togayachi, A. (2016). Formation of fibroblastic reticular network in the brain after infection with neurovirulent murine coronavirus. Neuropathology.

Wei, X., Melemedjian, O.K., Ahn, D.D.U., Weinstein, N., and Dussor, G. (2014). Dural fibroblasts play a potential role in headache pathophysiology. Pain.

Wei, X., Yan, J., Tillu, D., Asiedu, M., Weinstein, N., Melemedjian, O., Price, T., and Dussor, G. (2015). Meningeal norepinephrine produces headache behaviors in rats via actions both on dural afferents and fibroblasts. Cephalalgia.

Welsh, D.G., Tran, C.H.T., Hald, B.O., and Sancho, M. (2018). The Conducted Vasomotor Response: Function, Biophysical Basis, and Pharmacological Control. Annual Review of Pharmacology and Toxicology *58*, 391-410.

Wendling, O., Bornert, J.M., Chambon, P., and Metzger, D. (2009). Efficient temporally-controlled targeted mutagenesis in smooth muscle cells of the adult mouse. Genesis *47*, 14-18.
Winkler, E.A., Bell, R.D., and Zlokovic, B.V. (2010). Pericyte-specific expression of PDGF beta receptor in mouse models with normal and deficient PDGF beta receptor signaling. Mol Neurodegener *5*, 32-32.

Wynn, T.A. (2008). Cellular and molecular mechanisms of fibrosis. The Journal of pathology *214*, 199-210.

Xie, T., Wang, Y., Deng, N., Huang, G., Taghavifar, F., Geng, Y., Liu, N., Kulur, V., Yao, C., Chen, P., Liu, Z., Stripp, B., Tang, J., Liang, J., Noble, P.W., and Jiang, D. (2018). Single-Cell Deconvolution of Fibroblast Heterogeneity in Mouse Pulmonary Fibrosis. Cell Rep *22*, 3625-3640.

Yahn, S.L., Li, J., Goo, I., Gao, H., Brambilla, R., and Lee, J.K. (2020). Fibrotic scar after experimental autoimmune encephalomyelitis inhibits oligodendrocyte differentiation. Neurobiology of Disease *134*, 104674-104674.

Yang, T., Guo, R., and Zhang, F. (2019). Brain perivascular macrophages: Recent advances and implications in health and diseases. CNS Neuroscience & Therapeutics *25*, 1318-1328.

Ying, H.Z., Chen, Q., Zhang, W.Y., Zhang, H.H., Ma, Y., Zhang, S.Z., Fang, J., and Yu, C.H. (2017). PDGF signaling pathway in hepatic fibrosis pathogenesis and therapeutics (Review). Mol Med Rep *16*, 7879-7889.

Yiu, G., and He, Z. (2006). Glial inhibition of CNS axon regeneration. Nature reviews Neuroscience *7*, 617-627.

Yoshioka, N., Hisanaga, S.-I., and Kawano, H. (2010). Suppression of fibrotic scar formation promotes axonal regeneration without disturbing blood-brain barrier repair and withdrawal of leukocytes after traumatic brain injury. The Journal of Comparative Neurology *518*, 3867-3881.

Yoshioka, N., Kimura-Kuroda, J., Saito, T., Kawamura, K., Hisanaga, S.I., and Kawano, H. (2011). Small molecule inhibitor of type I transforming growth factor-β receptor kinase ameliorates the inhibitory milieu in injured brain and promotes regeneration of nigrostriatal dopaminergic axons. Journal of Neuroscience Research.

Yung, Y.C., Stoddard, N.C., Mirendil, H., and Chun, J. (2015). Lysophosphatidic Acid signaling in the nervous system. Neuron *85*, 669-682.

Zarbalis, K., Siegenthaler, J.A., Choe, Y., May, S.R., Peterson, A.S., and Pleasure, S.J. (2007). Cortical dysplasia and skull defects in mice with a Foxc1 allele reveal the role of meningeal differentiation in regulating cortical development. Proceedings of the National Academy of Sciences of the United States of America *104*, 14002-14007.

Zehendner, C.M., Sebastiani, A., Hugonnet, A., Bischoff, F., Luhmann, H.J., and Thal, S.C. (2015). Traumatic brain injury results in rapid pericyte loss followed by reactive pericytosis in the cerebral cortex. Scientific Reports.

Zhang, E.T., Inman, C.B., and Weller, R.O. (1990). Interrelationships of the pia mater and the perivascular (Virchow-Robin) spaces in the human cerebrum. J Anat *170*, 111-123.

Zhou, T., Zheng, Y., Sun, L., Badea, S.R., Jin, Y., Liu, Y., Rolfe, A.J., Sun, H., Wang, X., Cheng, Z., Huang, Z., Zhao, N., Sun, X., Li, J., Fan, J., Lee, C., Megraw, T.L., Wu, W., Wang, G., and Ren, Y. (2019). Microvascular endothelial cells engulf myelin debris and promote macrophage recruitment and fibrosis after neural injury. Nature Neuroscience, 1-1.

Zhou, Y., Kipps, T.J., and Zhang, S. (2017). Wnt5a Signaling in Normal and Cancer Stem Cells. Stem cells international *2017*, 5295286-5295286.

Zhu, Y., Soderblom, C., Krishnan, V., Ashbaugh, J., Bethea, J.R., and Lee, J.K. (2015). Hematogenous macrophage depletion reduces the fibrotic scar and increases axonal growth after spinal cord injury. Neurobiol Dis *74*, 114-125.